ISTANBUL TECHNICAL UNIVERSITY ★ GRADUATE SCHOOL OF SCIENCE ENGINEERING AND TECHNOLOGY

STRENGTHENING OF LOW-STRENGTH SHORT COLUMNS WITH SPRAYED UP TEXTILE REINFORCED GFRC

M.Sc. THESIS

Soheil KHOSHKHOLGHI

Department of Civil Engineering

Structural Engineering Programme

JULY 2015

ISTANBUL TECHNICAL UNIVERSITY ★ GRADUATE SCHOOL OF SCIENCE ENGINEERING AND TECHNOLOGY

STRENGTHENING OF LOW-STRENGTH SHORT COLUMNS WITH SPRAYED UP TEXTILE REINFORCED GFRC

M.Sc. THESIS

Soheil KHOSHKHOLGHI
(501121091)

Department of Civil Engineering

Structural Engineering Programme

Thesis Advisor: Prof. Dr. Alper ILKI

JULY 2015

İSTANBUL TEKNİK ÜNİVERSİTESİ ★ FEN BİLİMLERİ ENSTİTÜSÜ

PÜSKÜRTME BAZALT TEKSTİL TAKVİYELİ GFRC İLE DÜŞÜK DAYANIMLI KOLONLARIN GÜÇLENDİRMESİ

YÜKSEK LİSANS TEZİ

Soheil KHOSHKHOLGHI
(501121091)

İnşaat Mühendisliği Anabilim Dalı

Yapı Mühendisliği Programı

Tez Danışmanı: Prof. Dr. Alper İLKİ

TEMMUZ 2015

Soheil KHOSHKHOLGHI, a **M.Sc.** student of ITU **Graduate School of Science Engineering and Technology** student ID 501121091, successfully defended the **thesis** entitled "**STRENGTHENING OF LOW-STREGNTH SHORT COLUMNS WITH SPRAYED UP TEXTILE REINFORCED GFRC**", which he prepared after fulfilling the requirements specified in the associated legislations, before the jury whose signatures are below.

Thesis Advisor: **Prof. Dr. Alper ILKI**   ....
İstanbul Technical University

Jury Members: **Doç. Dr. Abdullah Necmettin GÜNDÜZ**
Istanbul Technical University   ....

Doç. Dr. Kutay ORAKÇAL   ....
Boğaziçi University

Date of Submission: 4 May 2015
Date of Defense: 9 July 2015

To my Mom, Dad and my Sister

For their everlasting love and support.

FOREWORD

This thesis was written for my master degree in structural engineering at the Istanbul Technical University. For me, the experiences, which I earned, through this thesis study, moreover, working in laboratories and various projects, attending conferences and workshops are at least equally gratifying as, the knowledge I learned from the courses I have got at ITU. I would like to show my gratitude to my supervisor Prof. Dr. Alper ILKI for his advice, encouragement, guidance, and help me during different challenges throughout this thesis. Working with him is a great honor for me.

MAY 2015   Soheil KHOSHKHOLGHI

                                                                        (Civil Engineer)

x

TABLE OF CONTENTS **Page**

ABBREVIATIONS

AR-glass	: Alkali Resistance Glass
BGFRC	: Basalt Reinforced Glass Fiber Reinforced Concrete
FRP	: Fiber Reinforced Polymer
RC	: Reinforced Concrete
TRM	: Textile Reinforced Mortar
GFRC	: Glass Fiber Reinforced Concrete
A_e	: Effectively Confined Area
A_g	: Gross Section Area
E_j	: Elastic Modulus of Jacket in Lateral Direction
f_{c0}	: Maximum Unconfined Concrete Stress
f_{cc}	: Maximum Confined Concrete Stress
f_{lu}	: Lateral Confining Stress on the Concrete
f_{je}	: Effective Strength of Jacket in Lateral Direction
K_s	: Confinement Effectiveness Coefficient
K	: Empirical Constants
m	: Empirical Constants
n	: Empirical Constants
n_f	: The Number of Plies of Wrapping Material
t_f	: The Effective Thickness of One Ply of Wrapping Material
t_j	: Thickness of Jacket
r_c	: Radius at Corners of Rectangular Sections
ε_{cc}	: Strain at Maximum Concrete Stress f_{cc}
ε_{co}	: Strain at Maximum Stress f_{co} of Unconfined Concrete
ε_{ccu}	: Ultimate Strain of Confined Concrete
ε_j	: Jacket Strain in Lateral Direction
$\sigma_{l.b}$	: Lateral Stress Perpendicular to Side b
$\sigma_{l,h}$	: Lateral Stress Perpendicular to Side h
σ_{lu}	: Ultimate Lateral Stress Due to Jacketing
σ_l	: Lateral Stress Due to Jacketing

LIST OF TABLES

LIST OF FIGURES Page

STRENGTHENING OF LOW-STRENGTH SHORT COLUMNS WITH SPRAYED UP TEXTILE REINFORCED GFRC

SUMMARY

Many existing reinforced concrete structures suffer from effects of earthquakes due to low strength concrete and inadequate transverse reinforcement, which affect strength and ductility characteristics of structural elements adversely during earthquakes. One method to improve these characteristics is the external confinement of these elements. Different materials can be used for the purpose of external confinement. Nowadays FRPs (fiber-reinforced polymers) are popular for external confinement due to their advantages such as corrosion resistance, high strength to weight ratio, easy and prompt application and minimal geometry change after retrofitting. On the other hand, using FRPs have some drawbacks as well such as poor behavior of epoxy resins at temperatures above the glass transition temperature, high initial investment cost, difficulty of application of FRP on wet surfaces or low temperatures, incompatibility of epoxy resins and substrate materials, and emission of harmful gases during application.

The main objective of this study is to investigate the effectiveness of two external jacketing materials, GFRC (glass fiber reinforced concrete) and textile-reinforced GFRC. Into best knowledge of authors, GFRC have not been used for the external confinement of concrete before. Furthermore, another originality of investigation is the use of spraying technique during application of external jacketing this technique allows application of retrofitting in difficult and narrow areas as well as being much more rapid with respected to other techniques of jacketing.

In this study, effects of several parameters, which are effective on the behavior, such as type of jacket material (GFRC or textile-reinforced GFRC), cross-section shape (circular, square or rectangular), and number of basalt layers in textile reinforced

jackets (varies from one to three layers) are examined with focus on failure mechanisms of different jackets. The contribution of this retrofitting technique is investigated on short columns experimentally under axial loads while member level theoretical analysis are carried out for the cases of axial loads as well as combined actions of axial loads and flexural moments.

In this experimental study totally 26 low-strength (concrete compression strength less than 10 MPa) short columns with four different cross-section type were tested. Spans with circular section with 200 mm diameter, with square cross-section of 200x200 mm, with rectangular cross-section of 200x300 mm and with 200x400 mm, are included in testing program. The heights of all specimens were 500 mm. All specimens were tested under concentric monotonic compression load using Amsler universal testing machine with the capacity of 5000 kN. Additionally, 24 tensile test specimens representing each external jacketing type were also constructed and tested. The data from tensile tests were used in analytical study, and the investigation of tensile behavior for external jacketing. Experimental results showed that external confinement with glass fiber concrete provided a significant increase in axial compressive strength, while basalt textile was effective on enhancement of deformation capability in particular.

In the analytical part of the study; firstly, a method was established for estimation of ultimate strength and deformation capacity of concrete members retrofitted with the proposed method. Then, the prediction of the analytical approach possessed are compared with the result of similar tests in the literature. In the second part of the analytical study, the nonlinear flexural behavior of reinforced concrete columns retrofitted with the proposed retrofitting technique are studied by relying use of moment-curvature analysis through fiber analysis approach and relying use of proposed strength and deformation characteristics of reinforced concrete members retrofitted with the proposed method. Finally, in the third part of the analytical study, other models originally proposed for the concrete members externally jacketed with textile-reinforced mortar are used for prediction of tested specimens and obtained analytical results are compared with experimental founding.

DÜŞÜK DAYANIMLI KISA KOLONLARIN TEKSTİL TAKVİYELİ PÜSKÜRTME CAM LİFLİ BETON İLE GÜÇLENDİRİLMESİ

ÖZET

Mevcut yapıların depremlerde dayanım ve süneklik özelliklerini etkileyen düşük beton dayanımı ve yetersiz sargı donatısı gibi yetersizlikler, bu yapılarda deprem etkisi altında hasar oluşmasına neden olmaktadır. Betonarme elemanların dıştan sargılanması bu yapısal karakteristiklerin iyileştirilmesi için önemli yöntemlerden biridir. Dıştan sargılama ile güçlendirme yönteminde birbirinden farklı türde malzemeler kullanılabilmektedir. Lifli polimer kompozitler (LP); iyi korozyon dayanımı, yüksek dayanım/ağırlık oranı, kolay ve hızlı uygulaması ve güçlendirme sonrası geometri değişiminin küçük boyutlarda olması gibi avantajlar nedeniyle günümüzde dıştan sargılamada kullanılan malzemelerin en önemlilerinden olduğu yapılan deneysel çalışmalar ile ortaya konulmuştur. Belirtilen avantajlarının yanısıra, epoksi reçinenin yüksek sıcaklıklardaki düşük performansı, yüksek üretim maliyeti, ıslak yüzeylerdeki ve düşük sıcaklıklardaki uygulama zorluğu, epoksi reçine ile alt yüzeyin malzemesi arasındaki uyumsuzluk, uygulamada sağlığa zararlı gazların ortaya çıkması gibi LP ile güçlendirmenin çeşitli yetersizlikleri söz konusudur.

Bu çalışmanın ana amacı cam lifli püskürtme beton (GFRC) ve tekstil takviyeli cam lifli püskürtme beton olarak iki kompozit malzemenin, dıştan sargılama ile güçlendirme yönteminde etkinliğinin incelenmesidir. Yazarın bilgisi dahilinde GFRC ilk kez bu çalışma kapsamında düşük dayanımlı betonun sargılanmasında kullanılmaktadır. Ayrıca yöntemin öne çıkan diğer bir orjinal özelliği ise pskürtme olarak uygulanması sonucunda ulaşılması güç bölgelerin de güçlendirilebilirliği ve diğer yöntemlere göre daha hızlı olarak uygulanabilmesidir.

Bu çalışmada, sargılama malzemesi olarak kullanılan kompozitin içeriği (GFRC veya tekstil takviyeli GFRC), en kesit geometrisi (dairesel, kare veya dikgörtgen) ve tekstil takviyeli sargılamada ki basalt katmanı sayısı (bir, iki ve üç kat) gibi davranışta

etkinliği öngörülen bir çok parametre incelenmiştir. Bu güçlendirme tekniğinin davranışa katkısı eksenel yük altında kısa kolonlar üzerinde yapılan deneysel çalışmalar ile birlikte eleman seviyeinde gerçekleştirilen teorik analizler ile araştırılmıştır.

Deneysel çalışmada toplam 26 düşük dayanımlı (beton basınç dayanımı 10 MPa dan az) dört farklı en kesit geometrisine sahip kısa kolon numuneleri test edilmiştir. Dairesel kesitli numunelerin çapı 200 mm, kare kesitli numuneler 200x200 mm boyutlarında, dikdörtgen kesitli numuneler ise 200x300 mm ve 200x400 mm olmak üzere iki farklı boyuttadır. Numunelerin yüksekliği 500 mm dir. Bütün numuneler 5000 kN kapasiteli Amsler Universal deney aleti ile monotonik basınç yüklemesi altında test edilmiştir. Ayrıca kompozit malzeme davranışını belirlemek amacıyla 24 adet çekme numunesi üretilmiş ve test edilmiştir. Çekme deneylerinden elde edilen davranışa bağlı karakteristik değerler, analitik çalışmalarda sargılama sonucu değişen beton malzeme davranışının modellenebilmesi için kullanılmıştır.

Kısa kolon numuneleri üzerinde gerçekleştirilen deneylerden elde edilen sonuçlar cam lifli püskürtme betonun ve basalt tekstil takviyeli cam lifli püskürtme betonun dıştan sargılama şeklinde güçlendirmenin dayanım ve süneklik özelliklerini önemli oranda arttırdığını göstermiş ve bu kompozitlerin güçlendirme için kullanılabilecek uygun malzemeler olduğunu ortay koymuştur. Deneylerde güçlendirilmiş kısa kolon numunelerinin monotonic artan eksenel yük altındaki davranışında maksimum dayanıma ulaşmaya yakın bölgelerde püskürtme cam lifli betonun davranışa hakim olduğu, maksimum dayanım değerinden sonra cam lifli betonda çatlakların oluşmaya başladığını ve basalt tekstillerin içeriği ve mekanik karakteristiklerine göre deformasyon özelliğinin değiştiği gözlemlenmiştir. Ayrıca dikdörtgen kesitli numunelerde kenar boyutları oranı büyüdükçe srgılama etkinliğinin ve tüketilen şekildeğiştirme enerjidinin azaldığı gözlenmiş, bu durumun güçlendirme tasarımında dikkate alınması gereken bir parametre olduğu ortaya konulmuştur.

Çalışmanın analitik kısmında ilk olarak güçlendirilmiş beton numunelerinin en büyük dayanım ve deformasyon değerlerinin tahmini için ampirik bağıntılar deney sonuçlarının istatistiksel olarak değerlendirilmesinden elde edilmiştir. Sadece cam lifli püskürtme beton ile güçlendirilmiş numunelerde basalt tekstil bulunmaması ve buna bağlı olarak deformasyon kapasitesinde bir artış söz konusu olmaması nedeniyle

analatik çalışmalar kısmında değerlendirilmemiştir. Tekstil takviyeli cam lifli püskürtme beton için deneysel sonuçlardan elde edilen sargılı beton ve şekildeğiştirme bağıntıları literatürde yer alan benzer deneysel çalışma sonuçları ile karşılaştırılmıştır ve verilen bağıntıların bu deneysel çalışmaların sonuçlarıyla oldukça uyumlu sonuçlar verdiği ortaya konulmuştur. Analitik çalışmanın ikinci kısmında elde edilen sargılı betona ait dayanım ve şekildeğiştirme bağıntılarından elde edilen değerler ile güçlendirilmiş beton davranış modeli belirlenmiştir. Bu model göz önüne alınarak literatürde tersinir tekrarlı yükleme altında test edilmiş farklı kesitlerdeki betonarme kolonların moment-eğrilik ilişkisine bağlı doğrusal olmayan eğilme davranışları incelenmiştir. Gerçekleştirilen analizlerde tekstil takviyeli püskürtme cam lifli beton ile dıştan sargılama güçlendirmesinin betonarme kolonların eleman davranışını önemli oranda arttıracağı belirlenmiş, buna bağlı olarak bu güçlendirme yönteminin yetersiz yapıların devrem davranışını dayanım ve süneklik açısından önemli oranda iyileştireceği ortaya konulmuştur. Analitik çalışmanın son kısmında tekstil takviyeli harçlar ile dıştan sargılama için önerilmiş diğer literatürdeki diğer modeller çalışmanın deneysel sonuçlarının tahmini için kullanılmış ve analitik sonuçlar ile deneysel sonuçlar karşılaştırılmıştır.

Gerçekleştirilen geniş kapsamlı deneysel çalışmalar ve deneysel sonuçlara bağlı olarak yapılan analitik çalışmalar, tekstil takviyeli cam lifli püskürtme beton ile yetersiz betonarme elemanların güçlendirilmesininin dayanım ve süneklik özelliklerinin artışı açısından önemli bir yöntem olduğunu ortaya koymuştur. Sahip olduğu kolay ve hızlı uygulanabilirlik gibi avantajları, diğer alternatif dıştan sargılama yöntemlerine göre tekstil takviyeli cam püskürtme beton ile dıştan sargılama yöntemini ön plana çıkarmaktadır.

1. INTRODUCTION

Significant portion of existing buildings in earthquake prone developing countries, suffer from low quality of concrete and/or lack of adequate transverse reinforcement. In such cases, axial capacity and deformability of structural members should be enhanced to ensure satisfactory seismic performance in term of strength and deformability. Particularly in Turkey, this sort of buildings are far from complying the requirements of current Turkish seismic design code. Consequently, these buildings need to be demolished and reconstructed or, strengthened to prevent loss of lives.

Increasing of ductility and strength of RC members through external jacketing by using fiber-reinforced polymers (FRP) has become very popular in recent years, due to its several favorable properties. These are corrosion resistance, high strength to weight ratio, easy and prompt application and minimal geometry change after retrofitting. Despite these advantages ,using FRPs as external jacketing material has a number of drawbacks as poor behavior of epoxy resins at temperatures above the glass transition temperature, high initial investment cost, difficulty of application of FRP on wet surfaces or low temperatures, incompatibility of epoxy resins and substrate materials, difficulty of conducting post-earthquake assessment of the damage suffered by the reinforced concrete behind (undamaged) FRP jackets, lack of vapor permeability, and emission of harmful gases during application.

Most of these deficiencies are caused by the organic resin matrix. Hence, to overcome these weaknesses, an inorganic cement based matrix can be used. As the bonding agent. The composite materials, obtained from using inorganic cement based matrix and textile reinforcement together are generally named textile-reinforced mortar (TRM) in the literature. Several researchers have focused on the improvement of the behavior of concrete or RC members using textile reinforced mortars (Bisby et al. 2009, Triantafillou and Papanicolau 2006, Bournas 2007, Ombres 2014, Ortlepp 2009 and Garcia 2010).

In this study sprayed GFRC (glass fiber reinforced mortar) jacketing alone or with additional basalt embedded into GFRC jacket are used for retrofitting the concrete specimens. Remarkable benefits, which usage of this technique provides are, ease and prompt of application using automatic mixture machine and spraying gun. These advantages make this technique independent from applicators expertise and quiet occupant friendly.

Seven circular specimens with 200 mm diameter, eight square specimens with 200x200 mm, seven rectangular specimens with 200x300 mm, and four rectangular specimens with 200x400 mm were tested .The height of all specimens were same 500 mm and all specimens were constructed with low strength concrete. Additionally 24 tensile specimens were also tested to evaluate the direct tension characteristics of the GFRC and textile reinforced GFRC.

 To the best knowledge of the author's this jacketing technique is used for the first time in the literature. The experimental results showed that both axial compression capacity, deformability capacity and energy absorption capacity of specimens has been improved considerably. This enhancement has also been shown theoretically for members under axial load and combined action of axial load and flexural moment.

1.1 Purpose Of Thesis

The main objective of this study is to examine the effectiveness of two external jacketing materials (GFRC and textile-reinforced GFRC) .To accomplish these objectives the following methodology was followed:

- Design, construction, instrumentation, and testing of totally 26 low-strength short columns with four different cross-section type, circular with 200 mm diameter, square with 200x200 mm, rectangular with 200x300 mm and 200x400 mm. Jacketing was applied either by only sprayed GFRC or sprayed GFRC and wrapped basalt mesh of different plies.

- Design, construction, instrumentation, and testing of totally 24 tensile test specimens. These tested specimens was formed either with only GFRC, or with GFRC retrofitted with 1, 2, or 3 layer of basalt.

- Theoretical analysis toward establishment of a model that is capable of estimating the strength and deformation capability of structural members retrofitted with the proposed method.

1.2 Literature Review

Triantafillou et al. (2006) in this study the application of textile-reinforced mortars (TRMs) for increasing the axial capacity of concrete through confinement is experimentally investigated. The study was carried out on 1) cylindrical specimens with the diameter of 150 mm and a height of 300 mm, 2) short column-type specimens 250x250 mm and a height of 700 mm, corners of all rectangular prism were rounded at a radius of 15 mm .all specimens are unreinforced. The parameters were investigated with this study are 1) comparing inorganic mortars versus epoxy resins. 2) Investigating the effect of mortar strength on the effectiveness of inorganic mortars, 3) investigating the role of the number of textile layers on the effectiveness of jacketing and, 4) effectiveness of bonded versus unbounded confining system. Based on the response of confined cylinders, it is concluded that: 1) textile-mortar confining jackets provide substantial gain in compressive strength and deformability where it is higher as the number of confining layers increases and depends on the tensile strength of the mortar, which determines whether failure of the jacket will occur due to fiber fracture or debonding, 2) Comparing resin-impregnated counterparts with mortar-impregnated textiles it is obvious that resin-impregnated counter parts are more effective and, 3) failure of mortar-impregnated textile jackets.
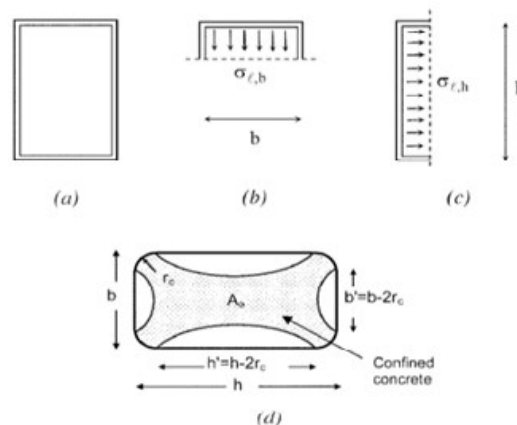
Figure 1.1: Confinement details: approximate average confining stresses (a) to (c); and (d) effectively confined area in columns with rectangular cross section (Triantafillou et al, 2006).

is less abrupt compared with that of their resin-impregnated counterparts, due to the slowly progressing fracture of individual fiber bundles. From the reaction of rectangular columns, it is concluded that mortar-impregnated textile jackets are quite effective in confining columns of rectangular cross sections for strength and axial deformability. In comparison with their epoxy-based counterparts, mortar-impregnated textile jackets gave approximately the same effectiveness in strength terms and a lower one in ultimate strain terms. The same conclusion applies in the case of spirally applied unbounded strips with end anchorages, except if the number of layers is quite low, which may unfavorably affect the deformability. Here is the confinement model that has been preferred in paper.

$$\frac{f_{cc}}{f_{c0}} = 1 + k_1\left(\frac{\sigma_{lu}}{f_{c0}}\right)^m \tag{1.1}$$

$$\varepsilon_{ccu} = \varepsilon_{c0} + k_2\left(\frac{\sigma_{lu}}{f_{c0}}\right)^n \tag{1.2}$$

$$k_1 = \alpha k_{1,R} \tag{1.3}$$

$$k_2 = \beta k_{2,R} \tag{1.4}$$

$$\sigma_l = \frac{\sigma_{l,h}+\sigma_{l,b}}{2} = \frac{1}{2}k_e\left(\frac{2t_j}{h}E_j\varepsilon_j + \frac{2t_j}{b}E_j\varepsilon_j\right) = \frac{k_e(b+h)}{bh}t_jE_j\varepsilon_j \tag{1.5}$$

$$k_e = 1 - \frac{b'^2+h'^2}{3A_g} \tag{1.6}$$

$$\sigma_{lu} = \frac{k_e(b+h)}{bh}t_jf_{je} \tag{1.7}$$

Ortlepp et al. (2009), in this study short columns with all possible cross-sections from Square to circle With different transition radiuses were tested (columns with a height of 300 mm The cross-section has been changed from a square with 150mm × 150mm to a circle with a diameter of 150mm. The transition radius has been enlarged evenly by steps of 15 mm), in order to find out the influence of the transition radius onto the local-bearing capacity of the reinforcing textile. Additionally, the impact of different fiber materials (textile out of AR-glass fibers and carbon fibers) and reinforcement degrees of the TRC (textile reinforced concrete) strengthening layer has been examined. The test parameters of the study were 1) the geometry, 2) the collapse load part of the pure fine-grained concrete, 3) the fiber material AR glass or carbon and 4) the fiber volume percentage. The results shows that a considerable inconsistent

increase of the confinement effect with rising transition radius. It is important for a practical use of TRC for strengthening columns to round the edges as far as possible to increase the effectiveness of the confinement. The load-carrying capacity increase by a Textile-Reinforced concrete layer is substantially achieved by the confinement of the core concrete. The load fraction being carried by the normal forces within the fine-grained concrete coat is small compared to the confinement effect. The size effect impact allows the opposing argument that the confinement effect should decrease with enlarging cross sectional area if the reinforcement degree remains the same. The fiber material carbon has obvious advantages due to its higher stiffness compared to AR-glass.

Table 1.1: The analytical expressions to predict peak strength f$_{cc}$ and ultimate axial strain (Ortlepp et al, 2009).

Model.	Analytical expressions.
Spoelstra and Monti (1999) (SM model)	$\dfrac{f_{cc}}{f_{c0}} = 2.254\sqrt{1 + \dfrac{7.4f_{lu}}{f_{c0}} - \dfrac{2f_{lu}}{f_{c0}}} - 1.254 \; ; \dfrac{\varepsilon_{cc}}{\varepsilon_{c0}} = 1 + 5(\dfrac{f_{cc}}{f_{c0}} - 1)$
Teng et al. (2002) (TL model)	$\dfrac{f_{cc}}{f_{c0}} = 1 + \dfrac{2.15f_{lu}}{f_{c0}} \; ; \dfrac{\varepsilon cc}{\varepsilon co} = 1.715 + 10(\dfrac{f_{lu}}{f_{c0}})$
Triantafillou et al. (1997) (TR model)	$\dfrac{f_{cc}}{f_{c0}} = 1 + 1.9(\dfrac{f_{lu}}{f_{c0}})^{1.27} \; ; \dfrac{\varepsilon_{cc}}{\varepsilon_{c0}} = 1 + (\dfrac{0.046}{\varepsilon co})(\dfrac{f_{lu}}{f_{c0}})^{1.44}$
Toutanji (1999) (TO model)	$\dfrac{f_{cc}}{f_{c0}} = 1 + 3.5(\dfrac{f_{lu}}{f_{c0}})^{0.85} \; ; \dfrac{\varepsilon_{cc}}{\varepsilon_{c0}} = 1 + (1.9 + 310.57\varepsilon fu)(\dfrac{f_{cc}}{f_{c0}} - 1)$
National Research Council–DT 200 (2004) (DT model)	$\dfrac{f_{cc}}{f_{c0}} = 1 + 2.6(\dfrac{f_{lu}}{f_{c0}})^{2/3} \; ; \dfrac{\varepsilon_{cc}}{\varepsilon_{c0}} = \dfrac{1}{\varepsilon co}(0.0035 + 0.015\sqrt{\dfrac{f_{lu}}{f_{c0}}})$
Ortlepp et al. (2011)(OLC model)	$\dfrac{f_{cc}}{f_{c0}} = 1 + 0.27\dfrac{f_{lu}}{f_{c0}} + 5.55(\dfrac{f_{lu}}{f_{c0}})^2 - 3.51(\dfrac{f_{lu}}{f_{c0}})^3$

Ombres (2013), in this paper the performances of plain concrete elements wrapped with PBO (Polypara-phenylene-benzo-bisthiazole) fiber meshes embedded into an inorganic cementitious matrix (Fiber Reinforced Cementitious Mortar, FRCM) were analyzed, (The analytical expression proposed by each author to predict peak strength fcc and ultimate axial strain, ecc), were reported in Table 1.1.To evaluate predictions of models the value of flu was determined by the relation

$$f_{lu} = k_e f_l = k_e \rho_f E_f \varepsilon_{fu} \tag{1.8}$$

In which ke is the strain efficiency coefficient. In the analysis, the mean

Value of ke = εflmax/εfu = 0.49, determined by tests

$$f_{lu} = k_e f_l = k_e k_\theta \rho_f E_f \varepsilon_{fu} \tag{1.9}$$

$$k_\theta = \frac{1}{1+3tan\theta} \tag{1.10}$$

Consequently the best fitting curve of experimental peak

Strength values is expressed as:

$$\frac{f_{cc}}{f_{co}} = 1 + 5.268(\frac{f_{lu}}{f_{co}}) \quad (R^2 = 0.94) \tag{1.11}$$

$$\frac{\varepsilon_{cc}}{\varepsilon_{co}} = \frac{0.41\left(\frac{f_{lu}}{f_{co}}\right)^{0.25}}{\varepsilon_{co}} - 1.02 \quad (R^2 = 0.86) \tag{1.12}$$

Moreover, experimentally (twenty cylindrical concrete specimens has been tested: two specimens were un-confined, while the remaining specimens were confined with different configurations. The fiber reinforcement ratio $\rho f = 4tf/D$ being D the specimen's diameter and t_f the thickness of the PBO-FRCM reinforcing system, and the angle, h, between the longitudinal fibers direction and the axis of the specimen, were parameters characterizing each confining configuration. For tested specimens ρf values were 0.12%, 0.24%, 0.36% and 0.47% corresponding to one, two, three and four layers of PBO fabric meshes, respectively, while h values were, h = 30, 45(degree), corresponding to configuration where fibers are spirally installed, and 90 (degree).The value of the compression strength of the mortar was 30.4 MPa and tensile strength of PBO fiber meshes are 5800 (N/mm2). All specimens were tested under uni-axial compression. Monotonically applied loading at a rate of 0.005 mm/s. in order to

find out 1) the effectiveness of the confinement of the concrete strengthened with the PBO-FRCM system, and, 2) to define analytical relationships able to characterize the stress–strain response of the PBO-FRCM confined concrete. Concluding remarks: The PBO-FRCM strengthening system, made by high-strength fabric mesh embedded into a cement-based matrix, is effective in confining concrete; a significant increase of both peak strength and axial strain was obtained by tests on confined specimens. The failure mode of tested specimens was loss of compatibility in the external reinforcement because of fiber–matrix separation. Axial strain and peak strength values of PBO FRCM confined concrete are influenced both on the number of PBO layers used inside the confining jacket and on the fiber orientation. The best performances were obtained in specimens confined with PBO fibers aligned with the axis of specimens (h = 90). Due to cracking of mortar, which increases the possibility of local stress concentration, the strain efficiency coefficient, ke, determined by experimental hoop strains values measured in the PBO reinforcement, was less than that of FRP confined concrete. For tested specimens, the average value of ke was near to 0.5. The ductility of PBO FRCM confined concrete, measured by the ''energy index'', increases with the number of PBO layers. The maximum ductility values were reached in specimens confined by fibers aligned with the axis of specimens.

Garcia et al. (2010), the aim of this study is to lighten the behavior of textile-reinforced mortar (TRM), used in jacketing technique in order to improve the performance of concretes with limited resistance capacity furthermore, to investigate the confinement effect of poor concrete with TRM. Moreover, the effect of the number of layers or the use of a different mortar matrix will be investigated in a proper experimental campaign. The investigation was carried out on 30 concrete cylindrical specimens with a diameter of 150mm and a height of 300mm (following the concrete Spanish Code EHE 2008). To reproduce the behavior of poor concrete structures, the specimens were made with low strength (mud slab) concrete, taken from a site civil work where was used as solid ground for pavements Tests were carried out on basalt fabrics and TRM under tension forces and low strength (mud slab) concrete cylindrical specimens.. At 28 aged days, the average compressive strength, fcm, was 21MPa. Two series of 12 cylinders each one were repaired with TRM. The difference between them was the matrix: puzolanic or cement based mortar. Each series was constituted by six cylinders wrapped with one layer of basalt, and six more samples confined with two layers. Due

to the risk of a premature debonding failure, an overlap of 120mm length was provided. specimens was tested in an Ibertest 3000kN compression machine whose load was applied with a load rate of 0.5MPa/s. TRM is a real solution for those cases where the use of FRP is limited because of the characteristics of the structure of decayed substrates and others in which organic binders are not adequate (hazard, humidity, fire, etc.). Several experiments showed that TRM confining systems achieved a considerable gain in terms of peak strength and axial ultimate strain. This increase is lower than that provided by FRP wrapping, but on the other side, the failure mode presents a more ductile behavior.

Bournas and Triantafillou (2009) experimentally investigated the effectiveness of a textile-reinforced mortar TRM and gave results of the confining old type reinforced concrete columns with limited capacity due to bar buckling or due to bond failure at lap splice regions. Comparisons with equal stiffness and strength fiber-reinforced polymer _FRP_ jackets allow for the evaluation of the effectiveness of TRM versus FRP. Tests were carried out on nearly full-scale non-seismically detailed RC columns subjected to cyclic uniaxial flexure under constant axial load. Ten cantilever-type specimens with either continuous or lap-spliced deformed longitudinal reinforcement at the floor level were constructed and tested. Experimental results showed that TRM jacketing is quite effective as a means of increasing the cyclic deformation capacity of old-type RC columns with poor detailing, by delaying bar buckling and by preventing splitting bond failures in columns with lap-spliced bars. Compared with their FRP counterparts, the TRM jackets used in this study were found to be equally effective in terms of increasing both the strength and deformation capacity of the retrofitted columns. From the response of specimens tested in this study, it can be concluded that TRM jacketing is a very promising solution for the confinement of reinforced concrete columns, including poorly detailed ones with or without lap splices in seismic regions. Ten large-scale reinforced concrete column specimens with the same geometry were constructed and tested under cyclic uniaxial flexure with constant axial load. Four of the columns were reinforced with continuous longitudinal reinforcement and six columns had lap-spliced rebar at the base. The specimens were flexure-dominated cantilevers with a height to the point of application of the load _shear span_ of 1.6 m _half a typical story height_ and a cross section of 250×250 mm. The columns were fixed into a heavily reinforced 0.5-m-deep base block, 1.2×0.5 m2 in plan, within

which the longitudinal bars were anchored with 90º hooks at the bottom. To represent old-type non-seismically designed and detailed columns, both series of continuous and spliced specimens were reinforced longitudinally with four 14-mm-diameter deformed bars with an effective depth of 225 mm and 8-mm diameter smooth stirrups at a spacing of 200 mm, closed with 90º hooks at both ends. The performance and failure mode of all tested specimens with continuous longitudinal reinforcement was controlled by flexure. The failure mode of the un-retrofitted specimen was controlled by buckling of longitudinal rebar above the column base, which led to strength degradation. TRM jackets are quite effective as a means of increasing the cyclic deformability and the energy absorption of old-type RC columns with poor detailing, by delaying bar buckling. Compared with equal stiffness and strength FRP, TRM jacketing has a higher effectiveness by about 50%. TRM confining jackets provide substantial gain in lateral strength and deformation capacity of cyclically loaded reinforced concrete columns with lap splices at the columns base. Compared with equal stiffness and strength FRP jackets. For columns with deformed lap-spliced bars, the Euro code 8 predicted drift ratios are in good agreement for FRP and TRM jacketed members with shorter lap lengths, while its predictions are quite conservative in the case of columns with longer lap splices.

Colajanni et al. (2014) investigated the structural behavior of concrete columns confined with a jacketing type made up of fiber nets embedded in an inorganic stabilized cementitious matrix under a uniaxial load. Specimens with circular and square cross-section were subjected to monotonic uniaxial compression, to lighten the efficiency of a Phenylene Benzobis Oxazole (PBO) Fiber Reinforced Cementitious Mortar (FRCM) system in increasing both strength and ductility. The experimental study was focused on investigating the effectiveness of various jacketing schemes (geometry, number of layers) based on the use of textile made of continuous fiber (PBO) in combination with inorganic matrix. Tests were carried out in two stages. In the first one, namely Series A, eight cylindrical specimens with diameter of 154 mm and height of 335 mm were cast; in the second one, namely Series B, seven cylindrical specimens with diameter of 200 mm and height of 335 mm and seven specimens with square cross-section having side of 200 mm and height of 425 mm were cast .and specimens confined with two or three layer of textile. All the four corners of square specimens were cast rounded with a curvature radius $r_c = 20$ mm.For the cylindrical.

Specimens were designed to obtain a cylindrical compressive strength equal to 25 MPa. The cementitious matrix was prepared to obtain, after 28 days curing, a minimum compressive strength equal to 15 MPa and a flexural strength of minimum 2 MPa. As showed by the experimental results obtained, the PBO-FRCM confinement system provides substantial gain in compressive strength and ductility. The efficiency of the confinement system is strictly related to the stiffness of the package of mortar and textile utilized depending on the following parameters: the thickness and stiffness of fiber; the number of layers used; and the bond between fiber and mortar related to their mechanical properties and the mortar layer thickness. For all square specimens, the failure was due to textile rupture at the corners. Modelling of concrete confined with FRCM is presented as a rather straightforward procedure through the sum of stress contributions of the confined concrete and the mortar of the confinement system, separately. Thus, the effective confining pressure for FRCM specimens in the adapted Spoelstra and Monti model can be evaluated as follows (the proposed formulation is accurate and consistent with experimental results):

$$f_{l,e} = \frac{1}{2} \rho \cdot E_f \cdot \varepsilon_f \cdot k_e \cdot k_{fl,FRCM} \qquad \textbf{(1.13)}$$

Where ρ=confinement volumetric ratio, E_f = elasticity modulus of fiber, k_e=shape efficiency coefficient, $k_{fl,FRCM}$ =confining pressure reduction coefficient for FRCM. The ultimate compressive strain (ε_{ccu}) was evaluated as empirically found by Spoelstra and Monti for RC members confined with FRP:

$$\frac{\varepsilon_{ccu}}{\varepsilon_{co}} = 2 + 1.25 \cdot \frac{E_c}{f_{co}} \cdot \varepsilon_{fu} \cdot \sqrt{\frac{f_{l,eu}}{f_{co}}} \qquad \textbf{(1.14)}$$

Where ε_{ccu}=strain at failure of confined concrete, ε_{co}= strain corresponding to cylindrical compressive strength of unconfined concrete, E_c =elasticity modulus of concrete, f_{co}=cylindrical compressive strength of unconfined concrete, ε_{fu}=experimental fibre strain at failure, $f_{l,eu}$=ultimate effectiveness confining pressure and $k_e \varepsilon_{fuo}$ and $f_{l,eu}$ is obtained assuming $\varepsilon_f = \varepsilon_{fu}$.

Based on test results it was concluded that: 1) a PBOFRCM confining system provides substantial gain in compressive strength and ductility which related to the number of confining layers and overlapping length, 2) as unexpected, the PBO-FRCM is quite

effective in confining columns of square cross-sections both for strength and axial deformability; 3) the use of a cementitiuos mortar in place of the resin-impregnated system determines a ''delay'' in activating the confinement system, and a post-peak stiffness degradation was observed, immediately retrieved by the specimen due to the effectiveness of the PBO-FRCM.

1.3 Research Significance

There are many existing reinforced concrete structures all around the world, which are designed and constructed according to the old codes. Many of these   structures were designed considering only gravity loads. Thus, these structures should be retrofitted and strengthened in order to comply the requirements of recent seismic design codes. Upgrading of existing reinforced concrete structures, through external jacketing of columns, has become a popular technique in recent years. Particularly, confinement with fiber-reinforced polymers (FRP) has gained considerable popularity among all jacketing techniques, due to several favorable properties presented by these materials, namely high strength to weight ratio, corrosion resistance, greater contact area, ease and prompt application, and minimal change of geometry. In spite of these advantages, FRP retrofitting technique has some drawbacks, e.g. being unsuitable at high temperatures; need of more initial investment cost; inapplicability on wet surfaces or at low temperatures; danger for the manual worker due to its toxic characteristics, and lack of vapor permeability. These are mainly caused by the organic epoxy resins used to bind the fibers. An interesting alternative to FRP materials are the so-called Textile-Reinforced Mortars, in which epoxies were replaced with inorganic binders.

In this study two nowel implements are presented on application of TRM jacketing; 1) use of GFRC in the matrix of TRM and 2)application of spraying technique during retrofitting .These two implements are significantly beneficial in terms of mechanical performance of TRM jacket and ease of application. The proposed method is shown to be effective through an extensive testing program as well as obtained theoretical analysis results.

2. EXPERIMENTAL STUDY

The main objective of the experimental study was to provide a better understanding on the effectiveness of sprayed up GFRC jacketing system on performance of poor concrete columns under concentric axial compression. The investigation was carried out on short columns; type:1) C series, cylindrical with a diameter of 200 mm; 2) S series, square with 200 x 200 mm, 3) R1.5 series, rectangular cross-section specimens with 200x300 ,and 4) R2 with 200x400 mm. All the specimens have the same height of 500 mm. The four corners of all square and rectangular prisms were rounded at a radius equal to 30 mm. All specimens were unreinforced. Jacketing configurations applied in this study were two type first, confining specimens with only GFRC (glass-fiber reinforced concrete) with the jacket thickness of 25 mm second, basalt textile reinforced GFRC sprayed up with one to three layer of basalt with the same thickness of 25mm. In both confining type mortar was the same.

2.1 Material Properties

Presented retrofitting methods is consist of two base material; GFRC is a glass fiber reinforced cement based composite jacket and basalt textile are used as a reinforcement to improve ductility properties of GFRC jacket.

2.1.1 Plain concrete

Design concrete mixture of short column specimens was selected to compressive strength less than 10 MPa for representing low strength concrete of existing old building. All the specimens were built up from one single batch of ready-mix concrete having the mixture of Portland cement 215 kg/rn^3, Crushed Aggregate No.1; 923 kg/m3 Crushed Sand 1104 kg/m^3, super plasticizer 2.75 kg/m^3, water 232 kg/m^3. Standard concrete cylinders 150 x 300 mm were prepared and cured under the same conditions of the specimens. These cylinders were tested according to ASTM C39

(2004) at 28 and 180days, and at the corresponding age at which the related specimens were tested. Amsler universal testing machine with the capacity of 5000 kN was used to test cylinders in accordance with ASTM method C39. A compress meter with three-point contacts was used with two Linear Variable Displacement Transducers (LVDTs) to measure concrete compressive strains. Stress-strain relationships from compression test at 180 days was shown in Figure 2.1 in which the average compressive strength was 8.6 MPa obtained from Stress-strain relationships.
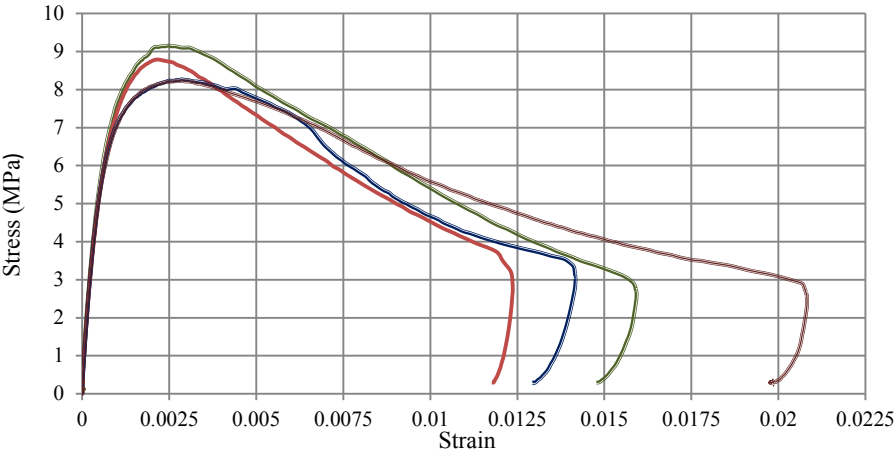
Figure 2.1: Concrete stress-strain diagram at the age of 180 days.

2.1.2 Basalt textile reinforcement mesh

Three layers of Basalt fiber mesh were sprayed with GFRC as column's jacket for specimen. The strips were wrapped around the columns in a spiral configuration and wrapping were started from one of the longer sides and was stopped at the same side by 300 mm overlap length. The technical details of the Basalt Textile, which was used in this experimental study as a strengthening material using Spinteks Corporation technical details (manufacturer corporation) are presented in Table 2.1. And 1900 MPa for Basalt textile tensile stress, 0.05 for ultimate strain and 32 Gpa for elastic modulus. Retrofitting system in this research program was manufactured either from basalt fibers, impregnated with Glass reinforced concrete (GFRC). The grids had a square configuration with 25 mm out-to-out dimension as shown in Figure 2.2.

Figure 2.2: Photo of Basalt mesh.

Table 2.1: Basalt mesh technical details.

Property	value	Tolerance
Mesh size	25X25 (mm)	+/-5%
Specific surface weight	303 (g/m2)	+/-5%
Thickness	0.8-0.9 (mm)	
Maximum load	3038.86 (warp) (N/5cm)	+/-5%
	2688.86 (weft) (N/5cm)	+/-5%
Elongation at break	6.67 (warp) (%)	+/-5%
	3.53 (weft) (%)	+/-5%

2.1.3 Glass fiber reinforced concrete

Glass fiber reinforced cementitious composites referred to as GFRC (Glass fiber reinforced concrete) or GRC (Glass fiber reinforced cement), and have been developed mainly for the production of thin sheet components, with a paste or mortar matrix, and nearly 5% fiber content. In the study, application of GFRC jacket is performed by spray-up method (figure 2.3), therefore mortar composition of GFRC was determined according to this method. Materials of the mortar mixture and weight ratios are given in the Table 2.2. Average compression strength of mortar is 43.53 MPa, obtained from compression test according to EN 1015.11:1999 were conducted on 28-day-old 40x40x40 mm cubic mortar specimens. AR-Glass fibers are chopped 24 mm length and sprayed with mortar to maintain proper fiber dispersion. Fiber content of GFRC is selected 3.5% of mixture weight to provide sufficient mechanical performance and workability Standards. Three point bending tests were performed by Fibrobeton's material laboratory on 600x100x12.5 mm GFRC sheets to determine flexural behavior according to EN 1015.11:1999. The transition point between linear and nonlinear range of flexural behavior is named as limit of proportional (LOP) is 7 MPa and ultimate flexural strength is called modulus of rupture (MOR) is 15 MPa.

Table 2.2: Mix-proportion of GFRC mortar.

Material	Amount
Cement	45 Kg/50dm^3
Sand	50 Kg/50dm^3
Metakaolin	5 Kg/50dm^3
Polymer	1.650 Kg/50dm^3
Plasticizer	0.12 Kg/50dm^3
Fiber	3.5 % of mixture weight

Figure 2.3: Application of GFRC with sprayed-up method.

2.1.4 Textile reinforced glass fiber reinforced concrete

Design, construction and test procedure of tensile test specimens for textile reinforced glass fiber reinforced concrete was done according to ACE 334 (acceptance criteria for masonry and concrete cementitous matrix (FRCM) composite system reinforced fabric strengthening) in annex A (tensile testing of FRCM composite specimens). Totally 24 tensile test specimens were constructed at the same time when the column specimens were retrofitted. For tensile specimens, the same material used as jackets. The investigation on the tensile test specimens aims to provide an understanding of the tensile behavior of jacket as well as essential data for analytical study and prediction model for ultimate strength and strain.

2.1.4.1 Construction of tensile test specimens

Details about tensile test specimens are given in Table 2.3.

Table 2.3: Details of tensile test specimens.

Label	Size	Detail	Number of tested specimens
T-G	100x450x12.5 mm	Only GFRC	5
T-B1	100x450x12.5 mm	GRC+1 basalt layer	5
T-B2	100x450x12.5 mm	GRC+2 basalt layer	5
T-B3	100x450x12.5 mm	GRC+3 basalt layer	4

For construction of tensile test specimens with the size of 100x600x12.5 mm, four plastic molds were used with inner dimensions of 600x600x12.5 mm .In each mold, tensile specimens represent a jacket type. The specimens were cast with the same materials and method used for columns retrofitting. First, the molds were sprayed with mold release oil and then a layer of GFRC were sprayed with the thickness of minimum 2 mm; afterwards, the basalt mesh was embedded in GFRC with the help of a hard type roller. At the end, another GFRC layer was sprayed (Figure 2.7 a-b) if there is more than one basalt layer, GFRC with 2mm thickness sprayed between them. One mold filled only with GFRC, one with GFRC+1 layer of basalt, one with GFRC+2 layers of basalt and the last one with GFRC+3 layers of basalt. Moreover, for all four type of tensile test specimens, two additional 150x600 mm basalt layer, were used at the top and the bottom of the specimens to prevent the formation of cracks near the chains (Figure 2.4 c).

| (a) | (b) | (c) |
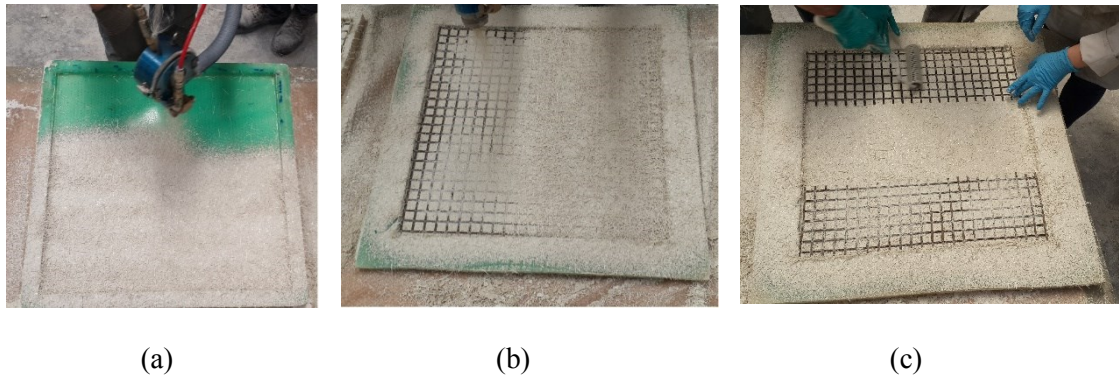
Figure 2.4: Casting of tensile test specimens.

After a week the molds were removed and the plates of tensile were cut by the width of 100 mm providing us 24 tensile test specimens with the dimensions of 100x600x12.5 mm.Geometry of a tensile specimen with one layer of basalt is given in Figure 2.5.
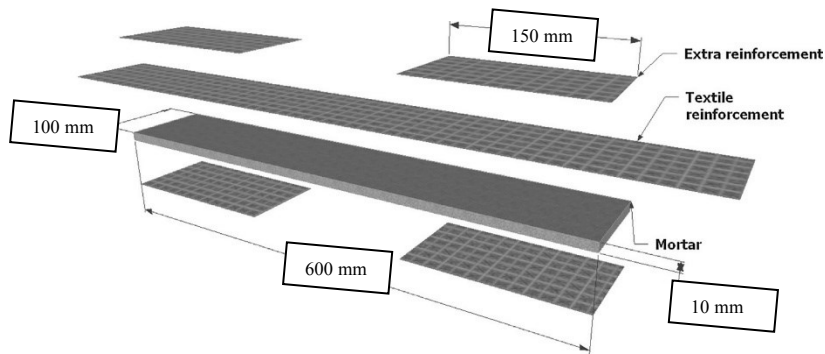
Figure 2.5: Geometry of tensile test specimens.

2.1.4.2 Test setup for tensile test specimens

All tensile test specimens were tested using Zwick-Roll tension-compression machine with the capacity of 250 KN. Due to the distance between two grips of the testing machine, the length of the specimens was 450 mm. Consequently, 75 mm, long parts from each end of the specimens were cut, and holes with the diameter of 10 mm were opened at each end using a rotary drill. Additionally, 100x100x4 mm aluminum plates were attached with a two-component epoxy adhesive at the ends (Figure 2.6). Hinges at the grips were used to prevent the formation of bending moment. For measurements, an external mechanical extensometer was used with the gauge length of 100 mm at mid-height of the specimens. After performing pilot tests, in order to avoid the stress concentration and splitting of the specimens from the zone that the aluminum plates were attached, the 150 mm top and bottom of the specimens were confined with additional CFRP (carbon fiber reinforced polymer) as shown in Figure 2.7. In the result section, the stress-strain diagrams of both, tensile test specimens wrapped with CFRP and tensile test specimens did not wrapped with CFRP are given and mentioned which are wrapped with CFRP.
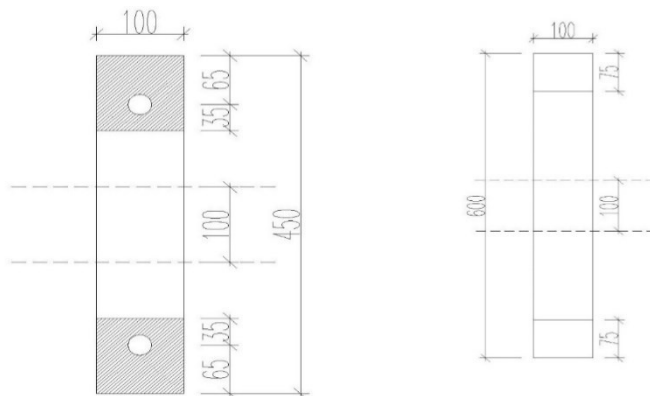
Figure 2.6: Preparation of tensile specimens for test.

Figure 2.7: Application of CFRP on tensile test specimens.
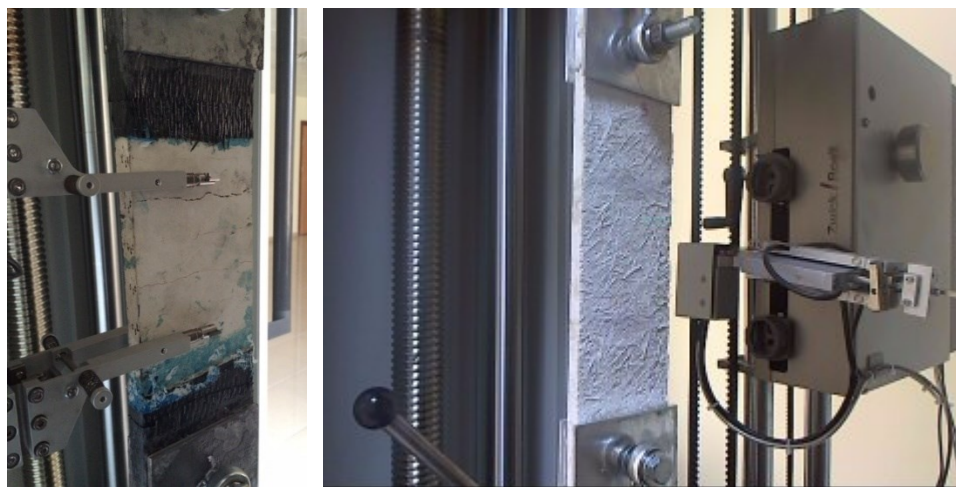
Figure 2.8: Extensometer and test set up of tensile specimens.

2.1.4.3 Test procedure of tensile test specimens

For tensile test specimens 500 N pre-load was applied. The loading was displacement controlled and the rate of loading was 0.2mm/min. As mentioned before, the gauge length for external extensometer was 100 mm at mid-height of the specimens.

2.1.4.4 Test results of tensile test specimens

In this section, tensile stress-strain diagrams related to each tensile test are presented. As it can be seen in a number of tests, the specimens could not reach the ultimate stress and failed early because of the rupture of specimens from the grips. In cases of a limited number of tests, after reaching the ultimate strength of the specimen, the extensometer read shortening because of the formation of cracks outside the measured span. As mentioned before to prevent this unwanted behavior a number of tensile test

specimens, which remained after pilot tests, were wrapped with CFRP in the top and bottom, where the tensile stress concentrated in that parts. Because of the mentioned reason, we use only the results of tensile tests for tensile test specimens, which CFRP used in them. In Figure 2.9 to 2.12 the tensile stress-strain diagrams of all tensile test include the tensile test specimens which were not wrapped with CFRP also presented.

In Figure 2.13 comparison of all tensile stress-strain diagrams of tensile test specimens which were wrapped with CFRP, and used in analytical study illustrated. It should be noticed that the thickness of tensile test specimens are not the same with jacket thickness consequently, the results obtained from tensile test specimens would not represent the exact tensile behavior of jackets. Further study is needed for this par.
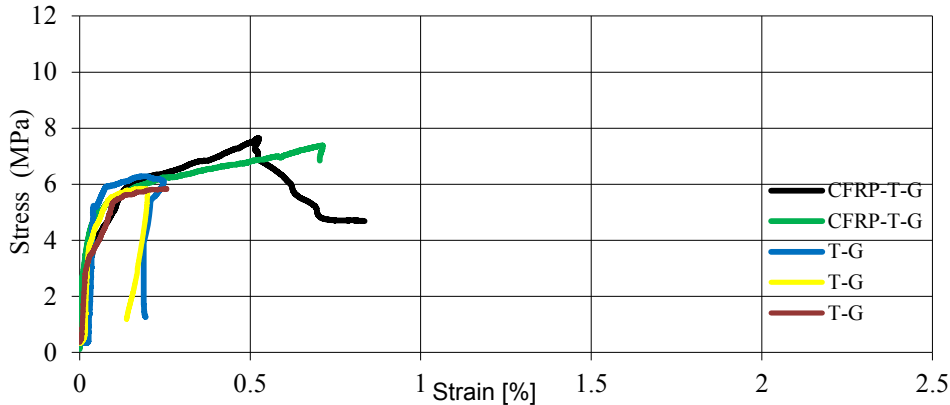
Figure 2.9: Stress-strain diagram related to tensile test specimens with only GFRC.
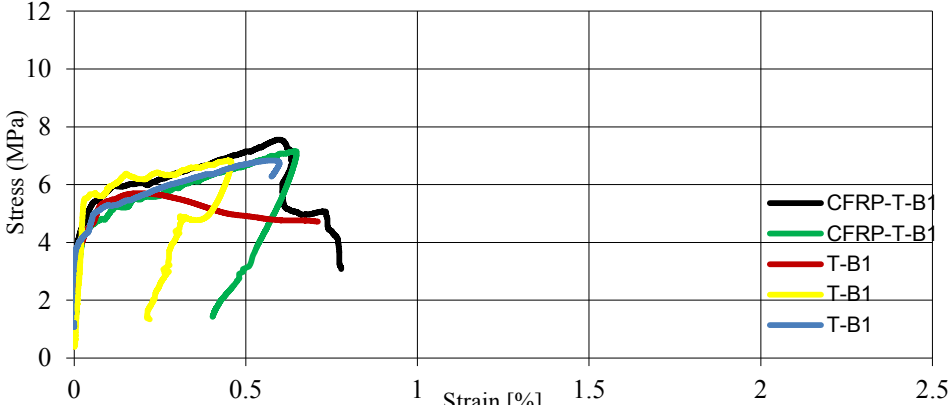
Figure 2.10: Stress-strain diagram related to tensile test specimens with GFRC+1layer of basalt.

20
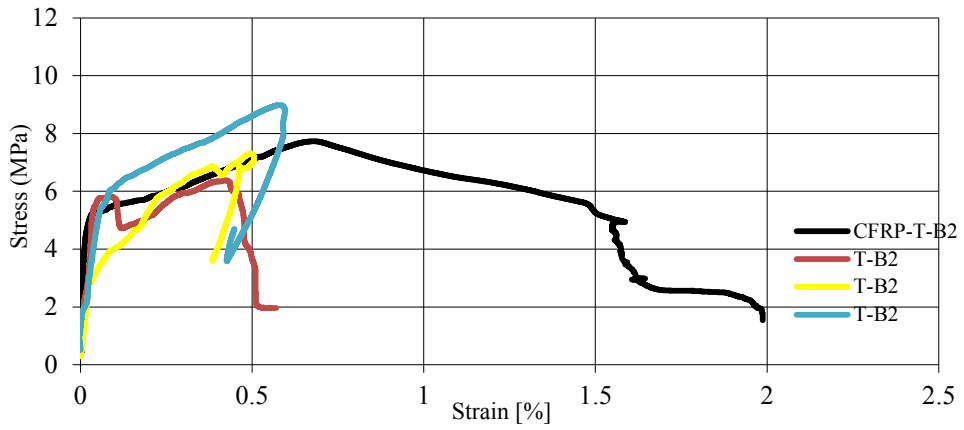
Figure 2.11: Stress-strain diagram related to tensile tests specimens with GFRC+2layer of basalt.
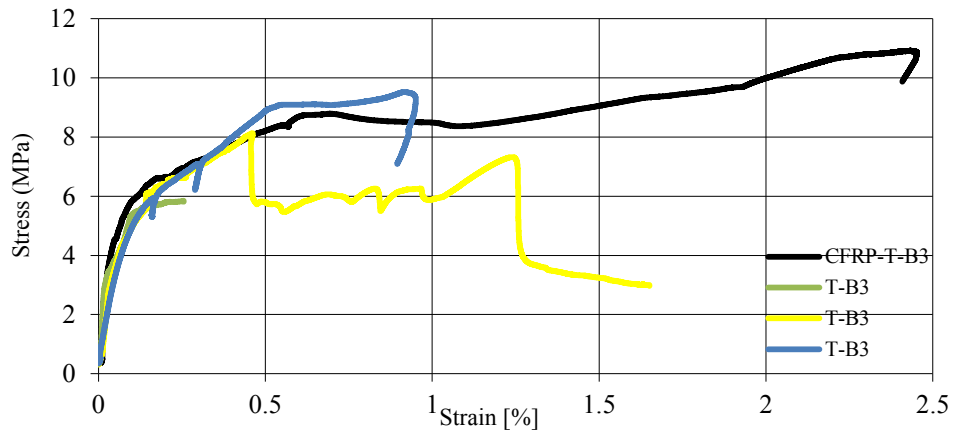
Figure 2.12: Stress-strain diagram related to tensile tests specimens with GFRC+3layer of basalt.
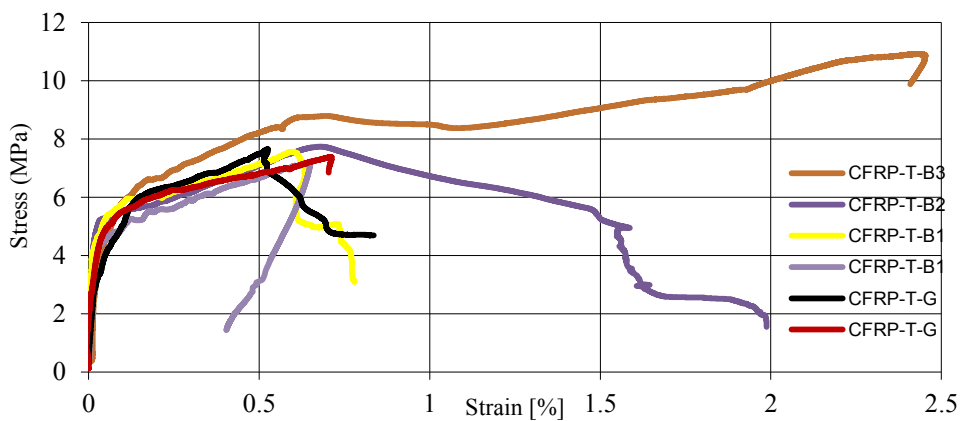
Figure 2.13: Comparison of all stress-strain curves for CFRP wrapped tensile test specimens.

As it is evident in the stress-strain diagrams of tensile test specimens from Figure 2.13, the behavior of specimens with only GFRC, specimens with GFRC+1 layer of basalt and, GFRC+2 layers of basalt is quite similar, and the ultimate tensile strength is approximately 7 MPa. However, the ultimate stress value for specimens with GFRC+3 layers of basalt is 10.82 MPa. For the tensile specimens with details of GFRC,GFRC+1layer of basalt and GFRC+2 layers of basalt the ultimate strain is approximately 0.007 while for the specimen with GFRC+3layers of basalt the ultimate strain is 0.024.

2.2 Construction of Specimens

The plywood molds were designed and prepared separately for each type of the column specimens, and were sprayed with a mound release oil before casting (as shown in Figure 2.4 b-c). The same low-strength (less than 10 MPa) ready-mix concrete was used in casting all the specimens, including columns and standard cylindrical specimens used to monitor the concrete strength. All the specimens were thoroughly vibrated using rod vibrators. At the same time, twenty 150 x 300 mm cylinder specimens were also cast to monitor concrete strength (Fig. 2.14.a). 7 days after curing, the molds were removed and all specimens were checked for irregularities. All the cylinders were kept with the column specimens at the outside temperature for 28 days before the application of retrofitting. The concrete column specimens, one week after retrofitting, were carefully moved from Duzce to Istanbul Technical University (ITU); and, cured in normal air conditions (kept at the outside temperature) until they were tested.

2.3 Application of Retrofitting System

Four series of concrete column specimens with circular (200 mm diameter), square (200x200 mm), rectangular (200x300 mm) and rectangular (200x400 mm) cross-sections, and 500 mm height were cast using the same low-strength (less than 10 MPa) ready-mix concrete. In the external jacketing of all series of column specimens, five different designs were used; the column specimens without wrapping (control specimens), specimens jacketed only with GFRC, specimens wrapped with one, two or three layers of basalt mesh embedded in GFRC. Before the application of retrofitting, the corners of the square and rectangular cross-section type specimens

were rounded to a radius of 30 mm and surfaces were prepared for jacketing (cleaned from dust and watered). Firstly, GFRC were sprayed directly to concrete columns surface with about 5 mm thickness and then basalt textile was wrapped around specimens (Figure 2.15 a-b). Additionally, a hard type of roller was used to make sure the basalt was completely embedded in GFRC and there were no air spaces inside the jacket. If specimens had more than one ply reinforcement, basalt mesh were continuously wrapped but at least 5 mm thick GFRC layer were consisted between each basalt mesh plies. In addition, a minimum 120 mm overlap length was provided at the end of the basalt mesh wrapping to prevent debonding failure of textile. At the end, GFRC was sprayed to the specimen for the last layer of jacket and GFRC surface was shaped by using a hand trowel.

Approximately, a 20 mm gap was left at the top and bottom of all jackets for considering only the confinement effects on strength and ductility characteristics of column specimens.

(a)

(b)

(c)

Figure 2.14: Casting of specimens: (a) all the column and standard cylinder specimens after casting. (b) Molds of columns with circular cross-section. (c) Molds of columns with square cross-section.

(a)

(b)

(c)

(d)

(e)

(f)

Figure 2.15: Application of jacketing: (a) spraying up the GFRC and (b-c-e) wrapping of basalt mesh. (d-f) Columns after confinement.

Figure 2.16: Columns with rectangular cross-section after confinement.

2.4 Test Setup

All specimens were constructed at the fibrobeton yapi elemanlar san.inş.tic.ltd.şti corporation in Duzce and were tested at Istanbul Technical University and Balikesir University material laboratories. The specimens were tested under monotonic compressive loads by using an Amsler universal testing machine with the capacity of 5000 kN (Figure 2.17). Lateral strains were measured at mid height by four surface strain gauges with the gauge length of 60 mm for a number of the specimens. Four vertical strain gauges were also used on two specimens with circular cross-section around the perimeter to lighten the axial strain distribution on the jacket surface. The locations of strain gauges on the specimens with circular cross-section, square cross-section, and rectangular cross-section specimens were at the mid-height of the specimens (as shown in Fig 2.17). For the measurement of the average axial strains, two different gauge lengths were used. Displacement transducers (LVDTs) were used for circular cross-section specimens, four transducers with 250 mm gauge length and four transducers with 500 mm gauge length were used; whereas, in square cross-section specimens, and rectangular cross-section specimens only four transducers with 500 mm gauge length were used (fig 2.17). For this study, data measured from 500 mm gauge length LVDTs was used as the data mesured from 250 mm gage length LVDTs were not appropriate due to; 1) by making holes in the column specimens we apply handicaps; consequently, the very first crack occurs just near the holes and it let the anchorages used for placing LVDTs to move or rotate. When the anchorages rotate or move, the displacement transducers could not measure the real responsive behavior of the specimen. 2) the behavior of the jacket and concrete are not the same so they don't show the same displacement. It led the anchorages to move or rotate while

providing a bigger hole in the jacket to prevent this problem, but it did not work. The measurements from the horizontal strain gauges provided us with a minimum value of jacket enlargement. Because after formation of cracks in the jacket strain gauges start to read shortening due to the fact that by concentration of strains near cracks while the cracks are becoming bigger other strain gages read shortening on the jacket. Before testing, loading caps was provided for all the specimens in order to make sure that the strains distributed uniformly on the specimens. Moreover, grease oil was used to minimize the friction between the loading plates and the specimens. All axial strains that are reported in this thesis, were obtained by the measurements of displacement transducers with the gauge length of 500 mm, otherwise mentioned.

(a)   (b)

(c)   (d)
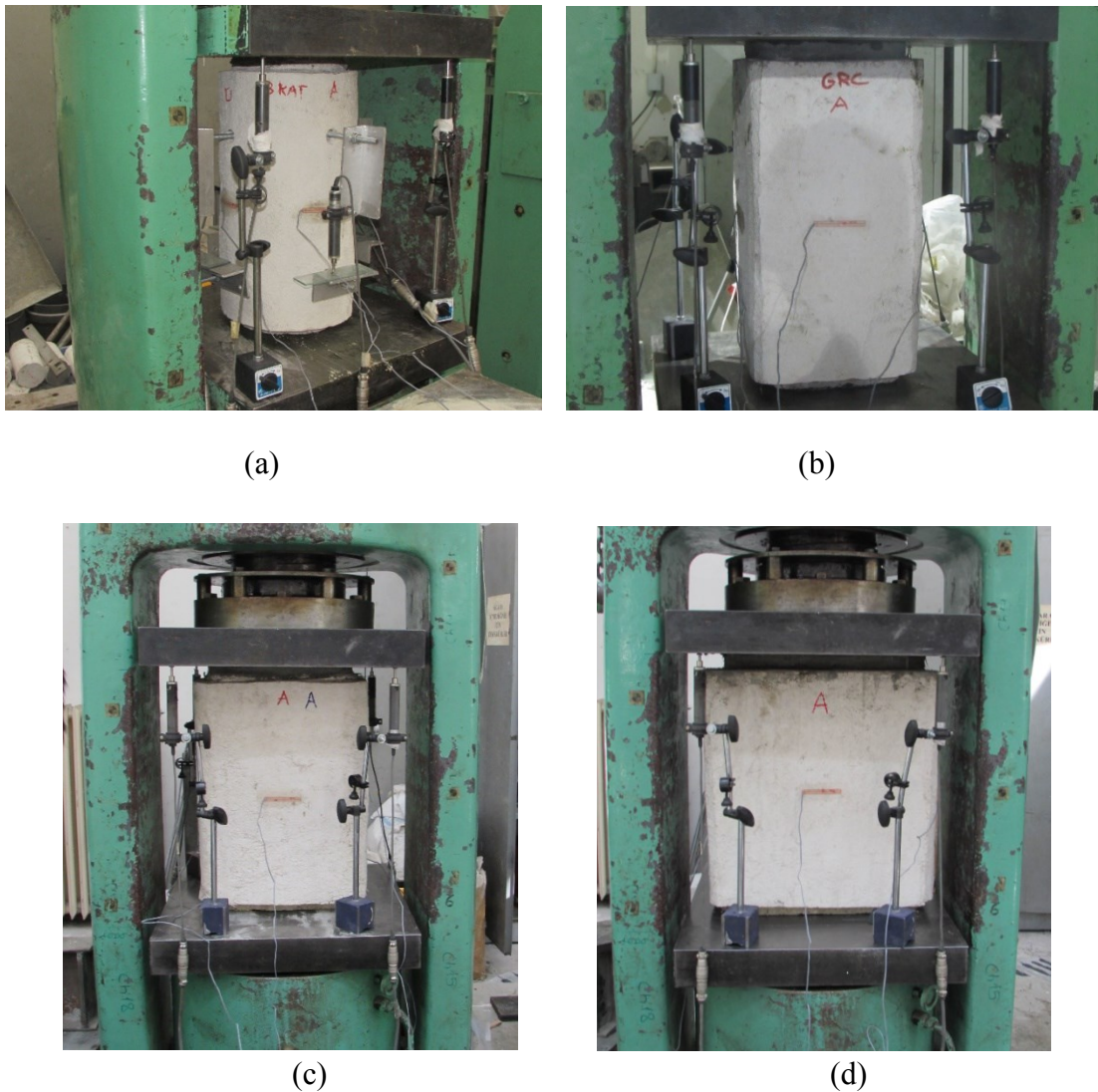
Figure 2.17: Test setup :(a) Test setup for columns with circular cross-section. (b) Test setup for columns with square cross-section. (c) and (d) Test setup for columns with rectangular cross-section.

2.5 Test Procedure

For the entire specimens, the first step was applying the pre-load in order to make sure that there is not any void between the loading cap and specimens to provide the uniform distribution of the strains. Then, all the channels going to the data logger were checked and the spans of gauge length for each transducer measured, and the constant values were entered to the software. After that, loading started with the rate of 100 kg per 3 seconds and remained the same until the end of each test. The difficulty faced here was the lack of place to use load cell; therefore, reading the loads was done manually. During the test, crack patterns were observed.

2.6 Identification of Column Specimens

Specimens in series A are given the notation C-XN-M where C stands for circular section type, X denotes the type of jacket (C for the unjacketed specimens (control), G for jacketing only with GFRC, T for textile reinforcement mortars). N denotes the number of basalt layer and M shows the number of specimens for each type. Specimens in series B are given the notation S-XN-M where S stands for square section type, X denotes the type of jacket as in series A. N denotes the number of basalt layer and M shows the number of specimens for each type. Specimens in series C are given the notation RW-XN-M where R stands for rectangular section type. W is ratio of length over width. X denotes the type of jacket as in series A. N denotes the number of basalt layer and M shows the number of specimens for each type.

Table 2.2: Detail of columns with circular (D=200mm) cross-section.

Name of specimen	Jacket detail	Mortar glass fiber % by weight of mortar mixture	Jacket thickness mm
C-C-1	-	-	-
C-C-2	-	-	-
C-G-1	Only GFRC	3.5	25
C-G-2	Only GFRC	3.5	25
C-T1-1	GFRC+1 layer basalt	3.5	25
C-T1-2	GFRC+1 layer basalt	3.5	25
C-T2	GFRC+2 layer basalt	3.5	25
C-T3	GFRC+3 layer basalt	3.5	25

Table 2.3: Detail of columns with square (200x200mm) cross-section.

Name of specimen	Jacket detail	Mortar glass fiber % by weight of mortar mixture	Jacket thickness mm
S-C-1	-	-	-
S-C-2	-	-	-
S-G-1	Only GFRC	3.5	25
S-G-2	Only GFRC	3.5	25
S-T1-1	GFRC+1 layer basalt	3.5	25
S-T1-2	GFRC+1 layer basalt	3.5	25
S-T2	GFRC+2 layer basalt	3.5	25
S-T3	GFRC+3 layer basalt	3.5	25

Table 2.4: Detail of columns with rectangular (200x300mm) cross-section.

Name of specimen	Jacket detail	Mortar glass fiber % by weight of mortar mixture	Jacket thickness mm
R1.5-C-1	-	-	-
R1.5-C-2	-	-	-
R1.5-G-1	Only GFRC	3.5	25
R1.5-G-2	Only GFRC	3.5	25
R1.5-T1	GFRC+1 layer basalt	3.5	25
R1.5-T2	GFRC+2 layer basalt	3.5	25
R1.5-T3-1	GFRC+3 layer basalt	3.5	25
R1.5-T3-2	GFRC+3 layer basalt	3.5	25

Table 2.5: Detail of rectangular (200x400mm) cross-section specimens.

Name of specimen	Jacket detail	Mortar glass fiber% by weight of mortar mixture	Jacket thickness mm
R2-C-1	-	-	-
R2-C-2	-	-	-
R2-G-1	Only GFRC	3.5	25
R2-G-2	Only GFRC	3.5	25

.

3. TEST RESULTS

Observations, which are made during column tests, are presented in this chapter. The failure process was documented for column specimens including cracking patterns.

3.1 General Behavior and Test Observations of Column Specimens

In Figure 3.1, an overall structural behavior of column specimens confined with basalt-reinforced GFRC, under concentric compression test is presented with related crack patterns.

Generally, the first crack on jacket occurs just before the specimen reaches its ultimate stress where GFRC is effective in this region. After formation of cracks on the jacket, the glass fibers lose their effectiveness on the behavior of externally jacketed specimens, and as the cracks grow the behavior of specimen controlled by basalt mesh. Consequently, deformation capacity of retrofitted column specimens after formation of crack in GFRC is governed by the basalt mesh within the GFRC matrix. The formation of first crack for circular specimens happened in the stress value of almost 12 MPa and strain value around 0.002. For columns with square cross-section, the first crack was formed in the stress value of approximately 13 MPa and strain value of 0.003. For columns with rectangular (200x300 mm) cross-section, the formation of firs crack was at the stress value of nearly10.53 Mpa and strain value of 0.0016. For columns with rectangular cross-section (200x400 mm), the formation of first crack was at the stress value of 10 MPa and the strain value of 0.002.

All stress-strain curves of confined concrete columns can be characterized by an ascending almost linear branch, followed by nonlinear climbing one up to ultimate stress. Then a nearly smooth linear branch followed by nonlinear descending one up to a sudden drop at a point where the jacket, fractured either due to the split of GFRC (if there is no basalt in jacket) or rupture of basalt mesh. More important the ultimate strain for the specimens that fails due to rupture of basalt mesh are very high in

comparison with the specimens, which fails by splitting of the GFRC. Failure mechanism directly related to physical and mechanical characteristics of textile in the GFRC jacket.
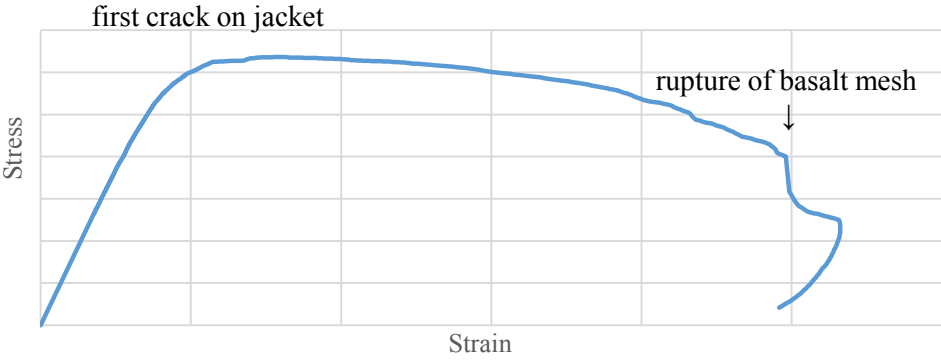
Figure 3.1: Overall behavior of basalt-reinforced GFRC confined column specimens

Stress-strain diagrams, test photos, f_{cc}/f_{co}, and $\varepsilon_{cu85}/\varepsilon_{c085}$ values for all column specimens are presented in appendix A.

3.2. Evaluation of Test Results

The details of all column specimens are given in Table 3.1.

In this part, axial stress average axial strain diagrams of concrete columns tested under concentric compression loads are presented. Ultimate compressive strengths (f_{cc}) and corresponding axial strains ($\varepsilon_{cu.}$) are calculated and presented in tables below. Additionally, compression strength enhancement ratios f_{cc}/f_{c0} (peak stress of confined concrete over peak stress of unconfined concrete) are calculated and presented in tables below. Deformability factor $\varepsilon_{cu85}/\varepsilon_{c085}$ (ε_{cu85} is the strain, related to the point that the stress drops by 15% and ε_{c085} is the strain, related to the point that the stress drops by 15% of unconfined concrete column specimen), calculated and presented in tables below. Characteristic points of column specimens illustrated in Figure 3.2.
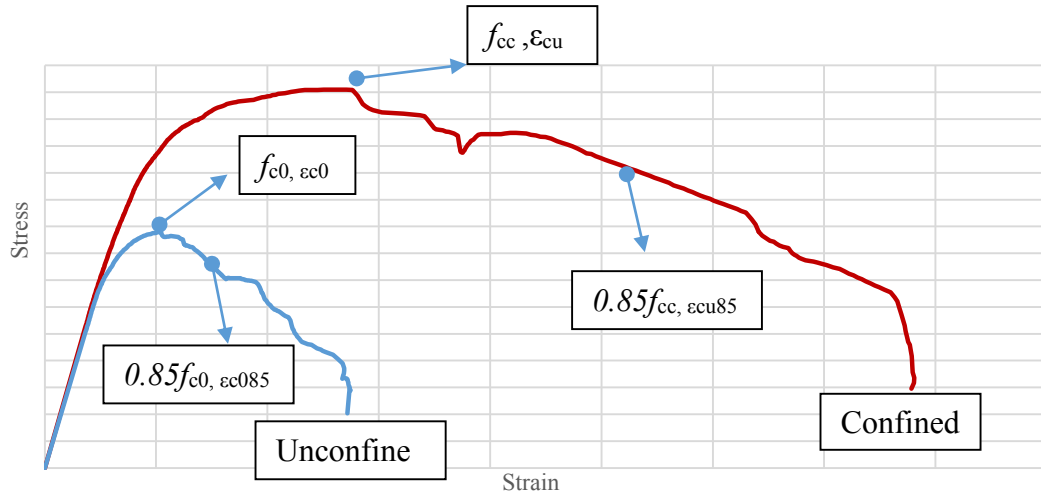
Figure 3.2: Characteristic points for column specimens.

Table 3.1: Details of column specimens.

Name of specimen	Dimension of cross-section (mm)	Height (mm)	Jacket detail	Mortar glass fiber % by weight of mortar mixture	Jacket thickness (mm)
C-C-1	D=200	500	-	-	-
C-C-2	D=200	500	-	-	-
C-G-1	D=200	500	Only GFRC	3.5	25
C-G-2	D=200	500	Only GFRC	3.5	25
C-T1-1	D=200	500	GFRC+1 layer basalt	3.5	25
C-T1-2	D=200	500	GFRC+1 layer basalt	3.5	25
C-T2	D=200	500	GFRC+2 layer basalt	3.5	25
C-T3	D=200	500	GFRC+3 layer basalt	3.5	25
S-C-1	200x200	500	-	-	-
S-C-2	200x200	500	-	-	-
S-G-1	200x200	500	Only GFRC	3.5	25
S-G-2	200x200	500	Only GFRC	3.5	25
S-T1-1	200x200	500	GFRC+1 layer basalt	3.5	25
S-T1-2	200x200	500	GFRC+1 layer basalt	3.5	25
S-T2	200x200	500	GFRC+2 layer basalt	3.5	25
S-T3	200x200	500	GFRC+3 layer basalt	3.5	25
R1.5-C-1	200x300	500	-	-	-
R1.5-C-2	200x300	500	-	-	-
R1.5-G-1	200x300	500	Only GFRC	3.5	25
R1.5-G-2	200x300	500	Only GFRC	3.5	25
R1.5-T1	200x300	500	GFRC+1 layer basalt	3.5	25
R1.5-T2	200x300	500	GFRC+2 layer basalt	3.5	25
R1.5-T3-1	200x300	500	GFRC+3 layer basalt	3.5	25
R1.5-T3-2	200x300	500	GFRC+3 layer basalt	3.5	25
R2-C-1	200x400	500	-	-	-
R2-C-2	200x400	500	-	-	-
R2-G-1	200x400	500	Only GFRC	3.5	25
R2-G-2	200x400	500	Only GFRC	3.5	25

Ductility ratio defines as $\varepsilon_{cu85}/\varepsilon_{c0}$ where ε_{c0} is assumed 0.002 for each column specimens. The values for ductility ratios are given in Tables 3.2 to 3.4.

3.2.1 Columns with circular cross-section

Axial stress average axial strain diagrams of column specimens with circular cross-section are given in Figure 3.3.

For columns with circular cross-section, the value of f_{c0} (average ultimate stress of two control specimen) is 8.80 MPa and ε_{c0} (strain related to average ultimate stress of control specimens) is 0.36 % while ε_{c085} is 0.53%.

The formation of cracks on GFRC began when the column specimen approximately reaches to its ultimate strength. These cracks, formed just near the provided holes for placing the LVDTs with gage length of 250 mm. By formation of cracks on jacket, basalt mesh engaged and the deformation of column specimens was controlled by basalt mesh mechanical characteristics. Then the column reached to its ultimate strength while the cracks get wider, we face a sudden drop in axial stress axial strain curves for column specimens that have basalt mesh embedded in GFRC because of rupture of basalt mesh.
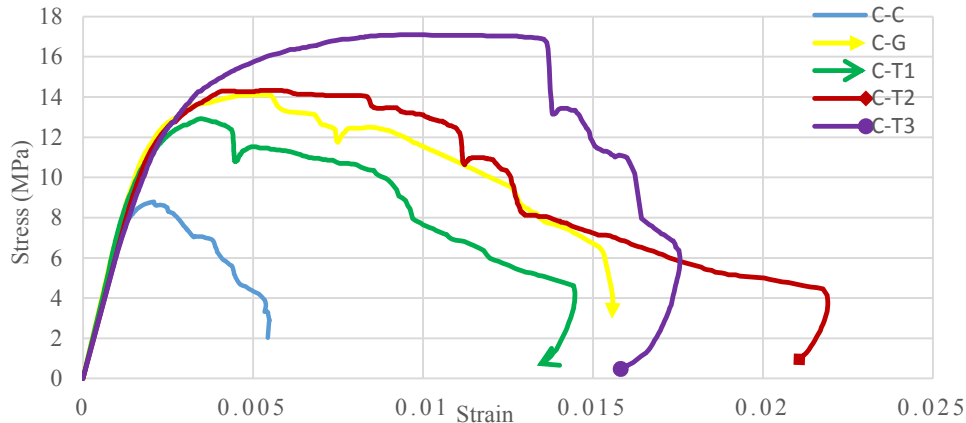
Figure 3.3: Stress-strain curves for column specimens with circular cross-section.

As it can be seen from Figure 3.3 and Table 3.2, in column specimens with circular cross-section confined only with GFRC, the gain in compressive strength is 53%, while the gain in deformability capacity is 80%. The gain in compressive strength, for circular column specimens GFRC+1, GFRC+2 and GFRC+3 are 47%, 63% and 94% respectively. The enhancement in deformability, are 27%, 109% and 159%.

Table 3.2: Strength and deformability characteristics of columns with circular cross-section.

Label	Jacket detail	f_{cc} (MPa)	$\varepsilon_{cu}\%$	$\varepsilon_{cu85}\%$	f_{cc}/f_{c0}	$\varepsilon_{cu85}/\varepsilon_{c085}$	$\varepsilon_{cu85}/\varepsilon_{c0}$
C-C-1	Control	9.58	0.17	0.25	1.09	1.46	1.25
C-C-2	Control	8.53	0.23	0.35	0.97	1.16	1.75
C-C(average)	**Control**	**8.80**	**0.21**	**0.30**	**1.00**	**1.00**	**1.50**
C-G-1	Only GFRC	13.50	0.70	0.95	1.53	1.80	4.76
C-G-2	Only GFRC	14.71	0.59	0.92	1.67	1.74	4.60
C-G(average)	**Only GFRC**	**14.10**	**0.54**	**0.95**	**1.60**	**1.79**	**4.74**
C-T1	GFRC+1 textile layer	12.92	0.35	0.67	1.47	1.27	3.36
C-T2	GFRC+2 textile layer	14.32	0.58	1.11	1.63	2.09	5.54
C-T3	GFRC+3 textile layer	17.09	1.00	1.37	1.94	2.59	6.87

The compression strength enhancement ratios f_{cc}/f_{c0} are calculated for circular column specimens (Table 3.2). The value of f_{cc}/f_{c0} is quiet similar for circular column specimens GFRC+1, GFRC+2 and GFRC+3 while for GFRC+3 is higher and it shows the gain in ultimate strength of confined column specimens. Deformability enhancement ratio, $\varepsilon_{cu85}/\varepsilon_{c085}$, also calculated for columns with circular cross-section (Table 3.2) which shows the gain in ultimate strain of confined specimens in comparison with the control specimen. The maximum enhancement is for GFRC+3 and the $\varepsilon_{cu85}/\varepsilon_{c085}$ value is 2.59.

As mentioned before ultimate tensile strength of jacket for GFRC, GFRC+1 ,GFRC+2 specimens are approximately the same and the value is 7 MPa this is the reason why the GFRC, GFRC+1 and, GFRC+2 specimens have quiet same axial behavior.

 From the Figure 3.2 it seems that, the behavior under axial load, of column jacketed with only GFRC is better than GFRC+1 layer of basalt, in case of ultimate strength and ultimate strain. This is because while embedding the basalt mesh into GFRC, some inevitable application errors were occurred such as air bubbles remained between the basalt mesh and GFRC and, basalt mesh could not well stretched during the confinement procedure.

3.2.2 Columns with square cross-section

Axial stress average axial strain diagrams of column specimens with square cross-section are given in Figure 3.4.

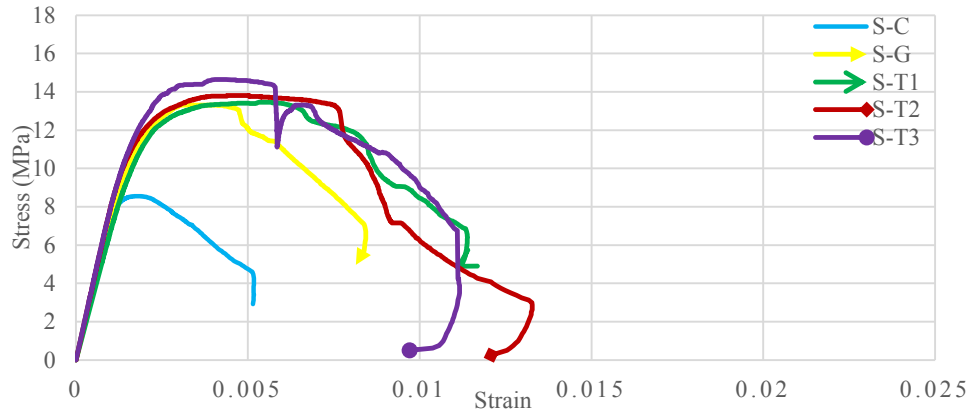**Figure 3.4:** Stress-strain curves for column specimens with square cross-section.

For columns with square cross-section, the value of f_{c0} is 8.55 MPa and ε_{c0} is 0.37 % while ε_{c085} is 0.6%.

Table 3.3: Strength and deformability characteristics of columns with square cross-section.

Label	Jacket detail	f_{cc} (MPa)	ε_{cu}%	ε_{cu85}%	f_{cc}/f_{c0}	$\varepsilon_{cu85}/\varepsilon_{c085}$	$\varepsilon_{cu85}/\varepsilon_{c0}$
S-C-1	Control	8.65	0.43	0.59	1.01	0.98	1.51
S-C-2	Control	8.45	0.42	0.61	0.99	0.98	1.51
S-C(average)	**Control**	**8.550**	**0.37**	**0.6**	**1.00**	**1.00**	**1.55**
S-G-1	Only GFRC	14.93	0.42	0.59	1.75	1.92	2.95
S-G-2	Only GFRC	13.13	0.38	0.54	1.54	1.75	2.69
S-G(average)	**Only GFRC**	**13.31**	**0.39**	**0.59**	**1.56**	**1.92**	**2.95**
S-T1-1	GFRC+1 textile layer	13.18	0.52	0.80	1.54	2.61	4.01
S-T1-2	GFRC+1 textile layer	13.75	0.57	0.88	1.61	2.86	4.39
S-T1(average)	**GFRC+1 textile layer**	**13.45**	**0.57**	**0.84**	**1.57**	**2.74**	**4.20**
S-T2	GFRC+2 textile layer	13.80	0.50	0.78	1.61	2.55	3.90
S-T3	GFRC+3 textile layer	14.65	0.61	0.99	1.71	3.22	4.94

The formation of cracks on GFRC began when the column specimen approximately reaches to its ultimate strength this cracks. By formation of cracks on jacket, basalt mesh engaged and the deformation ratio of column specimens control by basalt mesh's mechanical characteristics. Then the column reaches to its ultimate strength while the cracks get wider, we face a sudden drop in axial stress axial strain curves for column specimens that, have basalt mesh embedded in GFRC, because of rupture of basalt mesh.

From Figure 3.4 and Table 3.3, in column specimens with square cross-section, which confined only with GFRC, the gain in compressive strength is 56% while

deformability capacity is not enhanced. From Figure 3.3 and Table 3.3 the gain of compressive strength, for column specimens with jacketing type of GFRC+1, GFRC+2 and GFRC+3 are 57%, 61% and 71% respectively. The enhancements in deformability are 40%, 30% and 65%.

The compression strength enhancement ratios f_{cc}/f_{c0} are calculated for square column specimens (Table 3.3). The value of f_{cc}/f_{c0} is quiet similar for square column specimens GFRC+1, GFRC+2 and GFRC+3 while for GFRC+3 is higher and it shows the gain in ultimate strength of confined column specimens. Deformability enhancement ratio, $\varepsilon_{cu85}/\varepsilon_{c085}$, also calculated for columns with square cross-section (Table 3.3) which shows the gain in ultimate strain of confined specimens in comparison with the control specimen. The maximum enhancement is for GFRC+3 and the $\varepsilon_{cu85}/\varepsilon_{c085}$ value is 1.65.

As mentioned before ultimate tensile strength of jacket for GFRC, GFRC+1 ,GFRC+2 specimens are approximately the same and the value is 7 MPa this is the reason why the GFRC, GFRC+1 and, GFRC+2 specimens have quite similar axial behavior.

3.2.3 Columns with rectangular (200x300 mm) cross-section

Axial stress average axial strain diagrams of column specimens with rectangular (200x300 mm) cross-section are given in Figure3.5.
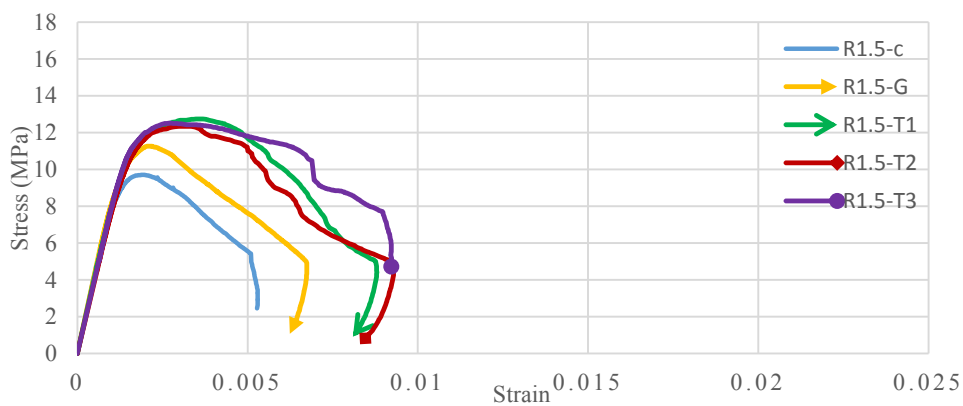

Figure 3.5: Stress-strain curves for column specimens with rectangular (200x300 mm) cross-section.

For columns with rectangular (200x300 mm) cross-section the value of f_{c0} is 9.7 MPa and ε_{c0} is 0.28 % while ε_{c085} is 0.47%.

Table 3.4: Strength and deformability factor of columns with rectangular (200x300 mm) cross-section.

Label	Jacket detail	f_{cc} (MPa)	ε_{cu} %	ε_{cu85} %	f_{cc}/f_{c0}	$\varepsilon_{cu85}/\varepsilon_{c085}$	$\varepsilon_{cu85}/\varepsilon_{c0}$
R1.5-C-1	Control	9.77	0.24	0.43	1.01	0.90	1.50
R1.5-C-2	Control	9.63	0.32	0.5	0.99	1.05	1.75
R1.5-C(average)	**Control**	**9.7**	**0.28**	**0.47**	**1.00**	**0.99**	**1.65**
R1.5-G-1	Only GFRC	11.27	0.22	0.36	1.16	1.08	1.80
R1.5-T1	GFRC+1 textile layer	12.73	0.37	0.56	1.31	1.68	2.80
R1.5-T2	GFRC+2 textile layer	12.33	0.33	0.52	1.27	1.56	2.60
R1.5-T3-1	GFRC+3 textile layer	12.5	0.30	0.62	1.29	1.86	3.10
R1.5-T3-2	GFRC+3 textile layer	12.73	0.32	0.79	1.31	2.37	3.95
R1.5-T3(average)	**GFRC+3 textile layer**	**12.51**	**0.30**	**0.67**	**1.29**	**2.01**	**3.35**

The formation of cracks on GFRC began when the column specimen approximately reaches to its ultimate strength this cracks. By formation of cracks on jacket, basalt mesh engaged and the deformation ratio of column specimens control by basalt mesh's mechanical characteristics. Then the column reaches to its ultimate strength while the cracks get wider, we face a sudden drop in axial stress axial strain curves for column specimens that, have basalt mesh embedded in GFRC, because of rupture of basalt mesh.

From Figure 3.4 and Table 3.4, in column specimens with square cross-section, which confined only with GFRC, the gain in compressive strength is 16% while deformability capacity is reduced 23%. From Figure 3.5 and Table 3.4 the gain of compressive strength ratio, for column specimens with jacketing type of GFRC+1, GFRC+2 and GFRC+3 are 31%, 27% and 29% respectively. The enhancement in deformability, are 19%, 11% and 43%.

The compression strength enhancement ratios f_{cc}/f_{c0} are calculated for square column specimens (Table 3.4). The value of f_{cc}/f_{c0} is quiet similar for square column specimens GFRC+1, GFRC+2 and GFRC+3 while for GFRC+3 is higher and it shows the gain in ultimate strength of confined column specimens. Deformability enhancement ratio, $\varepsilon_{cu85}/\varepsilon_{c085}$, also calculated for columns with rectangular (200x300 mm) cross-section (Table 3.4) which shows the gain in ultimate strain of confined specimens in comparison with the control specimen. The maximum enhancement is for GFRC+3 and the $\varepsilon_{cu85}/\varepsilon_{c085}$ value is 1.43.

3.2.4 Columns with rectangular (200x400 mm) cross-section

Axial stress average axial strain diagrams of column specimens with rectangular (200x400 mm) cross-section are given in Figure 3.6.

For columns with rectangular (200x400 mm) cross-section, the value of f_{c0} is 9.8 MPa and ε_{c0} is 0.45 % while ε_{c085} is 0.64%.
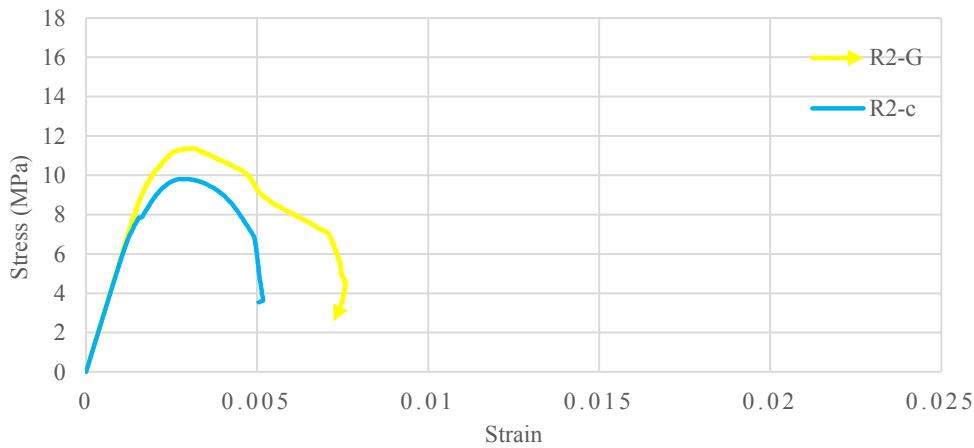

Figure 3.6: Stress-strain curves for columns with rectangular (200x400 mm) cross-section.

Table 3.5: Strength and deformability factor of columns with rectangular (200x400 mm) cross-section.

Label	Jacket detail	f_{cc} (MPa)	ε_{cu} %	ε_{cu85} %	f_{cc}/f_{c0}	$\varepsilon_{cu85}/\varepsilon_{c085}$	$\varepsilon_{cu85}/\varepsilon_{c0}$
R2-C-1	Control	10.38	0.30	0.47	1.06	1.09	2.35
R2-C-2	Control	9.66	0.34	0.45	0.99	1.03	2.25
R2-C	**Control(average)**	**9.80**	**0.30**	**0.43**	**1.00**	**1.00**	**2.15**
R2-G-1	Only GFRC	11.72	0.33	0.45	1.20	1.03	2.15
R2-G-2	Only GFRC	11.19	0.32	0.46	1.40	1.07	2.30
R2-G	**Only GFRC(average)**	**11.36**	**0.32**	**0.49**	**1.16**	**1.14**	**2.45**

As it can be seen from Figure 3.6 and Table 3.5, in column specimens with rectangular (200x400 mm) cross-section confined only with GFRC, the gain in compressive strength is 16% while deformability capacity could not enhanced.

From this part, it is concluded that the specimens jacketed with GFRC, GFRC+1 layer of basalt and GFRC+2 layers of basalt almost have the same behavior under concentric compression loads attributed to the fact that the effectiveness of jacketing is directly

The comparison of the deformability and compressive strength enhancement factors shows that as the cross sectional aspect ratios of columns increase, the effectiveness of the confinement decreases in term of gain in compressive strength and increase in deformability capacity. Nevertheless, for circular sections as well as rectangular sections with cross-sectional aspect ratios up to 1.5, the external basalt reinforced GFRC jacket positively effecting to the axial behavior.

3.3 Comparison of Energy Absorption Capacities

In this part, the effect of confinement on energy dissipation capacity of columns are presented. The diagrams in this part are prepared in the way that the vertical axis illustrates the ratio of area under stress-strain curves for each column over the area of control specimen's stress-strain diagram up to the strain value of 0.002; therefore, it is unitless (Figure 3.6). Energy dissipation ratio defined as Equation 3.1.
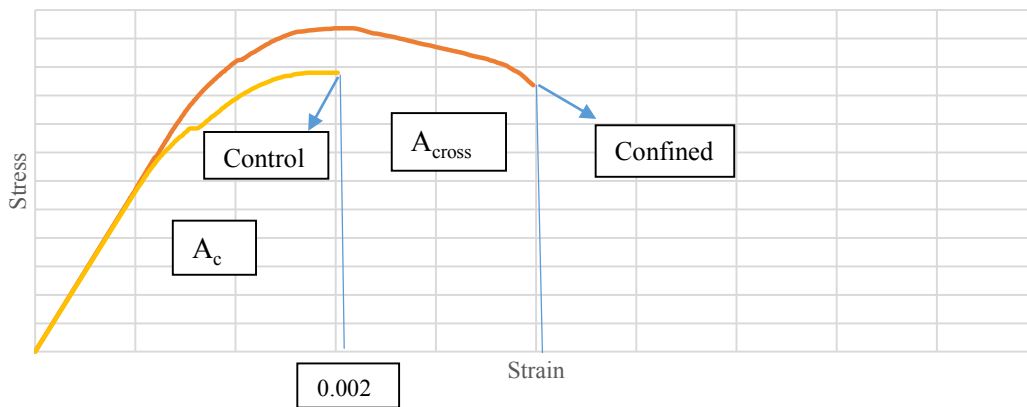

Figure 3.7: Definition of energy dissipation ratio.

$$Energy\ dissipation\ ratio = \frac{A_{cross}}{A_c} \qquad (3.1)$$

Horizontal axis shows the strain values starts from 0.002 up to the ultimate strain for the specimen jacketed with GFRC+3 layers of basalt which has the greater strain value in its own series. For the columns with rectangular cross-section with the cross-sectional aspect ratio of 2, the same method is applied for specimens jacketed only with GFRC and control specimens. It should be noticed that, for calculation of areas under stress-strain diagrams, the average stress-strain diagrams were used. In figures 3.7 to 3.10 energy dissipation ratios in different strains are illustrated for concrete column specimens.

According to Figure 3.7, in the strain value of 0.006, the control specimens energy absorption ratio is 3.85; while, for specimens jacketed with only GFRC this ratio is 8. For specimens jacketed with GFRC+1,2, and 3 layers of basalt, the energy absorption ratios are 6.81,7.41 and 7.8 respectively. The maximum energy absorption ratio calculated for columns up to their 15 % loss of ultimate strength. For columns with circular cross-section, the maximum energy absorption ratios are presented in Table 3.6. The maximum energy absorption ratios for columns with square, rectangular (200x300 mm) and rectangular (200x400 mm) cross-sections are presented in Table 4.6, Table 4.7 and Table 4.8, respectively.
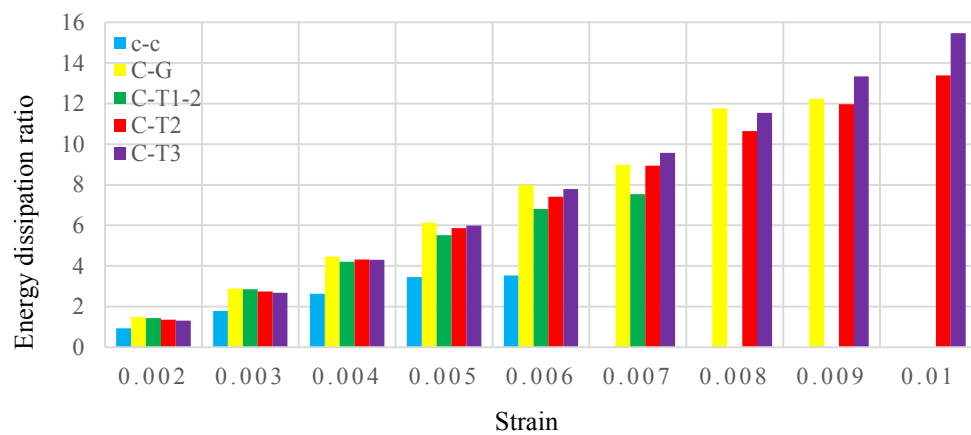

Figure 3.8: The effect of basalt GFRC jacketed on the area under stress-strain diagrams of columns with circular cross-section.
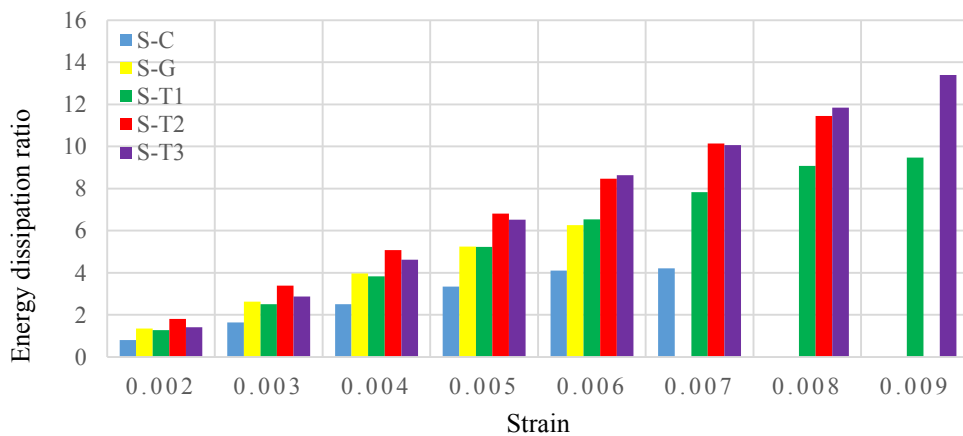

Figure 3.9: The effect of basalt GFRC jacketed on the area under stress-strain diagrams of columns with square cross-section.
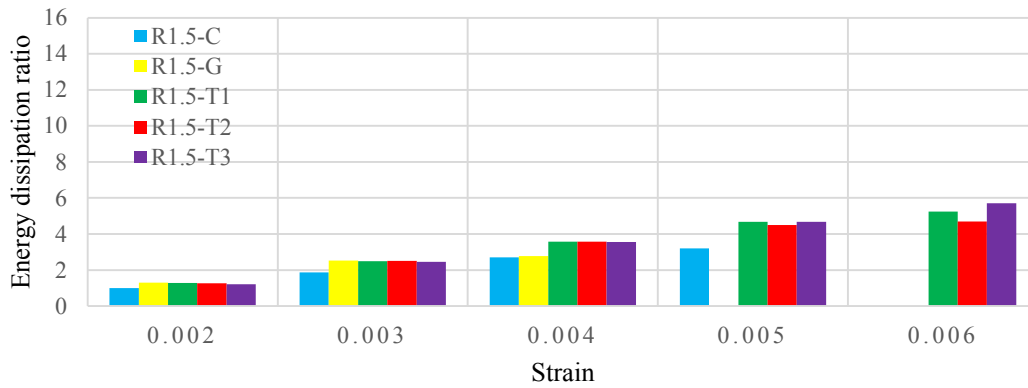
Figure 3.10: The effect of basalt GFRC jacketed on the area under stress-strain diagrams of columns with rectangular (200x300 mm) cross-section.
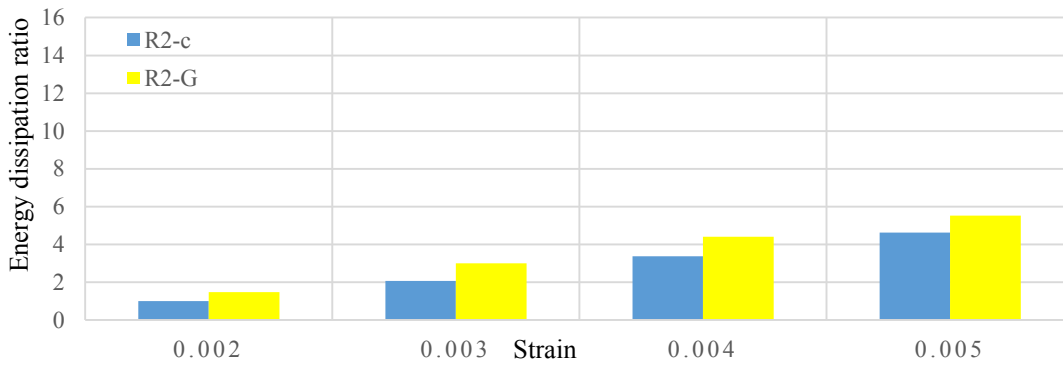
Figure 3.11: The effect of basalt GFRC jacketed on the area under stress-strain diagrams of columns with rectangular (200x400 mm) cross-section.

Table 3.6: Maximum energy dissipation ratios for columns with circular cross-section.

Label	Jacket detail	Energy dissipation ratio
C-C(average)	Control	3.85
C-G(average)	**Only GFRC**	**12.24**
C-T1	GFRC+1 textile layer	7.53
C-T2	GFRC+2 textile layer	13.39
C-T3	GFRC+3 textile layer	15.47

It can be concluded from comparison of maximum energy absorption ratios that, as the ratio of length over width of cross-section of specimens increases the energy absorption capacity of specimens' decreases significantly. For columns jacketed with only GFRC the dissipation ratio is less than for columns jacketed with BGFRC except

for C-G and C-T1. This is because of ultimate strength and strain of C-T1 could not enhanced in comparison with C-G.

Table 3.7: Maximum energy dissipation ratios for columns with square cross-section.

label	Jacket detail	Energy dissipation ratio
S-C(average)	Control	5.20
S-G(average)	Only GFRC	7.73
S-T1(average)	GFRC+1 textile layer	11.67
C-T2	GFRC+2 textile layer	11.46
C-T3	GFRC+3 textile layer	13.4

Table 3.8: Maximum energy dissipation ratios for columns with rectangular (200x300 mm) cross-section.

label	Jacket detail	Energy dissipation ratio
R1.5-C(average)	Control	3.20
R1.5-G	Only GFRC	2.77
R1.5-T1	GFRC+1 textile layer	5.23
R1.5-T2	GFRC+2 textile layer	4.69
R1.5-T3(average)	GFRC+3 textile layer	5.70

Table 3.9: Maximum energy dissipation ratios for columns with rectangular (200x400 mm) cross-section.

Label	Jacket detail	Energy dissipation ratio
R2-C(average)	Control	4.62
R2-G(average)	Only GFRC	5.53

4. THEORETICAL CONSIDERATION

In this part of the study, first, a method was established for estimation of ultimate axial strength and axial deformation capacity of concrete members retrofitted with the proposed method. Then, the predictions of the analytical approach proposed are compared with the results of similar tests in the literature. After all, three different available models from literature are used for comparing their predictions with the experimental result presented in this study.

4.1 A Simple Model for Axial Strength and Axial Deformation Capacity of Basalt Reinforced GFRC Jacketed Concrete Members

Simple equation for estimation of the axial strength and axial deformation capacity of concrete after confinement with basalt GFRC are proposed. The model estimates the confined concrete strength f_{cc} and ultimate strain ε_{cc} depending on the confining stress at failure, f_{lu}, as follows:

$$\frac{f_{cc}}{f_{c0}} = 1 + K_1 \times \left(\frac{f_{lu}}{f_{c0}}\right)^m \tag{4.1}$$

$$\varepsilon_{cu} = \varepsilon_{c0} + K_2 \times \left(\frac{f_{lu}}{f_{c0}}\right)^n \tag{4.2}$$

In above equations, K_1, K_2, m and n are empirical constants, which are computed, based on best fitting of experimental data. The ultimate tensile strength of the jacket, f_{lu} calculated as follows for columns with circular cross-section:

$$f_{lu} = \frac{2 \times t \times f_t}{D} \tag{4.3}$$

Where t is the jacket thickness, D is diameter of specimens, and f_t is the ultimate tensile stress of the jacket. In calculation of f_{lu} for square and rectangular cross-sections, f_{lu} is reduced by shape factor K_s which is defined by Equation (4.4).

$$K_s = 1 - \left(\frac{(b-2rc)^2 + (h-2rc)^2}{3A_g}\right) \tag{4.4}$$

In this equation A_g is total cross-section area of the column defined by Equation (4.5) and r_c is diameter of rounded corners if corners are rounded. If corners are not rounded r_c should be considered as zero.

$$A_g = b \times h - (4 - \pi)r_c{}^2 \qquad \textbf{(4.5)}$$

For square and rectangular cross-sections, D suggested by ACI 440 (2002) is defined with Equation (4.6).

$$D = \frac{2 \times b \times h}{(b+h)} \qquad \textbf{(4.6)}$$

In Table 4.1 the data used for four different cross-sections in finding the value of f_{lu}/f_{c0}, f_{cc}/f_{c0}, and $\varepsilon_{cu}/\varepsilon_{co}$ is given. While determining f_{lu}, f_t is taken from tensile tests carried out on BGFRC coupon specimens. The f_t values for jacket types only GFRC, GFRC+1 layer and GFRC+2 layers of basalt are 7 MPa, while for jacket type GFRC+3 layers of basalt it is 10.82 MPa. As mentioned before, f_{co} for columns with circular, square, rectangular (200x300 mm) and rectangular (200x400 mm) are 8.80, 8.55, 9.70 and 9.80 MPa, respectively. For all the confined specimens jacket thickness remained same as 25 mm, and n=1. As mentioned before, ε_{co} for circular, square, rectangular (200x300 mm) and rectangular (200x400 mm) are 0.0021, 0.0019, 0.002 and 0.003 respectively.

The values of D calculated for circular, square, rectangular (200x300) and rectangular (200x400) columns are 200, 200, 240 and 266.67 mm respectively.

Table 4.1: Value of f_{lu}/f_{c0}, f_{cc}/f_{c0} and $\varepsilon_{cu85}/\varepsilon_{co}$.

Specimen	f_{cc} (MPa)	f_{lu}(MPa)	ε_{cu85}	f_{cc}/f_{c0}	f_{lu}/f_{c0}	$\varepsilon_{cu85}/\varepsilon_{co}$
C-G	14.1	1.75	0.0054	1.60	0.20	1.00
C-T1	12.92	1.75	0.0038	1.47	0.20	1.79
C-T2	14.32	1.75	0.0063	1.63	0.20	1.27
C-T3	17.09	2.71	0.0078	1.94	0.31	2.09
S-G	13.31	1.08	0.0030	1.56	0.13	2.59
S-T1	13.45	1.08	0.0043	1.57	0.13	1.00
S-T2	13.80	1.08	0.0040	1.61	0.13	0.98
S-T3	14.65	1.68	0.0051	1.71	0.20	1.40
R1.5-G	11.27	0.76	0.0026	1.16	0.08	1.30
R1.5-T1	12.73	0.76	0.0040	1.31	0.08	1.65
R1.5-T2	12.33	0.76	0.0037	1.27	0.08	1.00
R1.5-T3	12.51	1.18	0.0048	1.29	0.12	0.77
R2-C-G	11.36	0.51	0.0033	1.16	0.05	1.19

For finding the K_1 coefficient, a linear trendline is used in Figure 4.1, where the horizontal axis is f_{lu}/f_{c0} and the vertical axis is f_{cc}/f_{c0}. Hence m and n coefficients in equations 4.1 and 4.2 are 1.
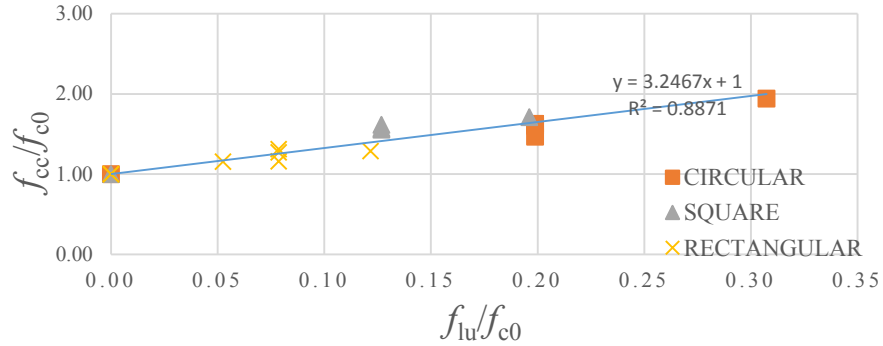

Figure 4.1: Experimental points and linear regression model for axial strength of GFRC/BGFRC jacketed columns.

Based on the satisfactory agreement of linear regression result (R^2=0.89), Equation (4.7) can be used for approximate determination of axial strength of concrete jacketed with GFRC and BGFRC.

$$\frac{f_{cc}}{f_{c0}} = 1 + 3.25 \times \left(\frac{f_{lu}}{f_{c0}}\right) \tag{4.7}$$

For finding the K_2 coefficient, again a linear trendline is used as seen in Figure 4.2 where the vertical axis is $\varepsilon_{cu85}/\varepsilon_{co}$ and horizontal axis f_{lu}/f_{c0}. During this regression analysis the specimens confined only with GFRC are excluded. Because the deformability performance of the specimens are directly related to basalt mesh behavior in agreement with this, for rectangular specimens the deformability of columns jacketed only with GFRC was not enhanced.
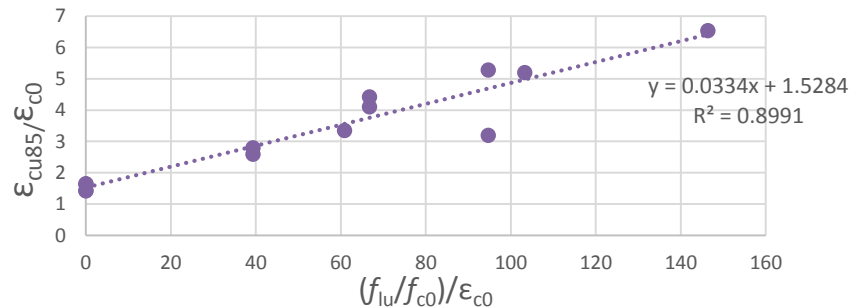

Figure 4.2: Experimental points and linear regression model for axial strain of GFRC/BGFRC jacketed columns.

Based on the satisfactory agreement of linear regression result (R^2=0.90), Equation (4.8) can be used for approximate determination of ultimate strain of concrete jacketed with GFRC and BGFRC.

$$\varepsilon_{cu85} = 1.53\varepsilon_{c0} + 0.033 \times \frac{f_{lu}}{f_{c0}} \qquad (4.8)$$

As mentioned before, the thickness of tensile test specimens are not the same with jacket thickness consequently, the results obtained from tensile test specimens would not represent the exact tensile behavior of jackets. Further study is needed for this part.

4.2 Comparison of Prediction of the Proposed Model with the Results of Similar Tests in Literature

In this part, the predictions of the proposed model for axial strength and ultimate strain are compared with the experimental results of tests available in the literature.

4.2.1 Similar experimental data from literature

In this part, four different experimental studies available in literature were selected for comparison. Experimental results obtained from the current study are also included for the comparison. The summary of the studies are presented below. It should be noticed that only current study includes sprayed mortar and glass fiber reinforced matrix.

Triantafillou et al. (2006), investigated 3 different types of unreinforced specimens confined with TRM. Two different types of mortar were used (The compressive strength at 28 days, for MI=8.56 MPa and for MII=30.61 MPa). For textile reinforcement, a commercial high-strength carbon textile was used with the equivalent thickness of 0.047 mm. The tensile strength of carbon fibers in this study was 3350 MPa. Details about the specimens of the experimental data and proposed model in this study is given in Table 4.2. Moreover, for two specimens with square cross-section (250x250 mm) with height of 700 mm the shape factor K_s was calculated using the Equation (4.5) and (4.6) (K_s=0.482). The corners rounded radius was 15 mm and diameter of specimens in series A and B was 150 mm. For all the specimens, ε_{c0} was 0.002.

In Table 4.2, f_{lu} is calculated using Equation (4.3). $f_{cc,E}$, $\varepsilon_{ccu,E}$ are ultimate axial strength and ultimate strain obtained from experimental study. $f_{cc,P}$ is ultimate axial strength found from Equation (4.7). $\varepsilon_{cu,P}$ is ultimate strains calculated using Equation (4.8) .

Table 4.2: Data obtained from experiments in the study of Triantafillou et al. (2006) and data obtained from proposed model in this study.

Label	f_{c0}(Mpa)	$f_{cc,E}$(Mpa)	$\varepsilon_{ccu,E}$	f_{lu}(Mpa)	$f_{cc,P}$(Mpa)	$\varepsilon_{cu,P}$
A-MI2	15.24	20.77	0.0096	4.20	28.87	0.0122
A-MII2	15.24	23.88	0.0108	4.20	28.87	0.0122
A-MI3	15.24	26.50	0.0113	6.30	35.69	0.0167
A-MII3	15.24	27.00	0.0122	6.30	35.69	0.0167
B-MII2	21.81	27.36	0.0098	4.20	35.44	0.0094
B-MII3	21.81	32.44	0.0108	6.30	42.26	0.0126
C-MII2	14.25	20.00	0.0118	2.52	18.19	0.0089
C-MII4	14.25	21.56	0.0176	5.04	22.14	0.0147

Ludovico et al. (2010), investigated the effectiveness of confinement based on basalt fibers preimpregnated with epoxy resins or latex and bonded with a cement based mortar over the specimen. The value ε_{lu}, for basalt fibers was 0.02. Details about the specimens and experimental values obtained from prediction model presented in this study are given in Table 4.3.

Table 4.3: Data obtained from experiments in the study of Ludovico et al. (2010) and data obtained from proposed model in this study.

Label	$\rho_f E_f$(Gpa)	f_{lu}(Mpa)	f_{c0}(Mpa)	$f_{cc,E}$(Mpa)	$\varepsilon_{ccu,E}$	$\varepsilon_{c0,E}$	$f_{cc,p}$	$\varepsilon_{cu,p}$
S4	10.9	1.09	15.52	22.50	0.0055	0.0023	19.06	0.0058
S5	21.8	2.18	15.52	22.81	0.0062	0.0023	22.60	0.0082
S14	10.9	1.09	17.83	24.07	0.0039	0.0029	21.37	0.0065
S15	10.9	1.09	17.83	26.57	0.0044	0.0029	21.37	0.0065
S16	21.8	2.18	17.83	28.71	0.0065	0.0029	24.91	0.0085
S17	21.8	2.18	17.83	27.99	0.0037	0.0029	24.91	0.0085
S6	10.9	1.09	15.52	19.71	0.0027	0.0023	19.06	0.0058
S7	21.8	2.18	15.52	22.50	0.0071	0.0023	22.60	0.0082
S18	10.9	1.09	17.83	26.39	0.0034	0.0029	21.37	0.0065
S19	10.9	1.09	17.83	19.43	0.0026	0.0029	21.37	0.0065
S20	21.8	2.18	17.83	27.64	0.0057	0.0029	24.91	0.0085
S21	21.8	2.18	17.83	25.85	0.0071	0.0029	24.91	0.0085

Trapko 2012 studied the effectiveness of FRCM (Fiber Reinforced Cementitious Matrix) and the usage of P-Phenylene Benzobisoxazole (PBO) fiber mesh and mineral mortar as confinement method. Details about the specimens and experimental values obtained from prediction model presented in this study are given in Table 4.4. The value for ε_{c0} is 0.00248.

Table 4.4: Data obtained from experiments in the study of Trapko (2012) and data obtained from proposed model in this study.

Label	f_{c0}(Mpa)	$f_{cc,E}$	f_{lu}	$f_{cc,p}$	$\varepsilon_{cu,E}$	$\varepsilon_{cu,p}$
20M1-1	22.6	32.48	4.24	36.36728	0.0062	0.0093
20M1-2	22.6	32.66	4.24	36.36728	0.0070	0.0093
20M2-1	22.6	42.42	8.49	50.16703	0.0121	0.0155
20M2-2	22.6	42.96	8.49	50.16703	0.0114	0.0155
20M3-1	22.6	58.07	12.73	63.93431	0.0181	0.0216
20M3-2	22.6	55.8	12.73	63.93431	0.0170	0.0216

Ombres (2013), investigated the effectiveness of PBO-FRCM confinement. Two types of specimens were used in this study. For the first type specimens; for CRP-I, f_{c0} and ε_{co} were 15.4 MPa and 0.0037, while for CRP-II the f_{c0} and ε_{co} were 29.26 MPa and 0.0074, respectively. The value of ε_{lu} for PBO fiber was 0.02. Details about the specimens and experimental values obtained from prediction model presented in this study are given in Table 4.5.

Table 4.5: Data obtained from experiments in the study of Ombres (2013) and data obtained from proposed model in this study.

Label	ρ_f%	$f_{cc,E}$(MPa)	f_{lu}(MPa)	$f_{cc,p}$(MPa)	$\varepsilon_{cu,E}$	$\varepsilon_{cu,p}$
CRP1-I	0.118	24.69	3.38	26.37	0.012	0.0103
CRP2-I	0.237	35,00	6.76	37.34	0.020	0.0175
CRP3-I	0.355	41.45	10.13	48.29	0.029	0.0248
CRP4-I	0.474	49.24	13.53	59.32	0.026	0.0321
CRP1-II	0.118	43.55	3.38	40.23	0.008	0.0103
CRP2-II	0.237	47.00	6.76	51.20	0.015	0.0175
CRP3-II	0.350	56.60	9.99	61.69	0.019	0.0245
CRP4-II	0.474	56.23	13.53	73.18	0.022	0.0321

In Table 4.6, the experimental data of this study used to calculate the values for ultimate axial strength and ultimate strain by using the proposed models in this study.

Table 4.6: Data obtained from experiments and proposed model in this study.

Label	f_{c0}	ε_{c0}	$f_{cc,E}$	$\varepsilon_{cu,E}$	f_l	$f_{cc,p}$	$\varepsilon_{cu,p}$
C-G	8.80	0.0036	14.10	0.0095	1.75	14.48	NA
C-T1-2	8.80	0.0036	12.92	0.0067	1.75	14.48	0.0096
C-T2	8.80	0.0036	14.32	0.0111	1.75	14.48	0.0096
C-T3	8.80	0.0036	17.09	0.0137	2.71	17.58	0.0132
S-G	8.55	0.0037	13.31	0.0059	1.08	12.07	NA
S-T1	8.55	0.0037	13.45	0.0084	1.08	12.07	0.0072
S-T2	8.55	0.0037	13.80	0.0078	1.08	12.07	0.0072
S-T3	8.55	0.0037	14.65	0.0099	1.68	13.99	0.0095
R1.5-G-1	9.70	0.0028	11.27	0.0036	0.76	12.18	NA
R1.5-T1	9.70	0.0028	12.73	0.0056	0.76	12.18	0.0056
R1.5-T2	9.70	0.0028	12.33	0.0052	0.76	12.18	0.0046
R1.5-T3	9.70	0.0028	12.51	0.0067	1.18	13.53	0.0060
R2-C-G	9.80	0.0045	11.36	0.0049	0.51	11.47	NA

4.2.2 Performance of the proposed model

Prediction of the compressive strengths and corresponding axial strains for columns retrofitted with TRM or BGFRC jacketing, made by the proposed model compared with the experimental data, gathered from the literature, in Figs 4.3, 4.4 and 4.6. The cross-section types of columns in the literature are circular, square and rectangular. According to these figures, it can be concluded that the proposed model shows a reasonably good performance in predicting the compressive strength of FRCM, TRM and BGFRC jacketed concrete members, as well as ultimate axial strains of these columns.
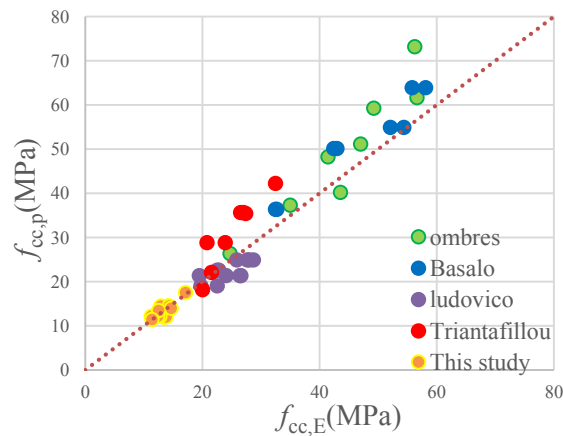
Figure 4.3: Performance of proposed model for compressive strength.
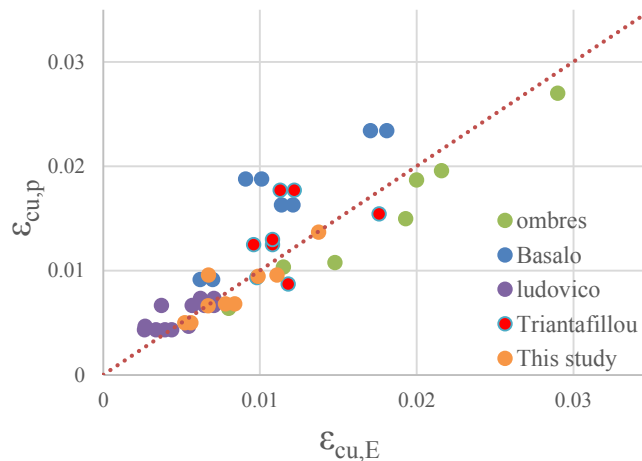
Figure 4.4: Performance of proposed model for axial strain using Equation (4.8).

The $f_{cc,E}/f_{cc,P}$ and $\varepsilon_{cu,E}/\varepsilon_{cu,P}$ values for comparison of experimental results gathered from literature and prediction of proposed model in this study are given in Tables 4.7 to

4.11. As the average values of $f_{cc,E}/f_{cc,P}$ and $\varepsilon_{cu,E}/\varepsilon_{cu,P}$ are nearer to 1, means prediction model is more accurate .

Table 4.7: The $f_{cc,E}/f_{cc,P}$ and $\varepsilon_{cu,E}/\varepsilon_{cu,P}$ values for comparison of experimental results of the study of Triantafillou et al. (2006) and prediction of proposed model in this study.

Triantafillou et al. (2006)		
Label	$f_{cc,E}/f_{cc,P}$	$\varepsilon_{cu,E}/\varepsilon_{cu,P}$
A-MI2	0.72	0.79
A-MII2	0.83	0.89
A-MI3	0.74	0.68
A-MII3	0.76	0.73
B-MII2	0.77	1.04
B-MII3	0.77	0.86
C-MII2	1.10	1.33
C-MII4	0.97	1.19
Average	**0.83**	**0.94**

Table 4.8: The $f_{cc,E}/f_{cc,P}$ and $\varepsilon_{cu,E}/\varepsilon_{cu,P}$ values for comparison of experimental results of the study of Ludovico et al. (2010) and prediction of proposed model in this study.

Ludovico et al. (2010)		
label	$f_{cc,E}/f_{cc,P}$	$\varepsilon_{cu,E}/\varepsilon_{cu,P}$
S4	1.18	0.94
S5	1.01	0.76
S14	1.13	0.60
S15	1.24	0.68
S16	1.15	0.77
S17	1.12	0.44
S6	1.03	0.46
S7	1.00	0.87
S18	1.23	0.53
S19	0.91	0.40
S20	1.11	0.67
S21	1.04	0.84
Average	**1.10**	**0.66**

Table 4.9: The $f_{cc,E}/f_{cc,P}$ and $\varepsilon_{cu,E}/\varepsilon_{cu,P}$ values for comparison of experimental results of the study of Trapko (2012) and prediction of proposed model in this study.

Trapko (2012)		
Label	$f_{cc,E}/f_{cc,P}$	$\varepsilon_{cu,E}/\varepsilon_{cu,P}$
20M1-1	0.89	0.67
20M1-2	0.90	0.76
20M2-1	0.85	0.78
20M2-2	0.86	0.74
20M3-1	0.91	0.84
20M3-2	0.87	0.79
Average	**0.88**	**0.76**

Table 4.10: The $f_{cc,E}/f_{cc,P}$ and $\varepsilon_{cu,E}/\varepsilon_{cu,P}$ values for comparison of experimental results of the study of Ombres (2013) and prediction of proposed model in this study.

Ombres (2013)		
Label	$f_{cc,E}/f_{cc,P}$	$\varepsilon_{cu,E}/\varepsilon_{cu,P}$
CRP1-I	0.94	1.16
CRP2-I	0.94	1.14
CRP3-I	0.86	1.17
CRP4-I	0.83	0.81
CRP1-II	1.08	0.78
CRP2-II	0.92	0.85
CRP3-II	0.92	0.78
CRP4-II	0.77	0.69
Average	**0.91**	**0.92**

Table 4.11: The $f_{cc,E}/f_{cc,P}$ and $\varepsilon_{cu,E}/\varepsilon_{cu,P}$ values for comparison of experimental results and prediction of proposed model in this study.

This study		
Label	$f_{cc,E}/f_{cc,P}$	$\varepsilon_{cu,E}/\varepsilon_{cu,P}$
C-G	0.97	NA
C-T1-2	0.89	0.70
C-T2	0.99	1.15
C-T3	0.97	1.04
S-G	1.10	NA
S-T1	1.11	1.16
S-T2	1.14	1.08
S-T3	1.05	1.04
R1.5-G-1	0.93	NA
R1.5-T1	1.05	0.99
R1.5-T2	1.01	1.13
R1.5-T3	0.92	1.11
R2-C-G	0.99	NA
Average	**1.01**	**1.04**

4.3 Comparison of Predictions of Other Models Proposed for TRM with the Experimental Results Obtained in This Study

In this part of the analytical study, other models originally proposed for the concrete members, which have been externally jacketed with TRM, are used for prediction of maximum compressive strengths and ultimate axial strains of the specimens tested in the current study. Prediction of models proposed by Triantafillou (2006), Ludovico (2010), Basalo (2010) and Caicedo (2007) are compared with the results of current experimental study. Models taken into consideration for this are presented in table 4.12.

Table 4.12: Analytical models originally proposed for TRM.

Model	Analytical expression
Triantafillou for TRM(2006)	$f_{cc}=f_{co}+1.897f_{lu}$ $\varepsilon_{cu}=\varepsilon_{c0}+0.0467(f_{lu}/f_{c0})$
Ludovico et al. BRM(latex) (2010)	$f_{cc}/f_{c0}=1+2.72(f_{lu}/f_{c0})^{0.85}$ $\varepsilon_{cu}=\varepsilon_{c0}+0.022(f_{lu}/f_{c0})^{0.85}$
Basalo et al. (cement base matrix) (2010)	$f_{cc}/f_{c0}=1+2.87(f_{lu}/f_{c0})^{0.775}$ $\varepsilon_{cu}=\varepsilon_{c0}+0.046(f_{lu}/f_{c0})^{0.775}$
Caicedo TRM(2007)	$f_{cc}/f_{c0}=1+2.6(f_{lu}/f_{c0})^{0.75}$ $\varepsilon_{cu}=\varepsilon_{c0}+0.015(f_{lu}/f_{c0})^{0.5}$

In Tables 4.13-4.16, the experimental data obtained from this study and predictions of the models proposed in literature are compared. Where $f_{cc,T}$, $f_{cc.E}$ stands for theoretical and experimental value of f_{cc}. $\varepsilon_{cu,T}$, $\varepsilon_{cu,E}$ are theoretical and experimental values of ε_{cu}.

Table 4.13: Comparison of experimental data with predictions model for (Triantafillou 2006) TRM model.

Label	$f_{cc,E}$(MPa)	$f_{cc,T}$(MPa)	Δf_{cc}	$\varepsilon_{cu,E}$	$\varepsilon_{cu,T}$	Δ, ε_{cu}
C-G	14.10	12.12	-16.34	0.0054	NA	NA
C-T1-2	12.92	12.12	-6.62	0.0038	0.013	47.83
C-T2	14.32	12.12	-18.17	0.0063	0.013	13.97
C-T3	17.09	13.93	-22.68	0.0079	0.018	23.47
S-G	13.31	10.61	-25.51	0.0030	NA	NA
S-T1	13.45	10.61	-26.81	0.0043	0.0096	12.69
S-T2	13.80	10.61	-30.11	0.0040	0.0096	18.84
S-T3	14.65	11.73	-24.88	0.0050	0.0129	23.16
R1.5-G-1	11.27	11.15	-1.10	0.0026	NA	NA
R1.5-T1	12.73	11.15	-14.20	0.0040	0.00645	13.49
R1.5-T2	12.33	11.15	-10.61	0.0037	0.0065	19.67
R1.5-T3	12.51	11.94	-4.79	0.0048	0.0085	21.00
R2-C-G	11.36	10.78	-5.43	0.0033	NA	NA

Table 4.14: Comparison of experimental data with prediction model for (Ludovico et al. (2010)) BRM (latex) model.

Label	$f_{cc,E}$(MPa)	$f_{cc,T}$(MPa)	Δ, f_{cc}	$\varepsilon_{cu,E}$	$\varepsilon_{cu,T}$	Δ, ε_{cu}
C-G	14.10	16.02	12.01	0.0054	NA	NA
C-T1-2	12.92	16.02	19.35	0.0038	0.0076	49.94
C-T2	14.32	16.02	10.61	0.0063	0.0076	17.44
C-T3	17.09	18.92	9.68	0.0079	0.0101	22.81
S-G	13.31	13.50	1.40	0.0030	NA	NA
S-T1	13.45	13.50	0.38	0.0043	0.0057	24.84
S-T2	13.80	13.50	-2.21	0.0040	0.0057	30.13
S-T3	14.65	15.49	5.45	0.0050	0.0074	31.96
R1.5-G-1	11.27	13.58	17.01	0.0026	NA	NA
R1.5-T1	12.73	13.58	6.26	0.0040	0.0045	12.40
R1.5-T2	12.33	13.58	9.21	0.0037	0.0045	18.66
R1.5-T3	12.51	15.14	17.37	0.0048	0.0056	16.20
R2-C-G	11.36	12.66	10.30	0.0033	NA	NA

Table 4.15: Comparison of experimental data with prediction model for (Basalo et al. (2010) cement base matrix model.

Label	$f_{cc,E}$(MPa)	$f_{cc,T}$(MPa)	Δ, f_{cc}	$\varepsilon_{cu,E}$	$\varepsilon_{cu,T}$	Δ, ε_{cu}
C-G	14.10	18.02	21.75	0.0054	NA	NA
C-T1-2	12.92	18.02	28.28	0.0038	0.0169	77.39
C-T2	14.32	18.02	20.51	0.0063	0.0194	67.49
C-T3	17.09	23.05	25.85	0.0079	0.0262	70.13
S-G	13.31	14.26	6.65	0.0030	NA	NA
S-T1	13.45	14.26	5.68	0.0043	0.0135	68.41
S-T2	13.80	14.26	3.23	0.0040	0.0132	69.97
S-T3	14.65	17.38	15.73	0.0050	0.0180	72.08
R1.5-G-1	11.27	13.72	17.85	0.0026	NA	NA
R1.5-T1	12.73	13.72	7.21	0.0040	0.0103	61.74
R1.5-T2	12.33	13.72	10.13	0.0037	0.0101	63.48
R1.5-T3	12.51	15.92	21.40	0.0048	0.0137	65.41
R2-C-G	11.36	12.51	9.18	0.0033	NA	NA

Table 4.16: Comparison of experimental data with prediction model for (Caicedo (2007)) TRM model.

Label	$f_{cc,E}$(MPa)	$f_{cc,T}$(MPa)	Δ, f_{cc}	$\varepsilon_{cu,E}$	$\varepsilon_{cu,T}$	Δ, ε_{cu}
C-G	14.10	15.62	9.70	0.0054	NA	NA
C-T1-2	12.92	15.62	17.24	0.0038	0.0105	63.51
C-T2	14.32	15.62	8.27	0.0063	0.0130	51.35
C-T3	17.09	18.25	6.32	0.0079	0.0161	51.43
S-G	13.31	13.27	-0.30	0.0030	NA	NA
S-T1	13.45	13.27	-1.33	0.0043	0.0096	55.48
S-T2	13.80	13.27	-3.97	0.0040	0.0093	57.27
S-T3	14.65	15.10	2.99	0.0050	0.0116	56.85
R1.5-G-1	11.27	13.45	16.18	0.0026	NA	NA
R1.5-T1	12.73	13.45	5.32	0.0040	0.0081	51.43
R1.5-T2	12.33	13.45	8.30	0.0037	0.0078	53.28
R1.5-T3	12.51	14.89	16.01	0.0048	0.0099	52.40
R2-C-G	11.36	12.59	9.79	0.0033	NA	NA

The experimental results and predictions of the models proposed in literature are compared in Figure 4.5 and 4.6 and for f_{cc} and ε_{cu}, respectively.
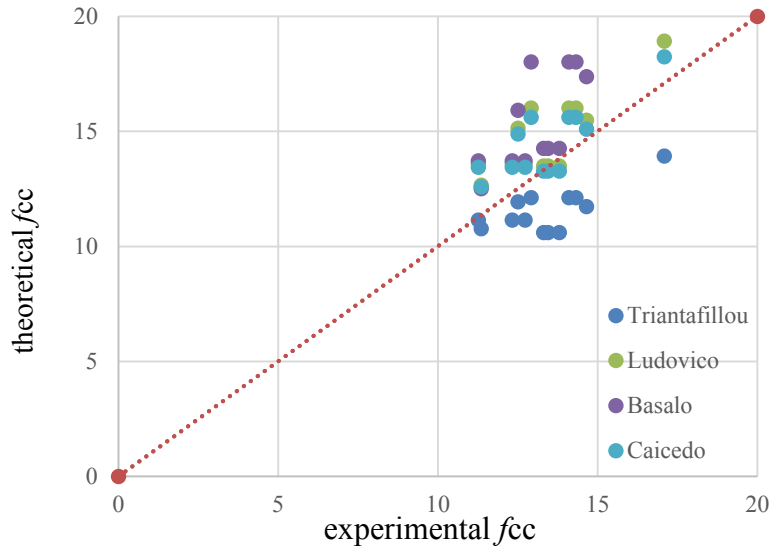

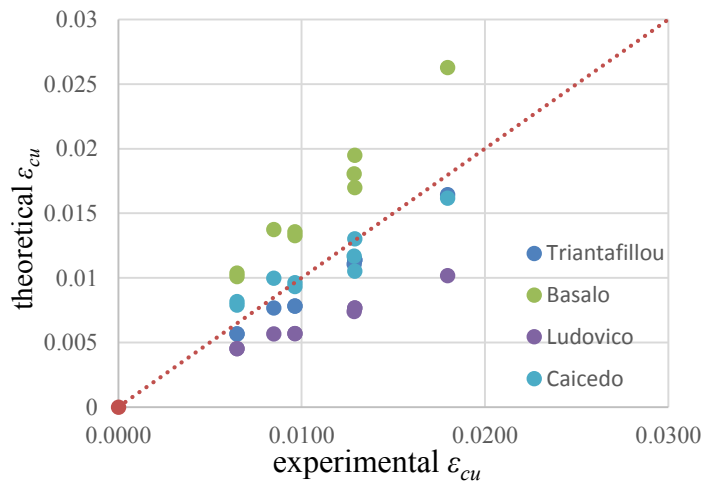**Figure 4.5:** Comparison of prediction values for f_{cc} from proposed model from literature with this study.

Figure 4.6: Comparison of prediction values for ε_{cu}, from proposed model from literature with this study.

Values of $f_{cc,E}/ f_{cc,P}$ and $\varepsilon_{cu,E}/\varepsilon_{cu,P}$ for comparison of prediction models proposed by Triantafillou (2006), Ludovico (2010), Basalo (2010), Caicedo (2007) and the results of current experimental study are given in Tables 4.17 to 4.20.

Table 4.17: Values of $f_{cc,E}/f_{cc,P}$ and $\varepsilon_{cu,E}/\varepsilon_{cu,P}$ for comparison of prediction models proposed by Triantafillou (2006) and the results of current experimental study.

Triantafillou (2006)		
Label	$f_{cc,E}/f_{cc,P}$	$\varepsilon_{cu,E}/\varepsilon_{cu,P}$
C-G	1.16	NA
C-T1-2	1.07	0.29
C-T2	1.18	0.48
C-T3	1.23	0.44
S-G	1.25	NA
S-T1	1.27	0.45
S-T2	1.30	0.42
S-T3	1.25	0.39
R1.5-G-1	1.01	NA
R1.5-T1	1.14	0.62
R1.5-T2	1.11	0.57
R1.5-T3	1.05	0.56
R2-C-G	1.05	NA
AVE	**1.16**	**0.47**

Table 4.18: Values of $f_{cc,E}/f_{cc,P}$ and $\varepsilon_{cu,E}/\varepsilon_{cu,P}$ for comparison of prediction models proposed by Ludovico (2010) and the results of current experimental study.

Loduvico (2010)		
Label	$f_{cc,E}/f_{cc,P}$	$\varepsilon_{cu,E}/\varepsilon_{cu,P}$
C-G	0.88	NA
C-T1-2	0.81	0.50
C-T2	0.89	0.83
C-T3	0.90	0.78
S-G	0.99	NA
S-T1	1.00	0.75
S-T2	1.02	0.70
S-T3	0.95	0.68
R1.5-G-1	0.83	NA
R1.5-T1	0.94	0.89
R1.5-T2	0.91	0.82
R1.5-T3	0.83	0.86
R2-C-G	0.90	NA
AVE	**0.91**	**0.76**

Table 4.19: Values of $f_{cc,E}/f_{cc,P}$ and $\varepsilon_{cu,E}/\varepsilon_{cu,P}$ for comparison of prediction models proposed by Basalo (2010) and the results of current experimental study.

Basalo (2010)		
Label	$f_{cc,E}/f_{cc,P}$	$\varepsilon_{cu,E}/\varepsilon_{cu,P}$
C-G	0.78	NA
C-T1-2	0.72	0.22
C-T2	0.79	0.32
C-T3	0.74	0.30
S-G	0.93	NA
S-T1	0.94	0.32
S-T2	0.97	0.30
S-T3	0.84	0.28
R1.5-G-1	0.82	NA
R1.5-T1	0.93	0.39
R1.5-T2	0.90	0.37
R1.5-T3	0.79	0.35
R2-C-G	0.91	NA
AVE	**0.85**	**0.32**

Table 4.20: Values of $f_{cc,E}/f_{cc,P}$ and $\varepsilon_{cu,E}/\varepsilon_{cu,P}$ for comparison of prediction models proposed by Caicedo (2007) and the results of current experimental study.

Caicedo (2010)		
Label	$f_{cc,E}/f_{cc,P}$	$\varepsilon_{cu,E}/\varepsilon_{cu,P}$
C-G	0.90	NA
C-T1-2	0.83	0.36
C-T2	0.92	0.48
C-T3	0.94	0.49
S-G	1.00	NA
S-T1	1.01	0.45
S-T2	1.04	0.43
S-T3	0.97	0.43
R1.5-G-1	0.84	NA
R1.5-T1	0.95	0.49
R1.5-T2	0.92	0.47
R1.5-T3	0.84	0.48
R2-C-G	0.90	NA
AVE	**0.93**	**0.46**

5. POTENTIAL APPLICATION FOR COLUMNS UNDER AXIAL LOAD AND FLEXURE

In this section firstly, a simple model for representing the behavior of basalt reinforced GFRC is proposed, then nonlinear analysis using XTRACT cross-section analyze program was done to figure out the moment-curvature diagrams and force-displacement diagrams as well, for unconfined (control) columns and externally jacketed columns with basalt reinforced GFRC. For columns and their reinforcement details, Peer column database was used. Afterwards, comparison of force-displacement relationships of columns jacketed with basalt reinforced GFRC and unconfined columns are presented in this section

5.1 A Simple Model for Axial Behavior of Concrete Externally Jacketed with Basalt Reinforced GFRC

For presenting the structural behavior of columns jacketed externally with basalt reinforced GFRC, a simple two-point stress-strain curve is proposed in the following part.

The experimentally determined values of ε_{co} and the corresponding axial stresses ($f_{\varepsilon c0}$) for columns externally jacketed with basalt reinforced GFRC are presented in Table 5.1. The peak stress values f_{cc} are also presented in this table for comparison.

Table 5.1: f_{cc} and $f_{\varepsilon c0}$ values for externally jacketed column with BGFRC.

Label	f_{cc}	$f_{\varepsilon c0}$	Δ
C-T1-2	12.92	12.86	-0.49
C-T2	14.32	13.88	-3.20
C-T3	17.09	14.48	-18.04
S-T1	13.45	13.29	-1.20
S-T2	13.80	13.73	-0.51
S-T3	14.65	14.05	-4.27
R1.5-T1	12.73	12.57	-1.27
R1.5-T2	12.33	12.3	-0.24
R1.5-T3	12.51	12.49	-0.16

It can be concluded from Table 5.1 that the values for fcc and $f_{\varepsilon c0}$ are quite close to each other and their differences are less than 5%, except for C-T3, for which the difference is 18%. Therefore, the first characteristics point of proposed model is defined as the point at which the strain value is ε_{co} and the stress value is f_{cc}. For connecting, the origin (0, 0) to the first characteristic point of the proposed model, a second-degree parabolic curve is defined as:

$$\sigma = a\varepsilon^2 + b\varepsilon + c \qquad (5.1)$$

By application of boundary conditions the constants a, b and c are defined as:

1) $\varepsilon=0$, $\sigma=0$; $0 = a0 + b0 + c$, $0 = c$ (5.2)

2) $\varepsilon=0$, $\sigma'=E_c$ $E_c = 2a0 + b$, $b = E_c$ (5.3)

For Equation (5.3), it is assumed that the jacket is not effective on the behavior (on axial stiffness) at small strains, where lateral dilation is minimal. The value E_c (elasticity modulus of concrete) is taken into consideration by Equation (5.4).

$$E_c = 4700\sqrt{f'_c} \text{ , ACI 318 (2008)} \qquad (5.4)$$

3) $\varepsilon=\varepsilon0$, $\sigma=f_{cc}$ $f_{cc} = a\varepsilon_{c0}{}^2 + E_c\varepsilon_{c0}$ (5.5)

$$a = \frac{f_{cc} - E_c\varepsilon_{co}}{\varepsilon_{co}{}^2} \qquad (5.6)$$

For the second characteristic point of the proposed model, coordinates on the stress-strain relationship are selected as $\varepsilon=\varepsilon_{cu}$, $\sigma=0.85f_{cc}$. Where ε_{cu} and f_{cc} could be defined using Equations 4.9 and 4.7, respectively. The first characteristic point of the proposed
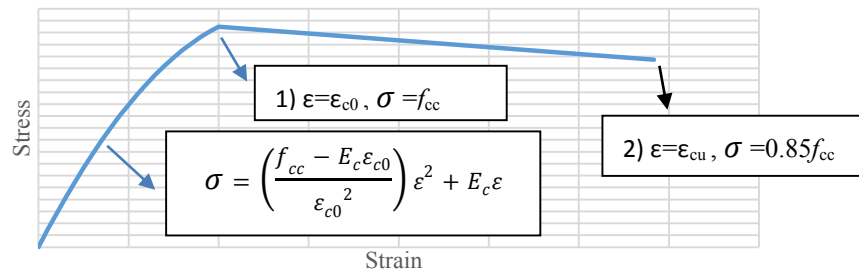
Figure 5.1: Proposed model for BGFRC jacketed concrete columns.

model is connected to the second characteristic point with a line as shown in Figure 5.1

5.2 Application of Confinement Model for Columns under Axial and Flexural

For obtaining analytical load-displacement relationships of the columns before and after BGFRC retrofitting, the elastic and plastic components of the top displacement of the columns (δ_y and δ_p) are calculated by Equations (5.7)-(5.9). As evident, the contributions of shear and potential slip to the top displacement are ignored based on the information that all these columns are flexural critical (PEER). The average moment-curvature relationships are obtained by making use of XTRACT (2007) cross-section analysis software. The calculated moment capacities are converted to lateral load capacities by dividing the moment capacity by the height of the column between load acting point and column base. While determining the plastic displacement, the plastic hinge length is assumed as h/2 as proposed by TSDC (2007), where *h* represents the effective depth of cross-section of column in the direction of bending.

For analyzing the reference column specimen the confined Mander model was used as the XTRACT program's default assumption. The internal reinforcement confinement only was used for reference column specimen. For retrofitted column specimens combination of internal reinforcement and external jacket used, by assuming the stress-strain relationship curves that illustrated in Figs 5.2 – 5.5 for retrofitted columns with BGFRC.

$$\delta_y = \theta_y \frac{2L}{3} = \frac{\varphi_y \ L}{2} \frac{2L}{3} = \frac{\varphi_y \ L^2}{3} \qquad (5.7)$$

$$\delta_p = (\phi-\phi_y)L_p \left(L-\frac{L_p}{2}\right) \qquad (5.8)$$

$$\delta_{Y+P} = \frac{\varphi_y \ L^2}{3} + (\phi-\phi_y)L_p \left(L-\frac{L_p}{2}\right) \qquad (5.9)$$

Here; δ_y, δ_p are the yield and plastic displacements, respectively, and δ_{Y+P} is the total ultimate displacement.

The stress-strain diagrams of material used for analyzing the columns are given in Figures 5.3 to 5.9.

59

The load-displacement curves following the theoretical approach summarized above are given in Figures 5.11 and 5.13 for reference and BGFRC retrofitted columns. The Moment-curvature curves obtained as given in Figures 5.10 and 5.12.
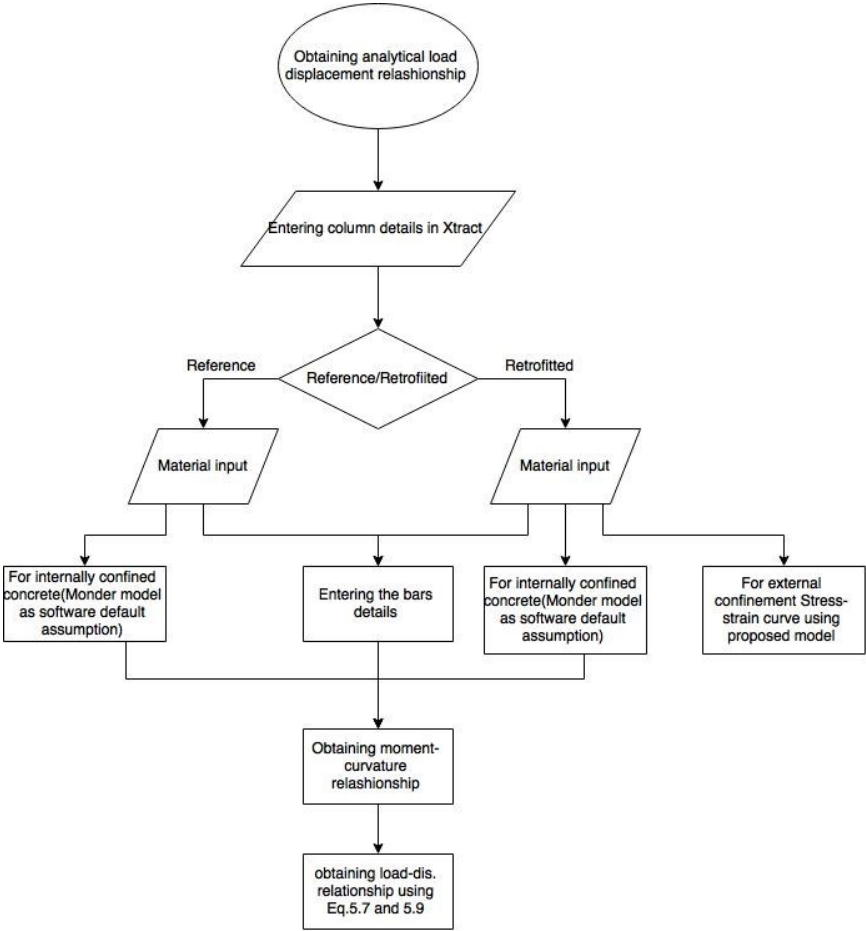
Figure 5.2: Flowchart of obtaining analytical load-displacement relationships.

It is clear that the limited contribution of external jacketing is due to heavy internal confinement reinforcement. The contribution of basalt reinforced GFRC jacket would be much more emphasized if the column had limited transverse reinforcement not fully satisfying the confinement reinforcement requirements per recent structural design documents. In this part, the details for columns (two substandard columns that contained insufficient amount confinement reinforcement before retrofitting)used as Table 5.2. For both columns as external jacket, 3 layers of basalt with GFRC is assumed to be used.

Table 5.2: Details of column No.1 and No.2.

Label	Section type	Section size(mm)	fc0(Mpa)	Num. Longitudinal bars	cover thickness (mm)	stirrups spacing(mm)
No.1	Circular	D=200	9.7	8	15	300
No.2	Square	300x300	9.7	4	20	400
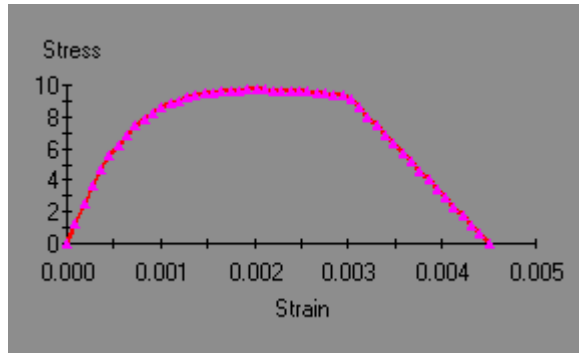
Figure 5.3: Stress-strain curve for unconfined concrete for column No.1and No.2.
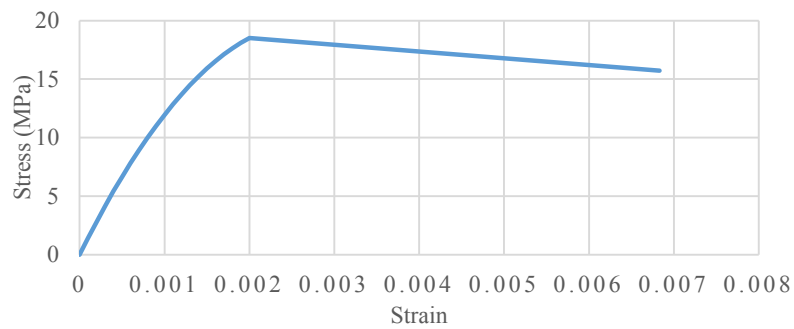
Figure 5.4: Stress-strain relationship for jacketed concrete with GFRC+3 layer basalt for column No1.
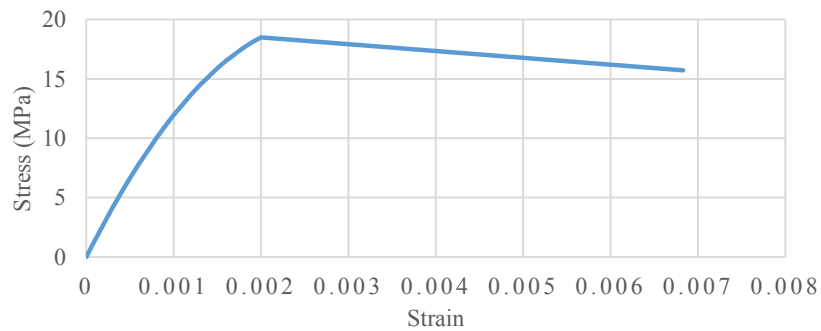
Figure 5.5: Stress-strain relationship for jacketed concrete with GFRC+3 layer basalt for column No2.
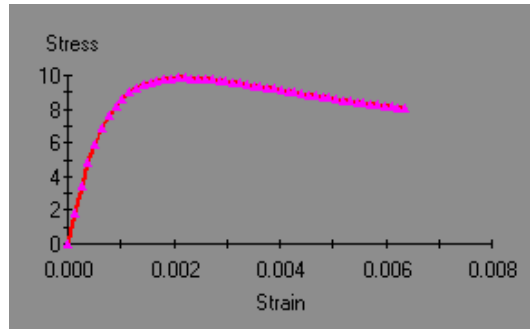
Figure 5.6: Stress-strain curve for concrete confined with internal stirrups for column No. 1.
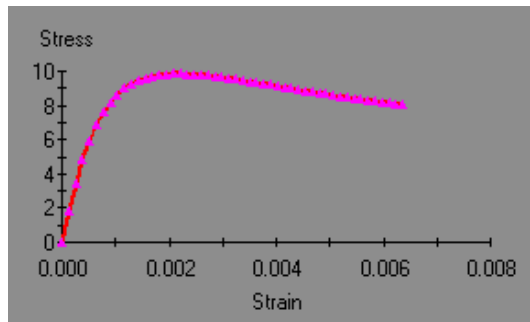
Figure 5.7: Stress-strain curve for concrete confined with internal stirrups for column No. 2.
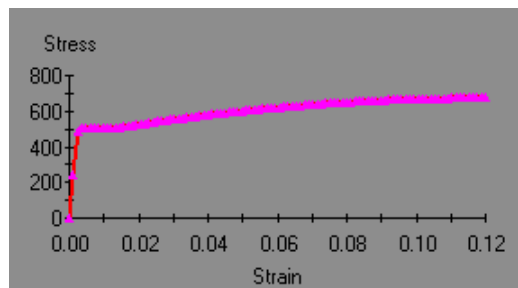
Figure 5.8: Stress-strain curve for longitudinal reinforcement for column No. 2.
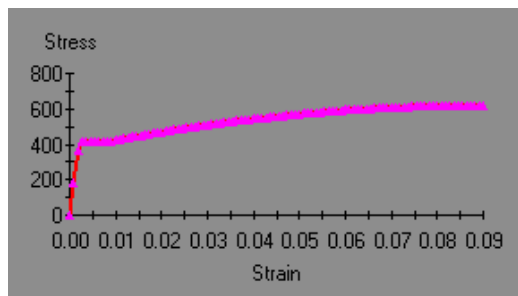
Figure 5.9: Stress-strain relationship for longitudinal reinforcement for columns No.1.

In Figs. 5.3 to 5.9 stress-strain relationships related to material used for analysis of the columns are presented.

In Figures 5.10 to 5.13 moment-curvature and load-displacement, relationships obtained from analysis using Xtract are presented.
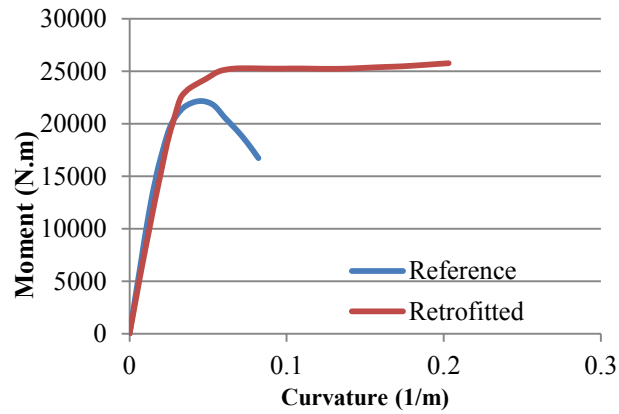
Figure 5.10: Moment-curvature relationships for substandard column No.1 before and after BGFRC retrofitting.
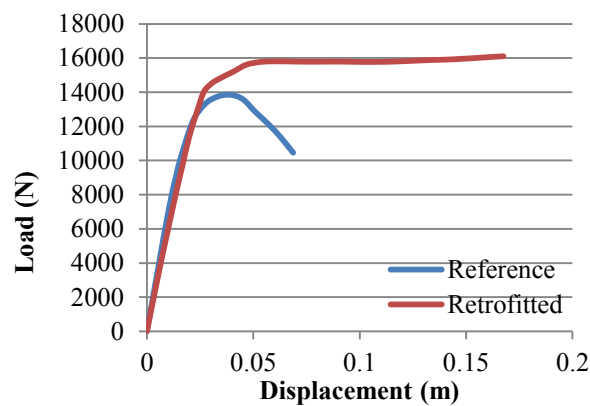
Figure 5.11: Load-displacement relationships for substandard column No.1 before and after BGFRC retrofitting.
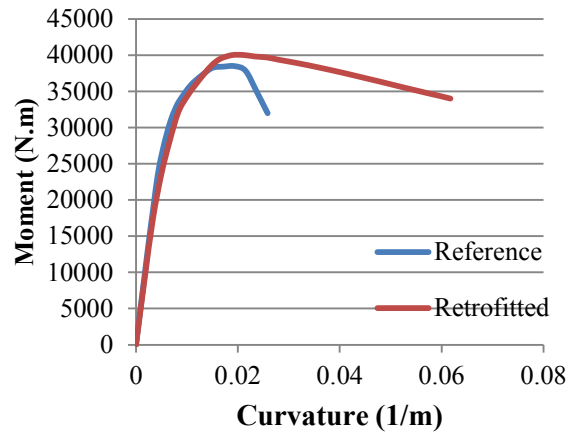
Figure 5.12: Moment-curvature relationships for substandard column No.2 before and after BGFRC retrofitting.
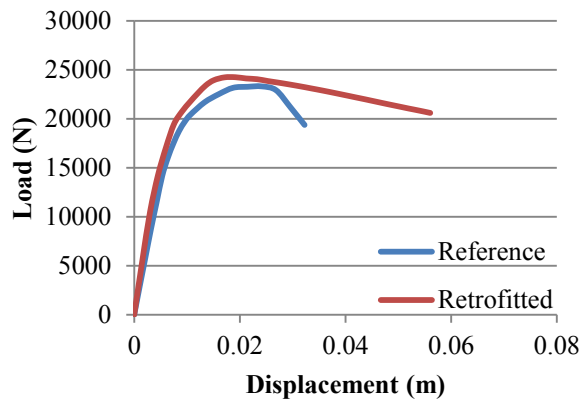
Figure 5.13: Load-displacement relationships for substandard column No.2 before and after BGFRC retrofitting.

6. CONCLUSIONS AND RECOMMENDATIONS FOR FURTHER RESEARCH

In this study, the effectiveness of two external jacketing materials GFRC and BGFRC developed for column retrofitting have been experimentally investigated. The effects of several parameters, such as type of the jacket material, cross-section shape and the number of the basalt mesh layers within the GFRC matrix are examined. The contribution of this retrofitting technique to the axial behavior of concrete members is investigated on short columns experimentally under concentric axial loads, while member level theoretical analyses are also carried out for the cases of axial loads as well as combined actions of axial loads and flexural moments. Additionally, tensile test specimens representing each external jacketing type were also tested under direct tension effects. The data obtained from the tensile tests were also used in analytical study. In the analytical part of the study, a method was established for the estimation of ultimate strength and deformation capacity of GFRC/BGFRC jacketed columns. Furthermore, a stress-strain relationship was also proposed for these members. The performance of the proposed model is investigated considering test data published by other researchers. Furthermore, accuracy of various models proposed by other researchers is also examined considering the test results presented in this study. It should be noted that the studies in literature examined for these comparisons were on textile reinforced mortar retrofitting. According to the best knowledge of the authors, the behavior of sprayed GFRC and BGFRC was not studied elsewhere before. Afterwards, the nonlinear flexural behaviour of RC columns retrofitted with the proposed retrofitting technique is studied under the combined actions of axial and lateral loads.

6.1 Conclusions

1-Sprayed GFRC and basalt reinforced sprayed GFRC methods for external confinement are suitable strengthening techniques in structural members, due to the enhancement observed in both compressive strength and deformability.

2-GFRC is effective in the region close to the ultimate compressive strength of the specimen. After formation of cracks in GFRC, the structural behavior of columns such as deformation capacity is controlled by the mechanical and physical characteristics of the basalt mesh.

3-Sprayed up GFRC has a significant impact on the behavior of specimens; therefore, determining the type of the textile as well as the number of textile layers should be done considering the tensile behavior of sprayed up GFRC.

4- Considering, the ease and prompt implementation, relatively low cost and renewability, sprayed up GFRC retrofitting method is an alternative to existing retrofitting methods.

5- For the specimens with rectangular cross-section, as the ratio of width/length increases the confinement effectiveness reduces (considering the value of f_{cc}/f_{c0}).

6-It can be concluded from the comparison of maximum energy absorption ratios that, as the ratio of length over width of cross-section of specimens increases, the rate of increase of energy absorption capacity of specimens decreases significantly.

7- The analytical study on concrete columns under axial and flexural loads concluded that, higher deformability and hence better seismic performance could be achieved by external jacketing of columns with large stirrups spacing through the proposed retrofitting technique with BGFRC.

7.2 Recommendations

The experimental and analytical results obtained in this study is valid for a limited number of specimens; therefore, further studies are needed to better determine the effectiveness of the proposed jacketing method in confining of structural members. According to the findings of this study, the following matters need further investigation:

-The effects of volumetric ratio and mechanical characteristics of basalt mesh within the BGFRC.

-The effects of volumetric ratio and mechanical characteristics of glass fibers within the GFRC mortar.

-The effect of jacket tensile strength on confinement effectiveness considering by, design of the tensile test specimens with the same exact details (thickness and fiber %) as jackets.

-The effects of mechanical characteristics of matrix of GFRC.

-The effects of environmental effects such as freeze and melt temperature variation and moisture.

-The effect of concrete strength and concrete columns cross-section size.

REFERENCES

ACI Committee 440 Report. Guide for the Design and Construction of Externally Bonded FRP Systems for Strengthening Concrete Structures. ACI Committee 440, Technical.Committee Document, 440.2R-02 (2002).

Bentur, A., and Mindess, S. (2007). Fibre Reinforced Cementitious Composites, second Ed., Taylor & Francis, New York.

Bournas, D. A., Lontou, P. V., Papanicolaou, C. G., and Triantafillou, T. C. (2007). Textile-Reinforced Mortar (TRM) versus FRP Confinement in Reinforced Concrete Columns. ACI Structural Journal, 104:6, 740-748.

DBYBHY (2007). Deprem Bölgelerinde Yapılacak Binalar Hakkında Yönetmelik.Turkish Earthquake Code, Ankara, Turkey.

Colajanni, P., De Domenico, F., Recupero, A., and Spinella, N. (2014). Concrete Columns Confined with Fibre Reinforced Cementitious Mortars: Experimentation and Modelling Construction and Building Materials, Vol. 52, pp. 375-384.

Di Ludovico, M., Prota, A., Manfredi, G., and Cosenza, E. (2008). Seismic Strengthening of an Under-Designed RC Structure with FRP. Earthquake Engineering & Structural Dynamics, Vol. 37(1), pp. 141-162.

Garcia, D., Alonso, P., Tomas, J., Jose, S., and Garmandia (2010). Confinement of Medium Strength Concrete Cylinders with Basalt Textile Reinforced Mortar.ICPI 2010 13th International congress on polymers in concrete.

Ilki, A., Demir, C., Bedirhanoğlu, I., and Kumbasar, N. (2009). Seismic Retrofit of Brittle and Low Strength RC Columns using Fiber Reinforced Polymer and Cementitious Composites. Advances in Structural Engineering, 12(3):325-347.

Ilki, A., and Kumbasar, N. (2002). Behavior of Damaged and Undamaged Concrete Strengthened by Carbon Fiber Composite Sheets. Int. Jour. Str. Eng. and Mech., 13(1): 75–90.

Mander, J. B., Priestley, M. J. N., and Park, R. (1988). Theoretical Stress-strain Model for Confined Concrete, *ASCE Journal of Structural Engineering*, 114 (8), 1804-1826.

Mirmiran, A., and Shahawy, M. (1997). Behavior of Concrete Columns Confined by Fiber Composites. ASCE Journal of Structural Engineering, 123(5): 583-590.

Nanni, A. (2012). A New Tool in the Concrete and Masonry Repair. Concrete International, 34(4), 43-49.

Nasrinpour, A. (2014). Seismic Retrofit of RC Columns with Sprayed Basalt Mesh Reinforced GRC: Effects of Stirrups Spacing. M.Sc. thesis.

Ombres, L. (2013). Concrete Confinement with a Cement Based High Strength Composite Material. Journal of Composite Structure 109 (2014) 294-304

Ortlepp, R., Brenz, A., and Curbach, M. (2009). Column Strengthening with TRC: Influence of The Geometry onto The Confinement Effect. Journal of Advanced in material science and engineering, Article ID 493097.

PEER (2014). Structural Performance Database [Report] Berkeley: The University of Washington, University of California, 2014.

Peled, A. (2007). Confinement of Damaged and Non-Damaged Structural Concrete with FRP and TRC Sleeves. Journal of Composites for Construction, 11(5): 514-523.

Toutanji, H. A. (1999). Stress-Strain Characteristics of Concrete Columns Externally Confined with Advanced Fiber Composite Sheets. ACI Materials Journal, 96(3), 397–404.

Trapko, T. (2012). Fiber Reinforced Cementitious Matrix Confined Concrete Elements. Material and Design 44 (2013) 382-391.

Triantafillou, T. C., Papanicolaou, C. G., Zissinopoulos, P., and Laourdekis, T. (2006). Concrete Confinement with Textile-Reinforced Mortar Jackets. ACI Structural Journal, 103(1): 28-37.

Triantafillou, T. C., and Papanicolaou, C. G. (2006). Shear strengthening of Reinforced Concrete Members with Textile Reinforced Mortar (TRM). Materials and Structures, 39(1): 93-103.

Saatcioglu, M., and Ozcebe, G. (1989). Response of Reinforced Concrete Columns to Simulated Seismic Loading [Journal] // ACI structural jurnal. - 1989.

XTRACT 3.0.8 (2007). Cross-sectional Structural Analysis of Components .TRC.

Yilmaz, A., Mezrea, P. E., Ispir, M., Bal, I. E., and Ilki, A. (2013). External Confinement of Brick Masonry Columns with Open-Grid Basalt Reinforced Mortar. APFIS 2013, the Fourth Asia-Pacific Conference on FRP Structures, Melbourne, December.

APPENDICES

APPENDIX A: details of column tests.

Name of specimen: C-C-1
Jacket detail: control specimen without jacket.
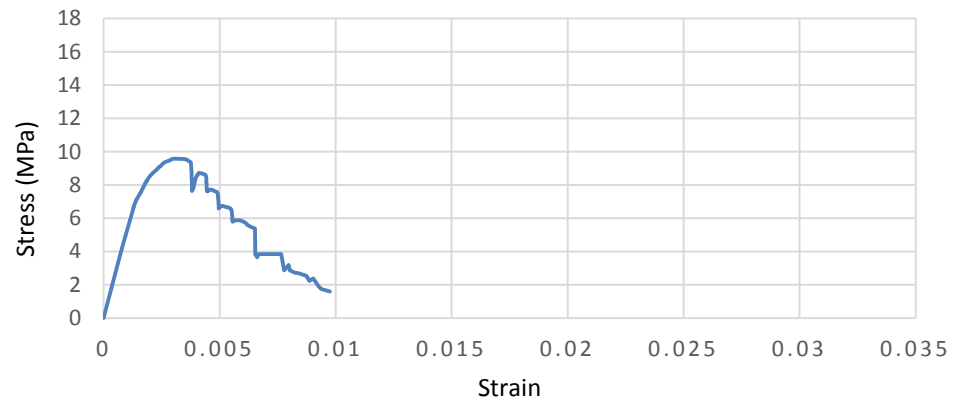
f_{cc}	ε_{cu}	f_{cc}/f_{co}	$\varepsilon_{cu85}/\varepsilon_{co85}$
9.58	0.0017	1.09	1.12

Name of specimen: C-C-2
Jacket detail: control specimen without jacket.
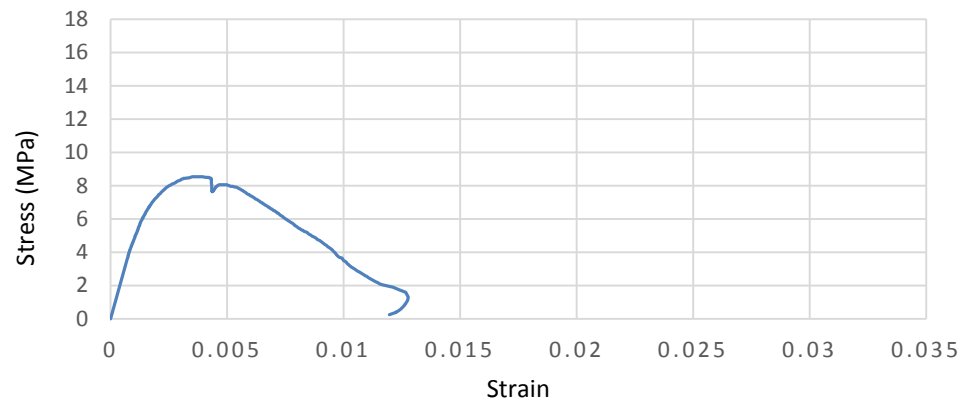
f_{cc}	ε_{cu}	f_{cc}/f_{co}	$\varepsilon_{cu85}/\varepsilon_{co85}$
8.53	0.0023	0.97	1.14

Name of specimen: C-G-1
Jacket detail: GFRC only.
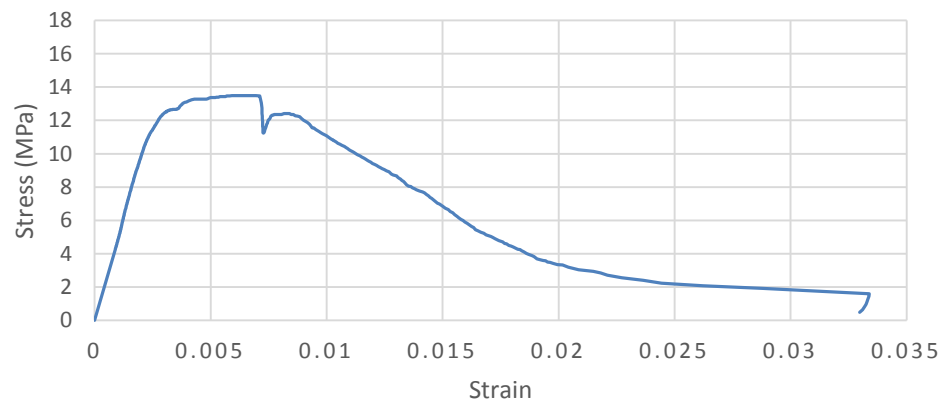
f_{cc}	ε_{cu}	f_{cc}/f_{co}	$\varepsilon_{cu85}/\varepsilon_{co85}$
13.50	0.007	1.53	1.8

Name of specimen: C-G-2
Jacket detail: GFRC only.
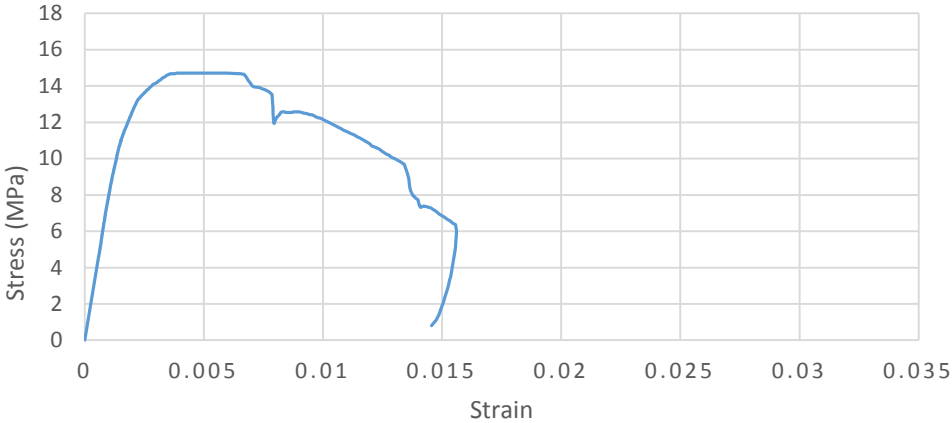
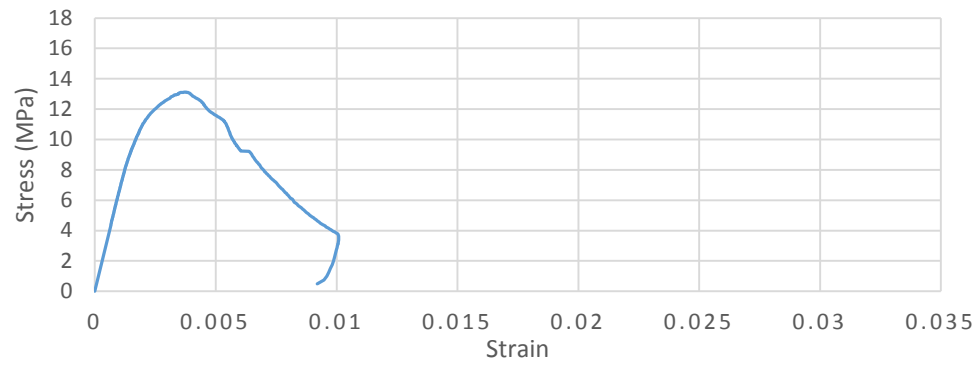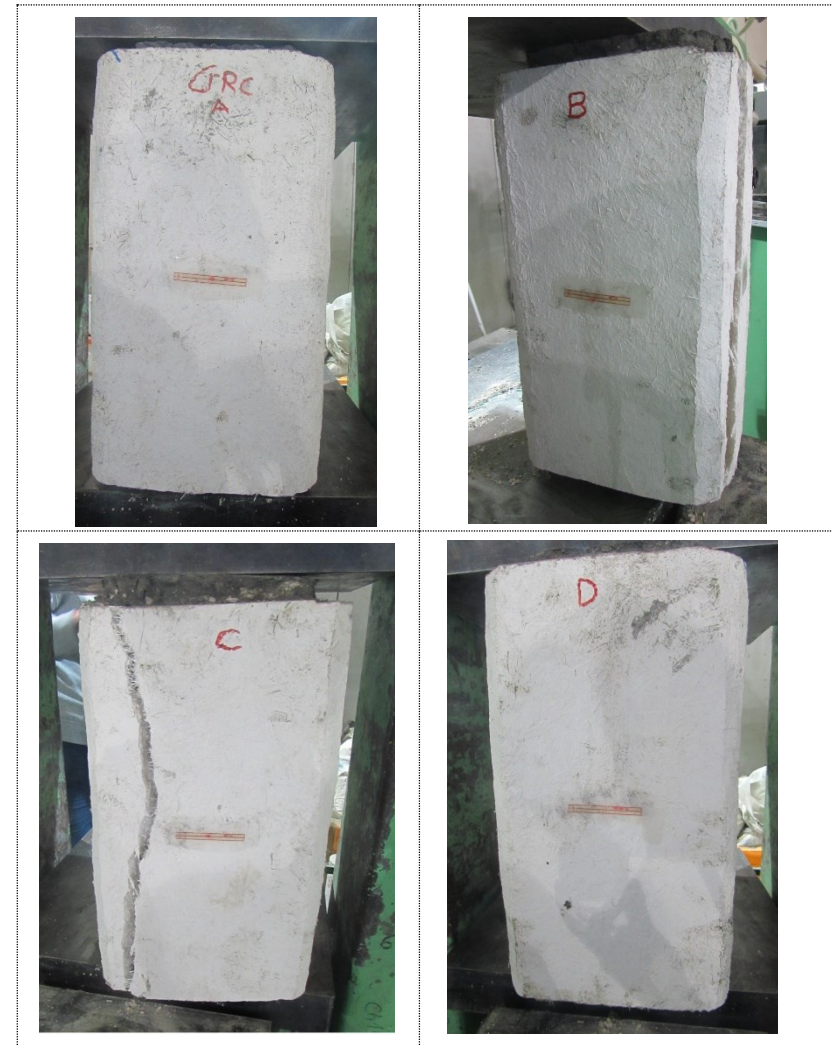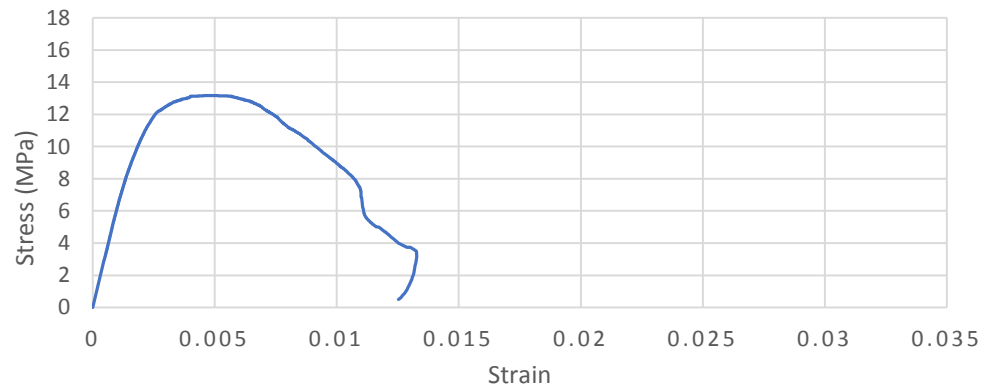| f_{cc}	ε_{cu}	f_{cc}/f_{co}	$\varepsilon_{cu85}/\varepsilon_{co85}$
14.71	0.006	1.67	1.74

Name of specimen: C-T1-2
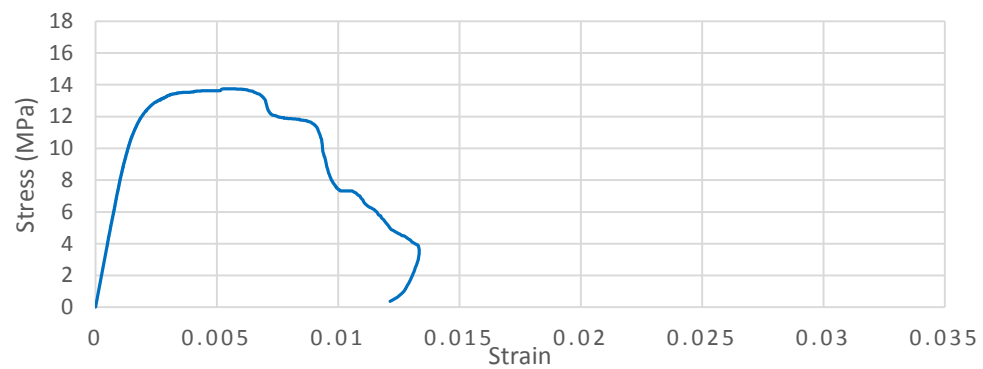Jacket detail: GFRC +1 layer of basalt.
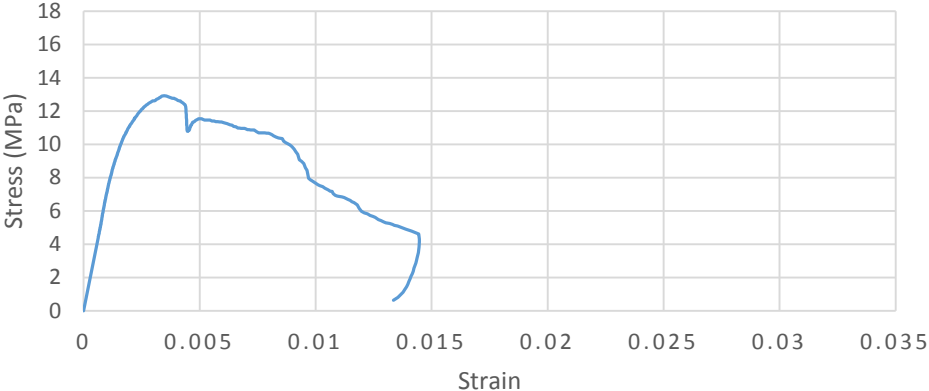
f_{cc}	ε_{cu}	f_{cc}/f_{co}	$\varepsilon_{cu85}/\varepsilon_{co85}$
12.92	0.003	1.47	1.27

Name of specimen: C-T2
Jacket detail: GFRC +2 layer of basalt.
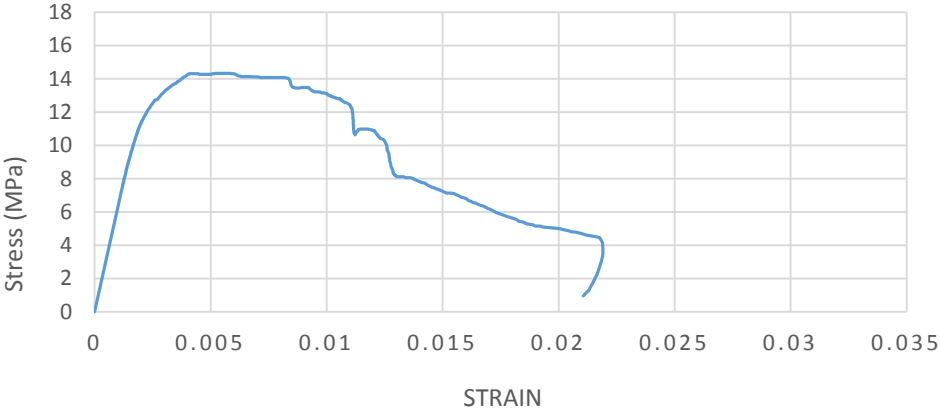
f_{cc}	ε_{cu}	f_{cc}/f_{co}	$\varepsilon_{cu85}/\varepsilon_{co85}$
14.32	0.006	1.63	2.09

Name of specimen: C-T3
Jacket detail: GFRC +3 layer of basalt.
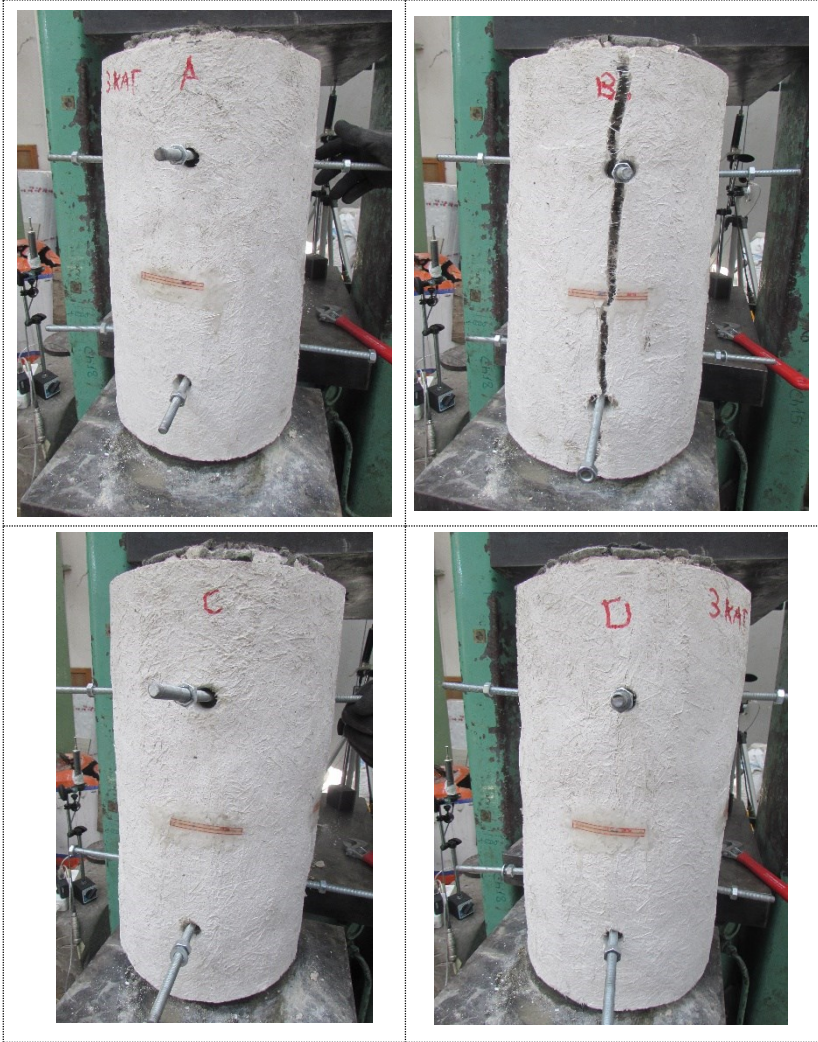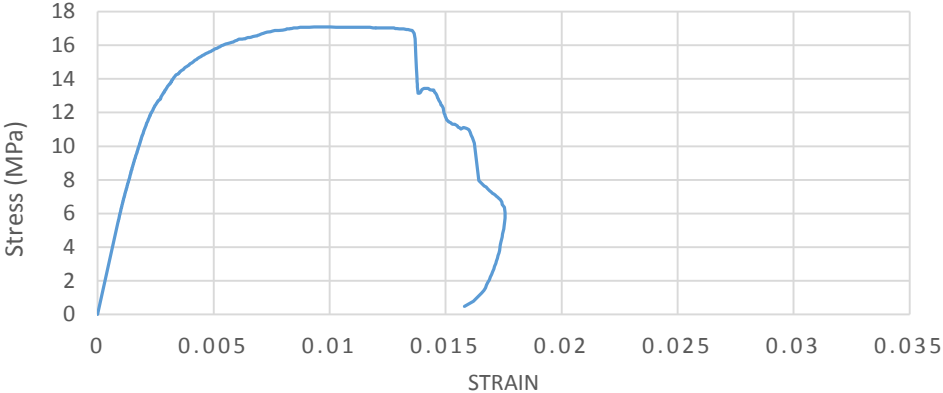
f_{cc}	ε_{cu}	f_{cc}/f_{co}	$\varepsilon_{cu85}/\varepsilon_{co85}$
17.10	0.010	1.94	2.59

Name of specimen: S-C-1
Jacket detail: control specimen without jacket.
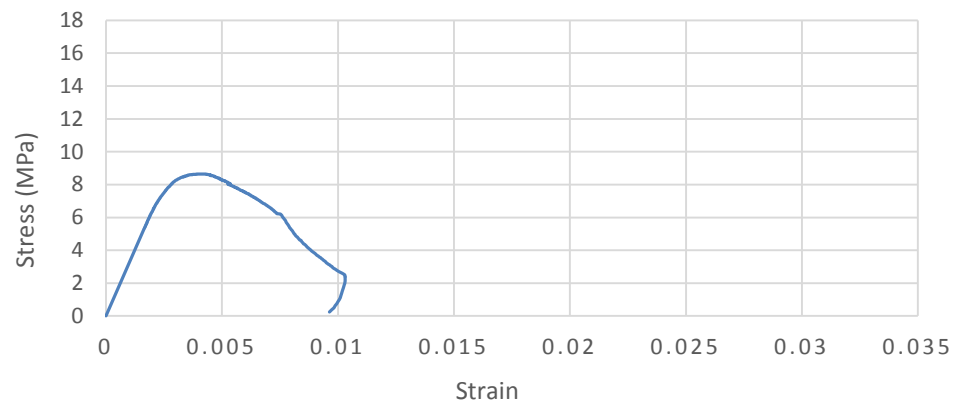
f_{cc}	ε_{cu}	f_{cc}/f_{co}	$\varepsilon_{cu85}/\varepsilon_{co85}$
8.65	0.0022	1.01	0.98

Name of specimen: S-C-2
Jacket detail: control specimen without jacket.
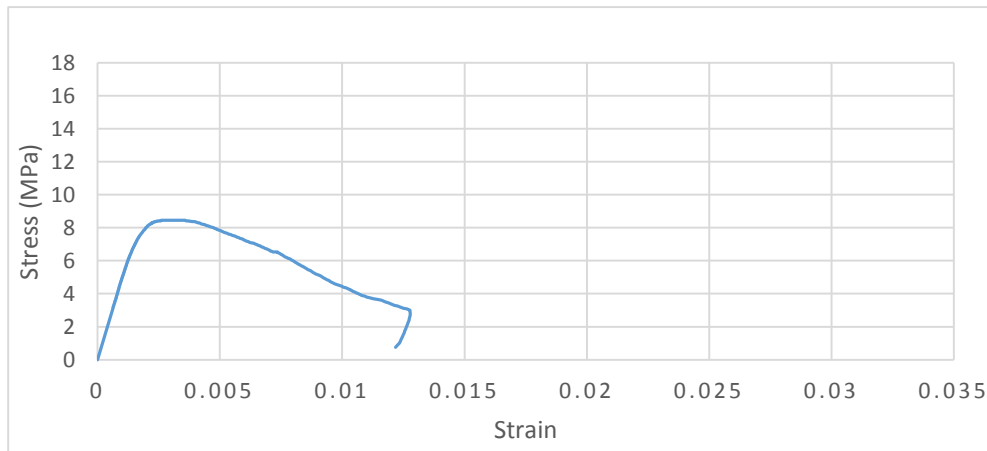
f_{cc}	ε_{cu}	f_{cc}/f_{co}	$\varepsilon_{cu85}/\varepsilon_{co85}$
8.65	0.002	0.988	1.01

Name of specimen: S-G-1
Jacket detail: GFRC only.
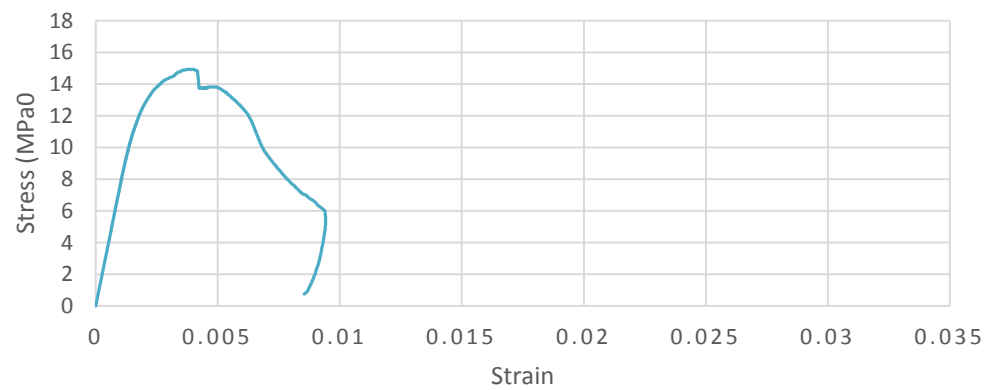
f_{cc}	ε_{cu}	f_{cc}/f_{co}	$\varepsilon_{cu85}/\varepsilon_{co85}$
14.93	0.004	1.75	0.98

Name of specimen: S-G-2
Jacket detail: GFRC only.

f_{cc}	ε_{cu}	f_{cc}/f_{co}	$\varepsilon_{cu85}/\varepsilon_{co85}$
13.13	0.004	1.54	0.90

Name of specimen: S-T1-1
Jacket detail: GFRC +1 layer of basalt.

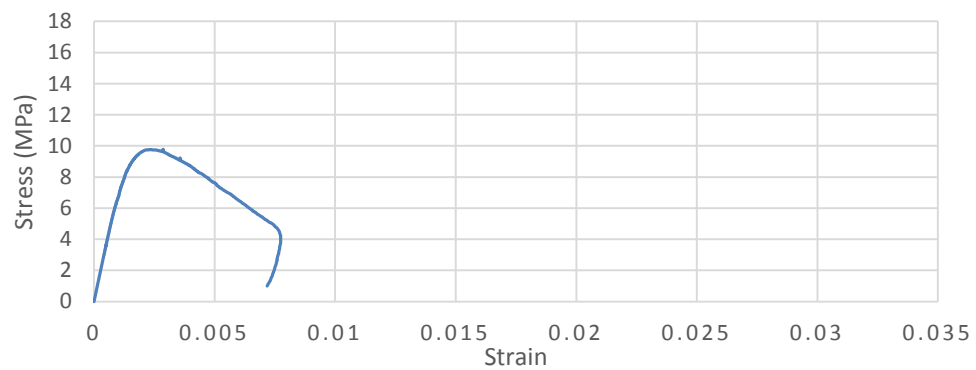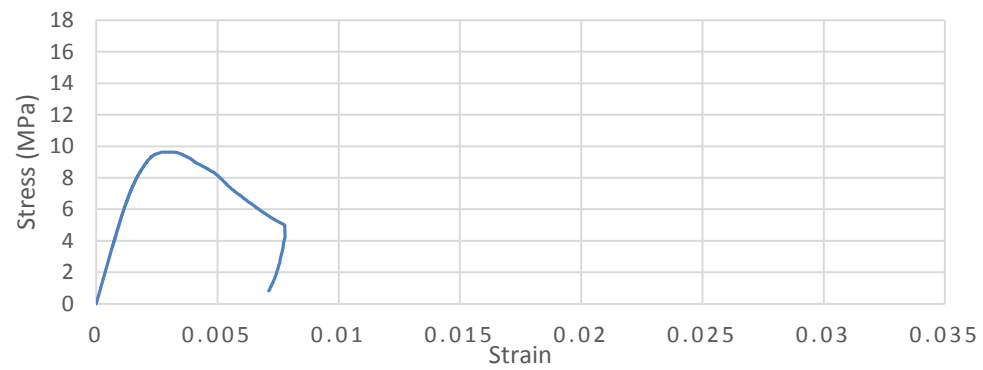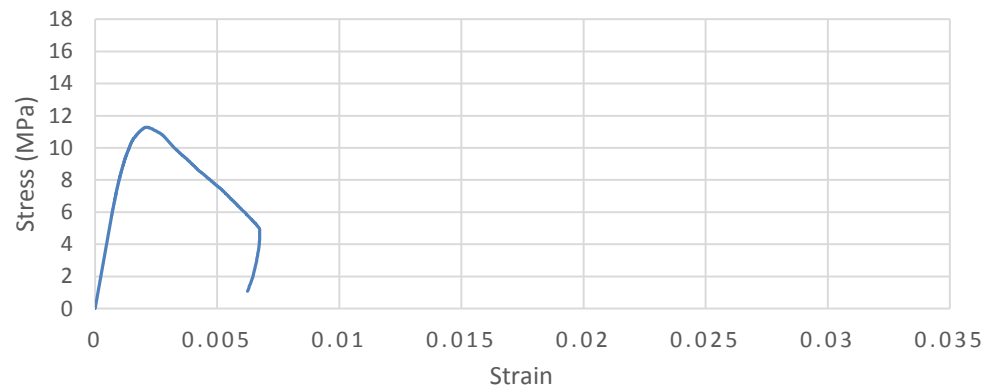| f_{cc}	ε_{cu}	f_{cc}/f_{co}	$\varepsilon_{cu85}/\varepsilon_{co85}$
13.18	0.005	1.54	1.34

Name of specimen: S-T1-2
Jacket detail: GFRC +1 layer of basalt.

f_{cc}	ε_{cu}	f_{cc}/f_{co}	$\varepsilon_{cu85}/\varepsilon_{co85}$
13.75	0.006	1.61	1.47

Name of specimen: S-T2
Jacket detail: GFRC +2 layer of basalt.
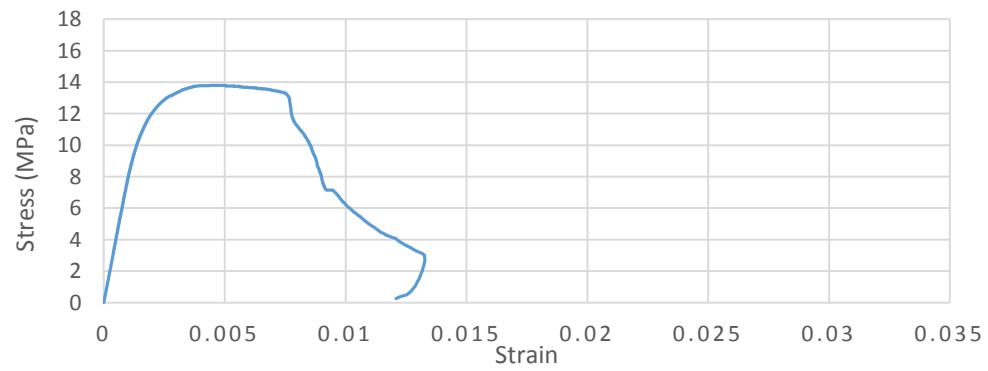
f_{cc}	ε_{cu}	f_{cc}/f_{co}	$\varepsilon_{cu85}/\varepsilon_{co85}$
13.8	0.005	1.61	1.30

Name of specimen: S-T3
Jacket detail: GFRC +3 layer of basalt.
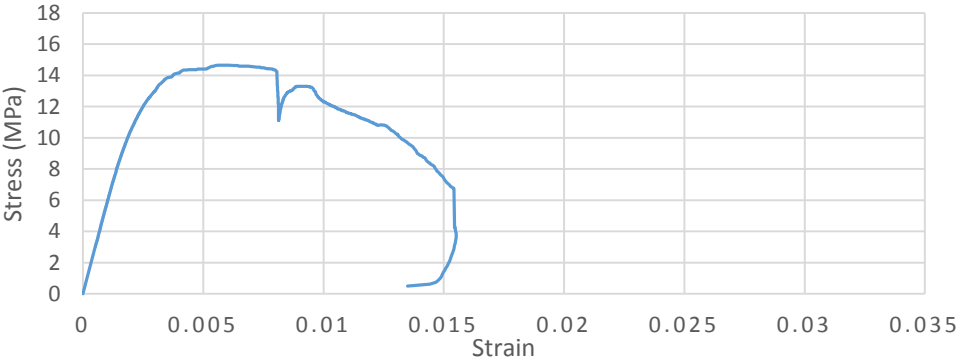
f_{cc}	ε_{cu}	f_{cc}/f_{co}	$\varepsilon_{cu85}/\varepsilon_{co85}$
16.65	0.0061	1.71	1.65

Name of specimen: R1.5-C-1
Jacket detail: control specimen without jacket.

f_{cc}	ε_{cu}	f_{cc}/f_{co}	$\varepsilon_{cu85}/\varepsilon_{co85}$
9.77	0.0023	1.04	0.93

Name of specimen: R1.5-C-2
Jacket detail: control specimen without jacket.

f_{cc}	ε_{cu}	f_{cc}/f_{co}	$\varepsilon_{cu85}/\varepsilon_{co85}$
9.63	0.0021	1.02	1.07

Name of specimen: R1.5-G-1
Jacket detail: GFRC only.

f_{cc}	ε_{cu}	f_{cc}/f_{co}	$\varepsilon_{cu85}/\varepsilon_{co85}$
11.27	0.002	1.19	0.77

Name of specimen: R1.5-T1
Jacket detail: GFRC +1 layer of basalt.
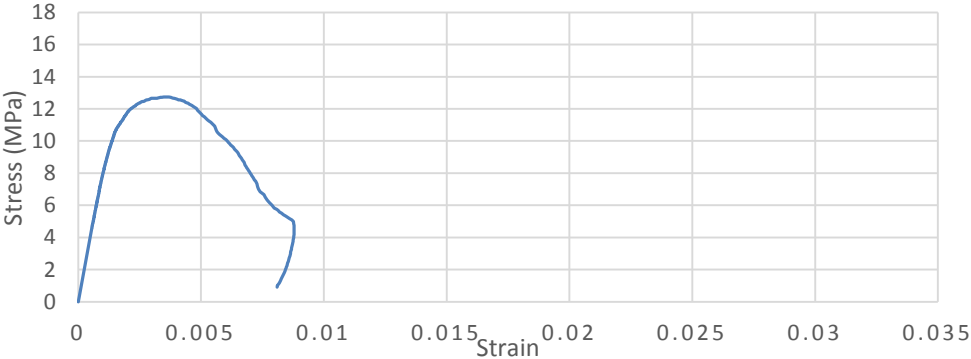
f_{cc}	ε_{cu}	f_{cc}/f_{co}	$\varepsilon_{cu85}/\varepsilon_{co85}$
12.73	0.004	1.35	1.2

Name of specimen: R1.5-T2
Jacket detail: GFRC +2 layer of basalt.
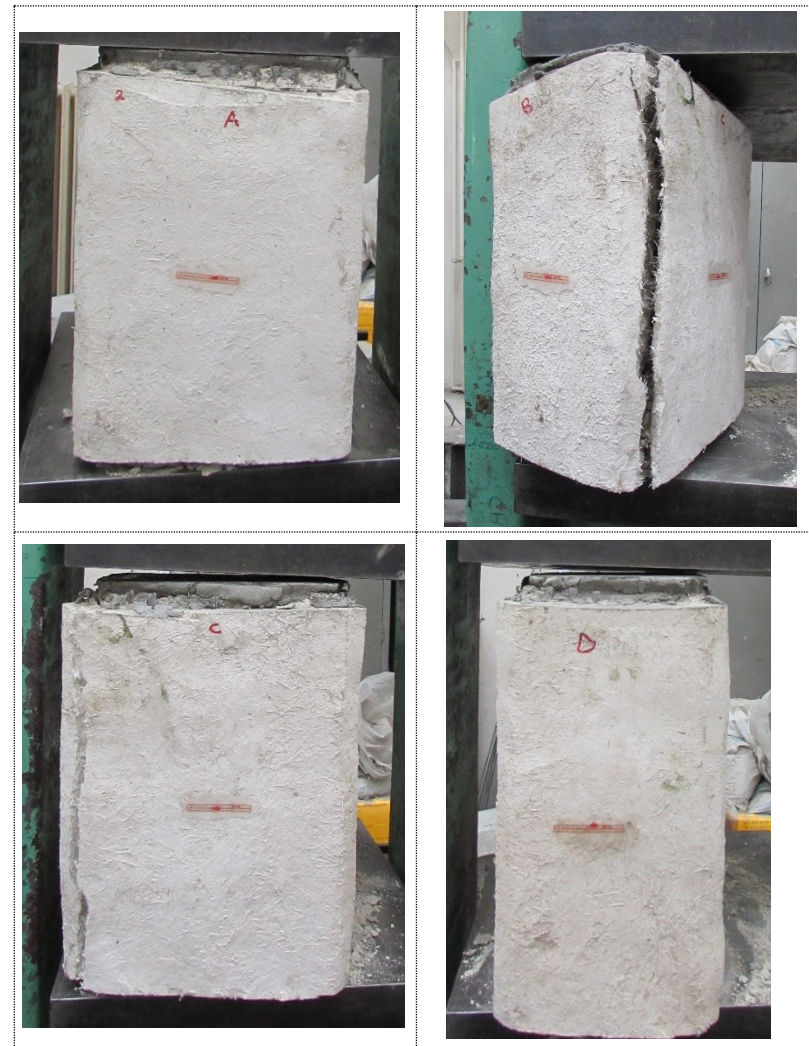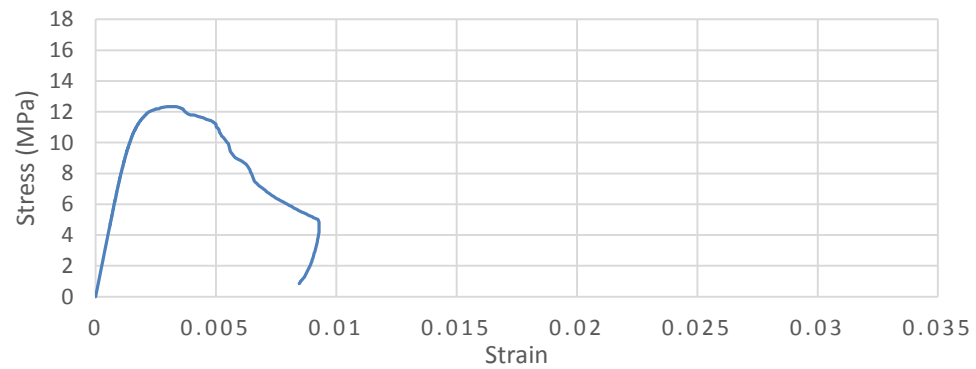
f_{cc}	ε_{cu}	f_{cc}/f_{co}	$\varepsilon_{cu85}/\varepsilon_{co85}$
12.33	0.003	1.31	1.12

Name of specimen: R1.5-T3-1
Jacket detail: GFRC+3layer of basalt
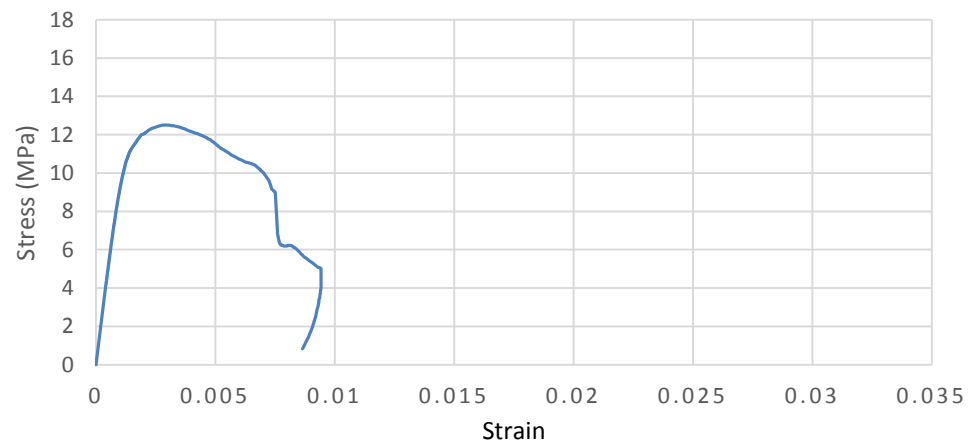
f_{cc}	ε_{cu}	f_{cc}/f_{co}	$\varepsilon_{cu85}/\varepsilon_{co85}$
12.5	0.003	1.33	1.33

Name of specimen: R1.5-T3-2
Jacket detail: GFRC+3layer of basalt
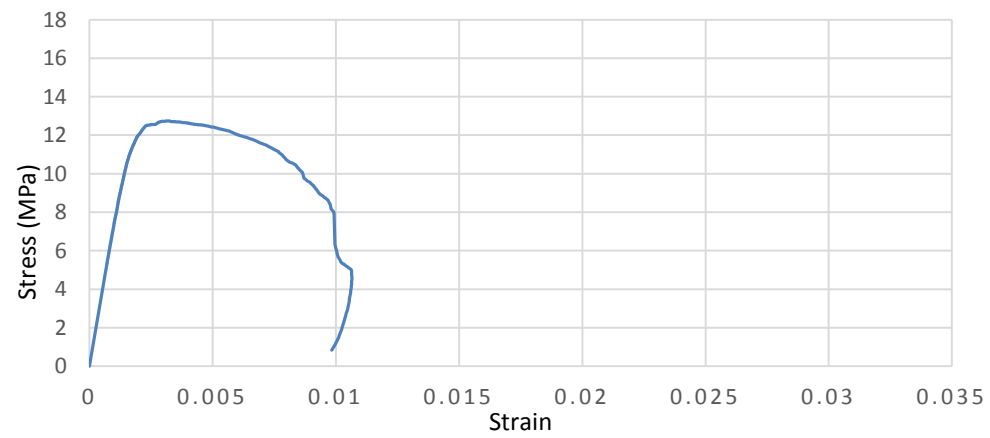
f_{cc}	ε_{cu}	f_{cc}/f_{co}	$\varepsilon_{cu85}/\varepsilon_{co85}$
12.73	0.003	1.35	1.71

CURRICULUM VITAE

Name Surname: Soheil KHOSHKHOLGHI

Place and Date of Birth: Oroumieh, Iran 1990

E-Mail: soheil.khoshkholghi@gmail.com

B.Sc.: Urmia Technical University, Civil Engineering, 2008-2012